ANALYSIS OF CYANATE ESTER RESINS AND GRAPHITE FABRIC FOR USE IN RESIN FILM INFUSION PROCESSING

Paul Joseph Myslinski

Thesis submitted to the Faculty of the
Virginia Polytechnic Institute and State University
in partial fulfillment of the requirements for the degree of

Master of Science
in
Materials Science and Engineering

Dr. A. C. Loos, Chair
Dr. R. G. Kander
Dr. B. J. Love

December, 1997
Blacksburg, Virginia

Keywords: Cyanate Esters, Cure-Kinetics, Graphite Fiber Composites,
Resin Film Infusion

ANALYSIS OF CYANATE ESTER RESINS AND GRAPHITE FABRIC FOR USE IN RESIN FILM INFUSION PROCESSING

Paul Joseph Myslinski

(ABSTRACT)

The objective of this investigation was to characterize two cyanate ester resins and a eight harness satin (8HS) graphite fabric for use in resin film infusion (RFI) processing. Two cyanate ester resin systems were characterized to determine their cure-kinetics, and viscosities during cure. A 8HS graphite fabric was tested in compaction and through the thickness permeability. A one-dimensional, through the thickness, flow and cure computer simulation was run.

The resin cure-kinetics models predicted the curing behavior of the resins as functions of time, temperature, and degree of cure. The proposed viscosity models determined the resin viscosity as a function of temperature and degree of cure. The 8HS graphite fabric was tested in compaction and through the thickness permeability to determine the effect of compaction pressure on fiber volume fraction and in turn on through the thickness permeability. The one-dimensional RFI flow and cure simulation combined the cure-kinetics and viscosity models of the resins with the characteristics of the graphite fabric and determined resin infiltration and cure times.

The proposed cure-kinetics and viscosity models were more than adequate in modeling the cure and flow behavior of the cyanate ester resin systems. Power law curve fits accurately represented the compaction and through the thickness permeability of the 8HS graphite fabric. Finally, the one-dimensional RFI flow and cure simulation showed that resin viscosity was the major influence on the infiltration times.

This research was supported under the NASA Grant NAG 1-343 and was monitored by Mr. Edward R. Long Jr. of the Environmental Interactions Branch in Langley, Virginia.

Acknowledgements

The author would like thank Dr. A. C. Loos, committee chairman, for his patience, support and perseverance, throughout the graduate program. Thanks are also due to the committee members, Dr. R. G. Kander and Dr. B. J. Love, for their time and effort.

This research was supported under the NASA Grant NAG 1-343 and was monitored by Mr. Edward R. Long Jr. of the Environmental Interactions Branch. This financial support was greatly appreciated.

In addition to those previously mentioned, the author would like to acknowledge the support and advice of several persons whose assistance was invaluable. Thanks are due to Dr. A. V. Rau, Dr. R. Clark, and T. Bullions for help with Differential Scanning Calorimetry. Dr. P. Shih provided great assistance with viscosity testing. A. Caba was of great assistance in running the one-dimensional simulations. The author would like to thank T. Knott and K. Furrow for their help in running all of the compaction and permeability tests. Thanks are also due to Dr. R. S. Gordon and J. Doran for their support and encouragement.

Finally, the author would like to thank his family and friends who provided incredible support and encouragement during this ordeal.

Table of Contents

List of Figures

List of Tables

CHAPTER 1: INTRODUCTION

1.0 INTRODUCTION

Improved performance, coupled with cost savings associated with the reduced weight of components, have been the key reasons that composites have been used extensively in a variety of space applications. Composite materials provide the designer the opportunity to tailor properties such as modulus, strength, and coefficient of thermal expansion (CTE) [1].

High modulus graphite / epoxy composites have been the materials of choice for space applications. However, the use of a conventional epoxy system has drawbacks due to excessive water absorption and residual stress, resulting in the propensity to microcrack when thermally cycled [1]. Alternatives to the epoxy resins have come about in recent years resulting in improvements in some critical composite properties.

The demand for matrix materials with improved toughness characteristics while maintaining high service temperatures, has focused attention on the use of cyanate ester resin systems. During the last decade, aromatic cyanate ester resins have emerged as a new class of thermosetting resins for use in the aerospace and electronics industries. As compared to epoxies, they are inherently tougher, have significantly better electrical properties and lower moisture uptake [2]. Cyanate esters also offer ease of handling and processing similar to that of epoxy resin systems.

Cyanate ester resin systems brought a significant improvement in toughness to the composite matrix. In primary structural aerospace applications, however, an even greater increase in matrix toughness was required. Work has shown that cyanate ester

resins lend themselves to toughening via incorporation of thermoplastic polymers [3]. Traditional toughening mechanisms such as this typically resulted in a significant decrease in service temperature. Efforts have been made to toughen cyanate ester resins without sacrificing any hot/wet performance.

A class of toughened cyanate ester resin systems has been developed, which include the incorporation of a proprietary thermoplastic into a thermosetting cyanate ester. This resin system maintains the processing ease characteristic of epoxies while significantly improving damage tolerance. By toughening the cyanate ester with a thermoplastic, significant increases in minimum melt viscosity were characteristic. Since this increase in viscosity was large, a different composite fabrication technique was considered.

Resin transfer molding (RTM) [4], a low viscosity resin injection process, is the typical fabrication method in making near net shape composite parts with two or three dimensional woven fabrics. Resin film infusion (RFI) is a composite manufacturing process which has evolved from earlier work on vacuum impregnation and RTM. The RFI process is similar to RTM except for the fact that RFI uses a hot melt resin film instead of a liquid resin. Low minimum viscosities are not a requirement as in the RTM process. Dry textile preforms are resin impregnated, consolidated, and cured in a single step [5]. The resin film is placed between the metal tool plate and the fabric preform. Inner and outer mold line tools (IML and OML) are used to accurately define and locate all structural detail as well as transfer autoclave pressure and temperature to the part [6].

Due to the many variables involved in the RFI process - resin viscosity, preform permeability, and resin / preform interaction - an iterative approach would be extremely

costly in determining such details as time required to fully saturate the preform, and the time to completely cure the composite part. Instead, cure-kinetics and viscosity models have been proposed for the cyanate ester resins. These models can be used to predict the cure rate, degree of cure, and viscosity as functions of temperature and time.

In order for analytical models to be accepted as valid replacements for experimental results, the accuracy of the models must be verified. This can be accomplished by comparing the proposed models to the experimental data. Using the proposed models and a reasonable temperature range (40-50°) an accurate model is expected.

It is also important to understand and measure the flow characteristics of the preform. Compaction tests are performed to determine how the fabric porosity changes under an applied load. The compressibility of the fiber bed will have a significant effect on the resistance to flow or permeability of the fabric. Compaction and permeability data are integral parameters in determining the time required for the resin to flow through and fill the preform.

A computer simulation model of the RFI process can be used to predict resin infiltration into the preform and cure of the resin saturated preform for a given processing cycle [5, 7]. Input into the simulation model are the cure-kinetics and viscosity models of the resin, and the compaction and permeability characteristics of the fabric. Additional input parameters include part thickness and autoclave temperature and pressure. Results of the simulation model included infiltration time and time required for the resin to fully cure. The simulation gives an overall look at how each parameter affects the RFI process.

The goal of this project was to investigate two cyanate ester resin systems and a new eight harness satin graphite fabric for their possible use in satellite applications. Properties of the materials are discussed in detail and various models are proposed. Background information on the two cyanate ester resins and the fabric are presented in chapter 2. The DSC cure-kinetics models are discussed in chapter 3. Chapter 4 contains the details of the viscosity model, while permeability and compaction information is explained in chapter 5. In chapter 6, a one-dimensional through-the-thickness RFI simulation model for infiltration of the cyanate ester resins into the carbon fabric is discussed. Finally, the conclusions are presented in Chapter 7 along with a brief discussion of future work..

CHAPTER 2: MATERIALS

2.0 MATERIALS

This chapter will detail the resin and fiber materials used in this research. The two resins were Fiberite 954-3 and 954-2a cyanate ester resins. The graphite fiber was Amoco ThermalGraph™ Fabric EWC-600X 8HS. Characteristics of the materials will be discussed in detail as well as the reasons why they were studied.

2.1. RESINS

Aromatic cyanate esters can be used in a wide variety of situations. When comparing them to epoxies, they are inherently tougher, have significantly better electrical properties and lower moisture uptake. Many applications in the aerospace and electronics industries require material properties such as these. ICI Fiberite has developed a family of modified cyanate resins for various uses ranging from radomes and primary aerospace structures to space applications [2]. Their properties can be explained on the basis of the molecular structure of the cured cyanate networks.

During the cure of cyanate resins, there is an initial shrinkage. However, unlike epoxies, cyanate esters cure via a ter-molecular reaction to form thermally stable triazine rings [1, 8, 9], as seen in Figure 2.1. As a consequence of this trimerization reaction and the structure of the resultant network, a large amount of free volume is created as the cure proceeds to completion after gelation. This is manifested as an overall cure

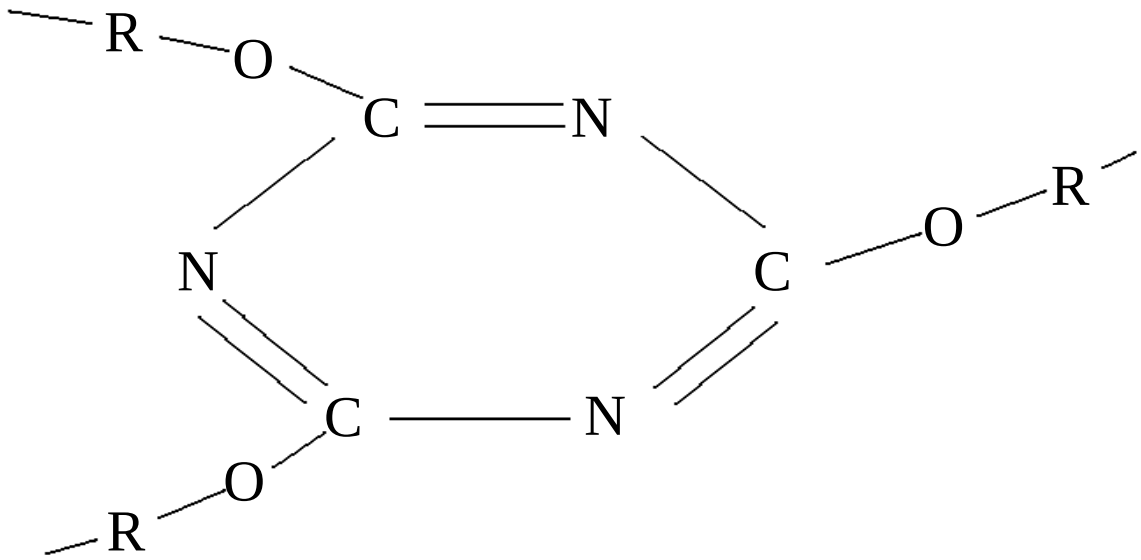

Figure 2.1: Schematic drawing showing the triazine ring structure.

shrinkage of less than 1% and reduced levels of residual stress. It is the large free volume present on a molecular level that is responsible for the inherent toughness that is characteristic of cyanate esters. This improved toughness greatly reduces the tendency to microcrack when exposed to thermal cycling [1].

Another characteristic of the molecular structure of the cured network is that it is extremely low in polarity due to the symmetry of the triazine rings formed. During the cure of epoxies, polar hydroxyl groups are generated. These have a strong affinity for water due to the thermodynamically favorable hydrogen bonds that can be formed. In contrast, no such functionality that is capable of hydrogen bonding with water is generated while curing cyanate esters. Relative to epoxies, cyanates are considerably more hydrophobic and cured neat resins typically exhibit a low moisture uptake of only 0.5%-2.5% [2].

The inherent hydrophobicity of the cured matrix is an important advantage in applications where dimensional stability is critical since it reduces hygrostrain. Additionally, along with the absence of volatiles evolved during cure, the inherent hydrophobicity is responsible for the low outgassing behavior observed with cyanate esters [1]. Cyanates are excellent at maintaining their electrical performance across a wide range of environmental conditions because of their inherent hydrophobicity. They also have extremely low dielectric constants (D_k) and dissipation factors (D_f) due to the absence of polarity in the crosslinked cyanurate network. Despite their attractive properties, modifications to both rheology and fracture toughness have been necessary to facilitate their use in certain demanding areas of the aerospace industry.

2.1.1. 954-3 CYANATE ESTER RESIN

Aerospace applications have created the demand for new resin systems that offer an improvement in performance. These are driven by the need for improved dimensional stability of structures which experience repeated cycling over a large range of temperatures (typically -128°C to 121°C). Under such conditions, composite materials microcrack to relieve residual stresses that are built in during fabrication. Predictability of the extent of microcracking and its effect on the coefficient of thermal expansion (CTE) are often critical, so structures are often cycled before being used to ensure dimensional stability.

954-3 was designed in response to the demanding requirements of space applications. When heated to elevated temperatures it easily passes outgasing requirements, and still remains easily processable similar to epoxy resins. Cyanates, as a class of resins, are also radiation resistant.

One other important feature of 954-3 cyanate ester resin is its extremely low minimum viscosity. At modest temperatures (120°C) it experiences minimum viscosities below 0.1 Pa-s. This results in shorter times for the resin to infiltrate and completely fill the preform.

The selection of a more hydrophobic resin with a reduced propensity to microcrack may be crucial in designing structures with greater dimensional stability. Fiberite 954-3 offers significant improvements in these key properties that can be used to advantage in applications where dimensional stability is critical [1].

2.1.2. 954-2A TOUGHENED CYANATE ESTER RESIN

Primary structural applications have created a demand for materials with improved damage tolerance and high service temperatures. This has typically been achieved via the incorporation of engineering thermoplastics and / or elastomeric modifiers. Materials that have been toughened include epoxies, cyanates, and bismaleimides. However, toughness has often been gained at the expense of modulus and / or glass transition temperature, resulting in materials with reduced service temperature capability.

ICI Fiberite has developed a unique toughened thermoset technology which allows damage tolerance to be increased whilst minimizing the reduction in service temperature. Proprietary thermoplastics, with the necessary reactive functionality and optimum molecular weight are employed to produce homogeneous thermoset / thermoplastic blends [1]. Such blends can be prepregged and upon cure yield a “co-continuous”[10] morphology.

Open hole compression tests place the hot / wet service temperature at 177 to 191°C. This is comparable to several toughened bismaleimide systems that are presently available. The system also offers excellent electrical properties and is being evaluated for novel applications that demand a combination of toughness, hot / wet performance and electrical transparency.

954-2a has a significantly increased minimum viscosity (3.5 Pa-s) relative to the 954-3 resin system. 954-2a also requires degassing prior to use. During the mixing process, when the thermoplastic is added, either gas or moisture becomes entrapped

within the resin system. Violent bubbling behavior is witnessed at elevated temperatures if the resin is not degassed.

954-3 and 954-2a are 350°F (177°C) curing cyanate resins with -200°F to 250°F (-128°C to 121°C) service temperatures. They are formulated for autoclave or press molding. Standard cure is two hours at 350°F (177°C). Service temperatures are maximized by a post-cure of 428-450°F (220-232°C). Both can be impregnated via hot melt or solution techniques on all available fibers and fabrics [11].

2.2. EWC-600X 8HS GRAPHITE FABRIC

An eight (8) harness satin is a weave of carbon or graphite fibers oriented at 0° and 90°. The 0° direction is referred to as the warp direction and the 90° direction is the fill direction. The "eight" is essentially the repeat unit in the fabric. Each tow of fibers in the warp direction goes above seven tows and below one, but each tow of fibers in the fill direction goes below seven and above one. Figure 2.2 shows the basic weave of an eight harness satin [12].

ThermalGraph™ Fabric EWC-600X 8HS is a pitch-fiber based high thermal conductivity woven fabric developed for thermal management applications. Due to the orthotropic nature of the weave, and the high longitudinal thermal conductivity of the fibers, biaxial thermal conductivity is achieved. It is easily prepregged and processed into a composite form. EWC-600X is available as an eight harness satin weave fabric constructed from 2000 (2K) filament continuous pitch tows [13].

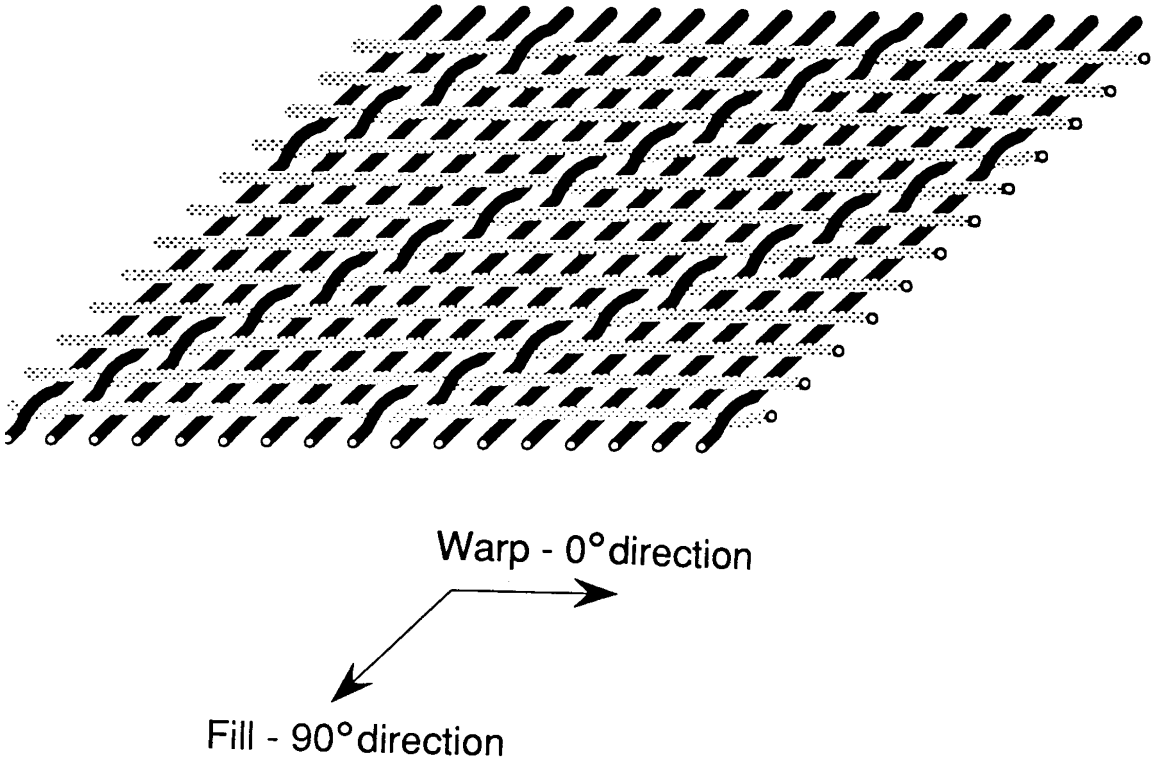

Figure 2.2: An eight harness satin fabric weave [12].

Some properties of the EWC-600X 8HS include the following: 20 tows per inch in both the warp and fill directions, areal weight of 491 g/m^2, and a nominal thickness of 0.84 mm (0.033 in.). The yarn density is 2.18 g/cc, the carbon assay is >99%, and there has been no surface treatment of the fibers [13].

CHAPTER 3: CURE-KINETICS

3.0 CURE-KINETICS

Cure kinetics models are often developed to relate the cure reaction rate to the temperature and degree of cure. The degree of cure of a thermosetting resin is related to the heat of reaction by the following expression,

$$\alpha = \frac{H(t)}{H_r} \qquad (3.1)$$

where H(t) is the heat given off as a function of time and H_r is the total heat of reaction. Characterizing the cure kinetics involves measuring the parameters associated with the exothermic cure reaction and then developing a mathematical model for the cure rate in terms of temperature and degree of cure.

3.1. EXPERIMENTAL PROCEDURE

DSC experiments were performed on Fiberite's 954-3 and 954-2a cyanate ester resins. The instrument employed in this investigation to make these measurements was a DuPont Model 910 differential scanning calorimeter (DSC) controlled by a TA Instruments Model 9900 computer. Sample sizes ranged from 5.0 to 10.0 mg and were encapsulated in hermetically sealed pans. All samples were prepared under the same conditions and from the same batch of resin.

Prior to running any tests, the sample chamber was heated to 600°C in air [14] in an effort to burn off any sources of contamination that may have accumulated from previous use. Following the cleaning, several calibration procedures were employed. A dynamic scan was run to confirm a static base-line of an empty chamber, followed by a temperature calibration using indium and lead. The calibration software automatically corrected the cell constant, a ratio of the measured to standard heat of fusion.

Sample preparation included weighing the resin sample and sealing the aluminum sample pan using the TA Instruments crimping tool. An empty sample pan and lid were used as the reference. A small hole was made in the lid of the 954-2a sample to allow entrapped gas to escape.

Once the sample was prepared, testing ensued. A set of dynamic scans were run [15] to determine the total heat of reaction and the temperature range for the isothermal scans. Heating rates ranged from 10 °C/min down to 1 °C/min**.** Shown in Figure 3.1 is an example of a 5 °C/min dynamic scan with the peak starting point and peak area (H_r), denoted. Isothermal scanning temperatures were selected in 10 or 15° increments between the peak starting temperature and the peak maximum temperature.

The resin sample was placed in the testing chamber preheated to the isothermal testing temperature. Data recording began when the cell temperature was within 5° of the desired temperature. The test ran until the curve flattened out, indicating that the extent of cure at that temperature had been reached. Shown in Figure 3.2 is an example of an isothermal scan with the important points labeled. Higher temperatures resulted in shorter testing times. Once the sample had cured the test was stopped and the sample

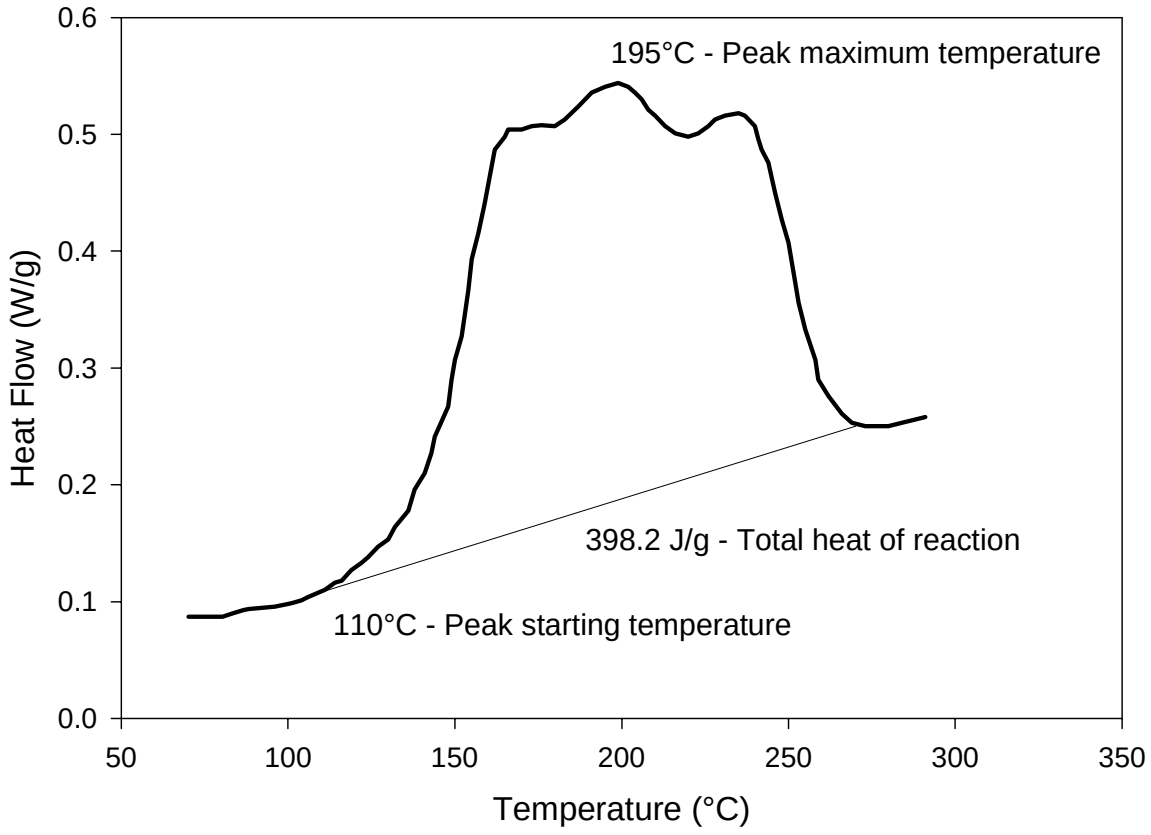

Figure 3.1: Example dynamic scan of 954-2a run at 5°C / minute up to 300°C showing the peak starting temperature, peak maximum, and total heat of reaction.

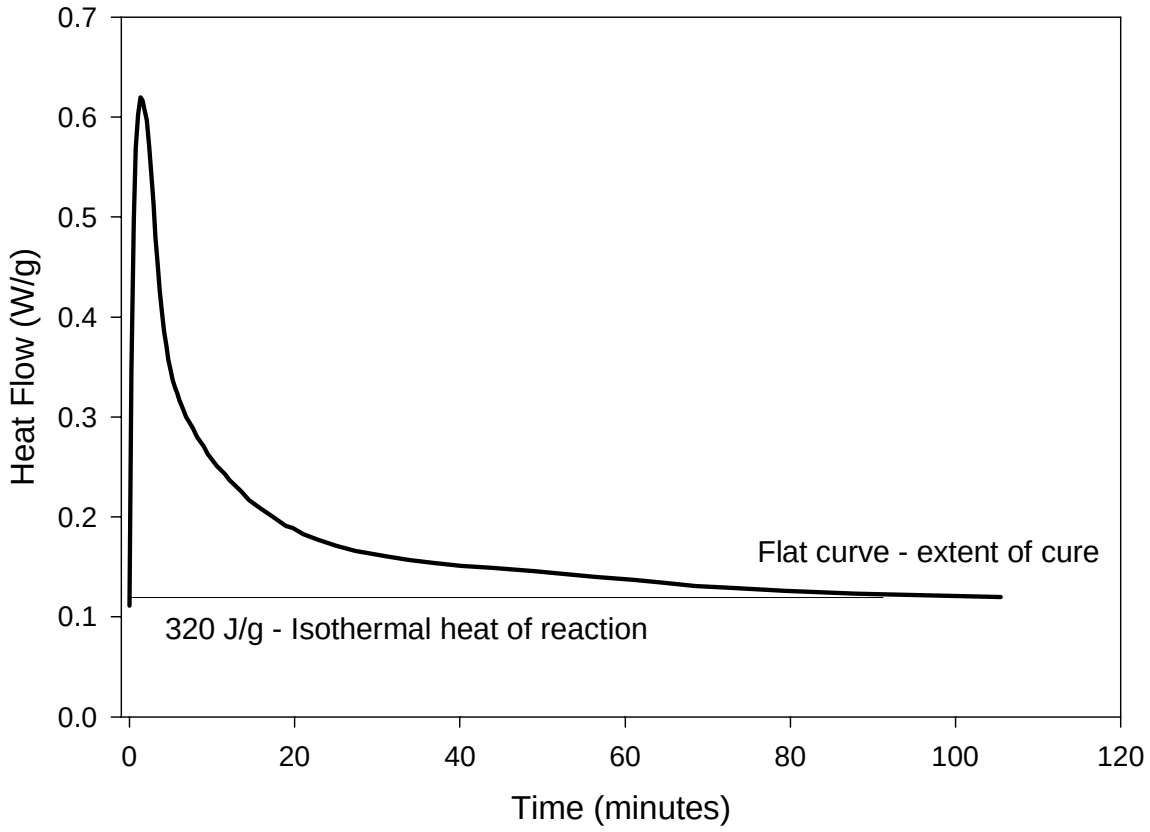

Figure 3.2: Example isothermal scan, run at 180°C for 110 minutes on the 954-2a resin, showing the isothermal heat of reaction (H_{iso}).

chamber cooled to room temperature. A residual scan, shown in Figure 3.3 (5°C/min up to 350°C) was then performed to determine the residual heat of reaction. The total heat of reaction H_T can be expressed as follows

$$H_T = H_{iso} + H_{res} \qquad (3.2)$$

where H_{iso} is the isothermal heat of reaction and H_{res} is the residual heat of reaction. The total heat of reaction, H_T, determined from the isothermal and residual scans should be equal to the total heat of reaction, H_r, from the dynamic scan.

The isothermal scans were used to determine the degree of cure and cure rate using the following procedure: A flat baseline, as seen in Figure 3.2, was determined by adjusting the starting point of the curve to be at the same y-value as the flat portion. The area between the curve and the flat baseline, H_{iso}, was determined by integration, and then broken up into small intervals. Figure 3.4 shows how the isothermal scan was broken up into intervals in order to measure area versus time data. Degree of cure was then determined by the following equation,

$$\alpha(t) = \frac{\sum_{i=0}^{t} A_i}{H_T} \qquad (3.3)$$

where A_i is the area under the curve at time, t.

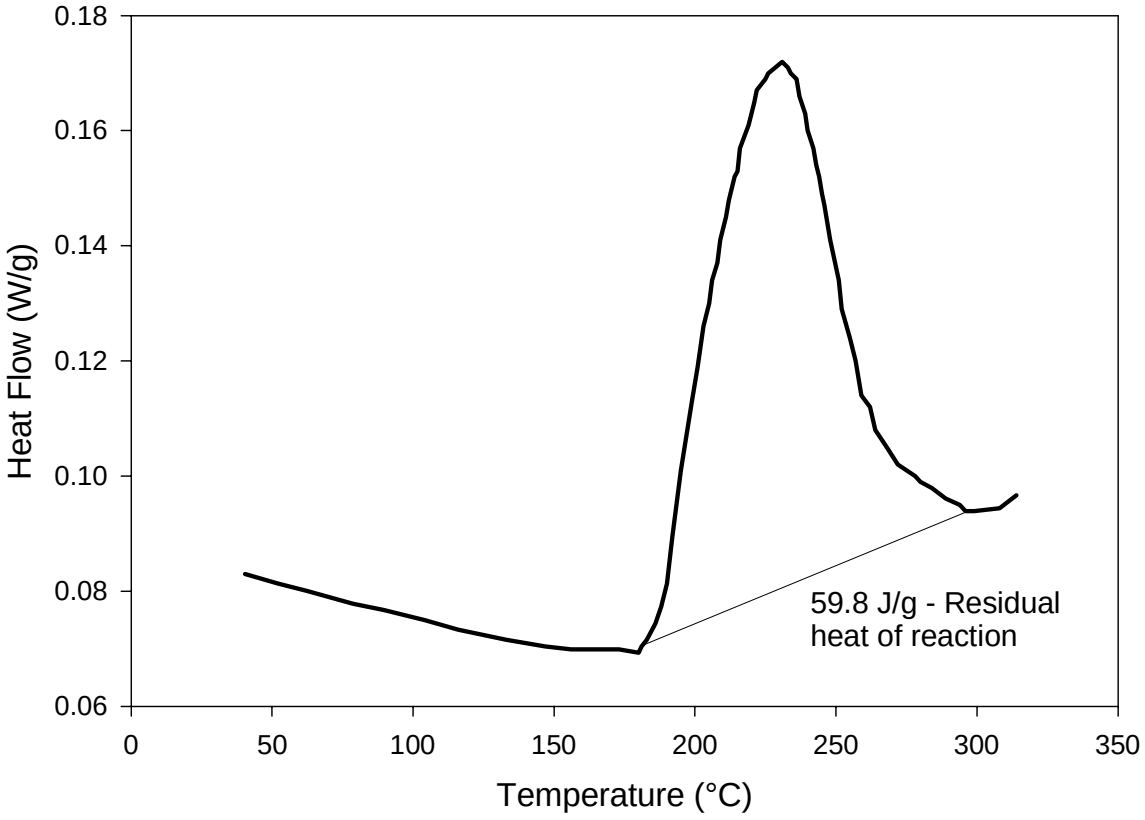

Figure 3.3: Residual dynamic scan run at 5°C / minute immediately after the 180°C isothermal scan, showing the residual heat of reaction (H_{res}).

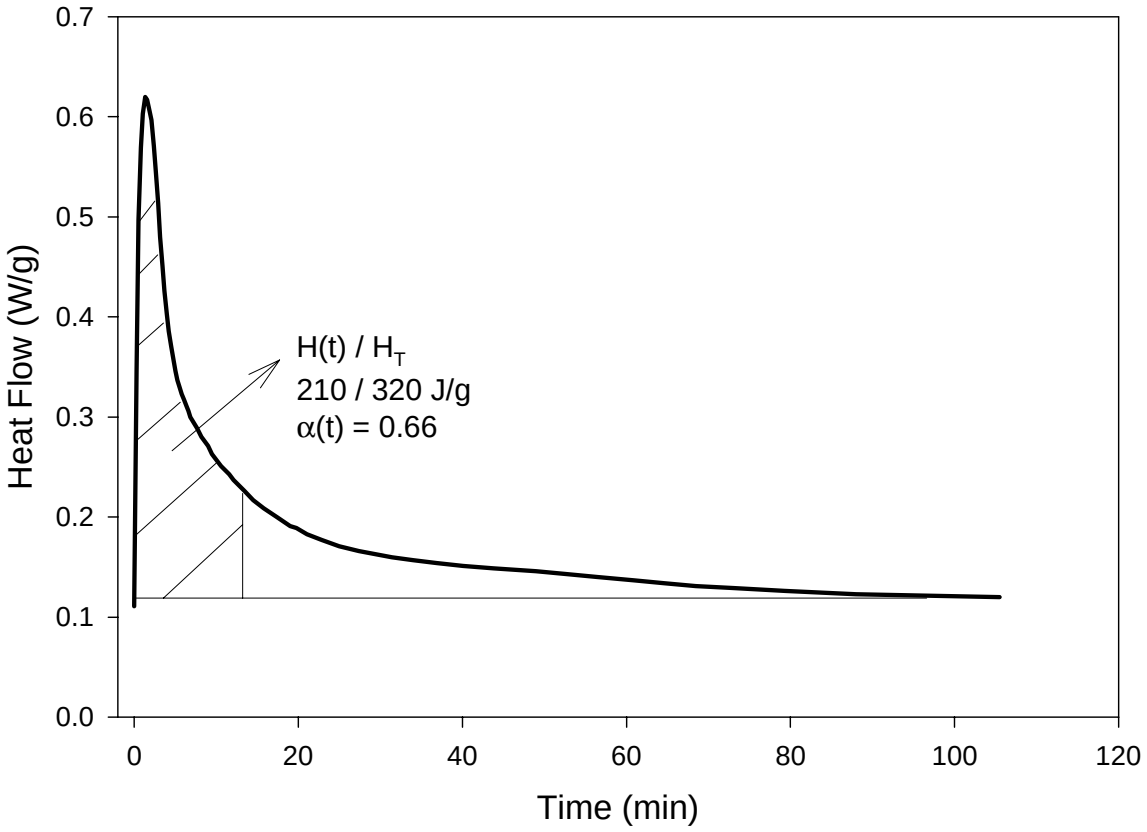

Figure 3.4: Example of an isothermal scan broken up into intervals to determine the degree of cure as a function of time.

Once degree of cure (α) was calculated as a function of time, reaction rate ($d\alpha/dt$) was determined as a function of degree of cure (α).

$$\frac{\alpha_2 - \alpha_1}{t_2 - t_1} = \frac{d\alpha}{dt} \qquad (3.4)$$

3.2. GOVERNING EQUATIONS

The data were then fit to a two part mathematical model proposed by Chen and Macosko [16],

$$\frac{d\alpha}{dt} = (k_1 + k_2\alpha^m)(1-\alpha)^{n_1} \; ; \; \alpha < \alpha_d \qquad (3.5)$$

$$\frac{d\alpha}{dt} = k_3(\alpha_p - \alpha)^{n_2} \; ; \; \alpha \geq \alpha_d \qquad (3.6)$$

where m and n_i are kinetic exponents, α_p is the maximum degree of cure that is reached at a specific temperature, and α_d is the onset of diffusion controlled kinetics. α_d was determined from the plots of reaction rate versus degree of cure [17, 18]. A change in slope signified the onset of diffusion controlled kinetics. Figure 3.5 shows how α_d was

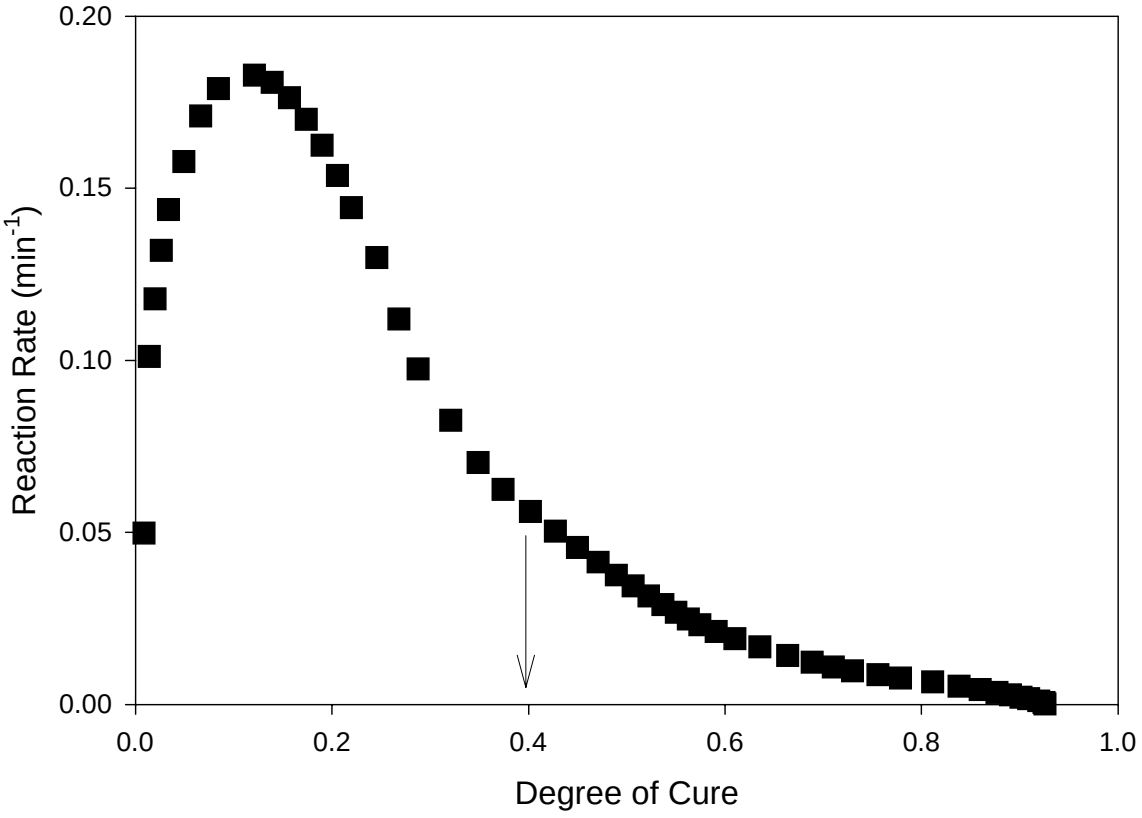

Figure 3.5: Plot of reaction rate vs. degree of cure for 954-2a, run at 180°C, showing the determination of α_d.

determined for the 954-2a cyanate ester resin. The reaction rate constants, k_i, were described by an Arrhenius type expression as follows

$$k_i = A_i e^{-\frac{E_i}{RT}}; \text{ i = 1 - 3} \qquad (3.7)$$

where A_i is the Arrhenius pre-exponential factor , E_i is the activation energy, R is the universal gas constant 8.314 J/mole-K, and T is the temperature in Kelvin.

SigmaPlot's nonlinear multiple regression algorithm was used for the analysis of the isothermal runs. The program read the values of α and $d\alpha/dt$ from an input file and iteratively solved equations (3.5) and (3.6) until the solutions with the desired degree of accuracy were obtained.

The SigmaPlot nonlinear regression uses the Marquardt Levenberg algorithm to find the coefficients (parameters) of the independent variable(s) that give the "best fit" between the equation and the data. This algorithm seeks the values of the parameters that minimize the sum of the squared differences between the values of the observed and predicted values of the dependent variable,

$$SS = \sum_{i=1}^{n} (y_i - \bar{y}_i)^2 \qquad (3.8)$$

where y_i is the observed and y_2 is the predicted value of the dependent variable [19].

This process is iterative; SigmaPlot begins with a "guess" at the parameters, checks to see how well the equation fits, then continues to make better guesses until the differences between the residual sum of squares no longer decreases significantly. This condition is known as convergence [19]. Upon completion of the iterations, output containing the values for k_1, k_2, k_3, m, n_1, and n_2 were displayed.

3.3. RESULTS

3.3.1. 954-3 CYANATE ESTER RESIN

From a series of six dynamic scans, H_T was determined to be 413 ± 27 J/g. Table 3.1 contains the six dynamic scans and their heats of reaction.

Table 3.1 - Heating rates and their respective heats of reaction for 954-3.

Heating rate (°C/minute)	H_r (J/g)
10.0	425.9
7.5	420.0
5.0	395.3
4.0	443.7
2.0	422.0
1.0	368.0

The isothermal range of temperatures was determined to be between 135°C and 195°C.

The values of A_1, A_2, A_3, E_1, E_2, and E_3 were found by constructing Arrhenius plots of the natural log of the rate constants (k_1, k_2 and k_3) versus inverse temperature (1/T). k_1 was fit in two parts; a high temperature region (170°C - 195°C) and a low temperature region (135°C - 170°C). A linear least squares fit was used and the following equations were the result.

$$k_1(\text{high}) = \exp\left(-4.0 \times 10^4 \, (1/T) + 63\right)$$

$$k_1(\text{low}) = \exp\left(-1.6 \times 10^4 \, (1/T) + 31\right) \qquad (3.9)$$

$$k_2 = \exp\left(-1.0 \times 10^4 \, (1/T) + 20\right)$$

$$k_3 = \exp\left(-8.6 \times 10^3 \, (1/T) + 17\right)$$

These plots are shown in Figures 3.6 - 3.9. The y-intercept of these curves is equal to the natural log of the pre-exponential constants (A_1, A_2 and A_3). The slope is equal to the value ($-E_i/R$). The resulting values are presented in Table 3.2.

Table 3.2 - The pre-exponential constants (A_i) and the activation energies (E_i) for 954-3 cyanate ester resin.

	A_i (1/min)	E_i (J/mole)
k_1(170°C - 195°C)	3.1×10^{27}	3.3×10^5
k_1(135°C - 165°C)	2.4×10^{13}	1.3×10^5
k_2	6.8×10^8	8.5×10^4
k_3	1.9×10^7	7.1×10^4

Kinetic exponents, m and n_i were plotted as functions of temperature in Figures 3.10-3.12. An average value was used to represent n_1 because no noticeable trend was observed. The data were fit with a linear least squares fit which resulted in the following equations.

$$n_1 = 1.1 \text{ (average)}$$

$$m = 3.5 \times 10^{-3} \, (T) - 1.24 \qquad (3.10)$$

$$n_2 = 3.5 \times 10^{-3} \, (T) - 0.60$$

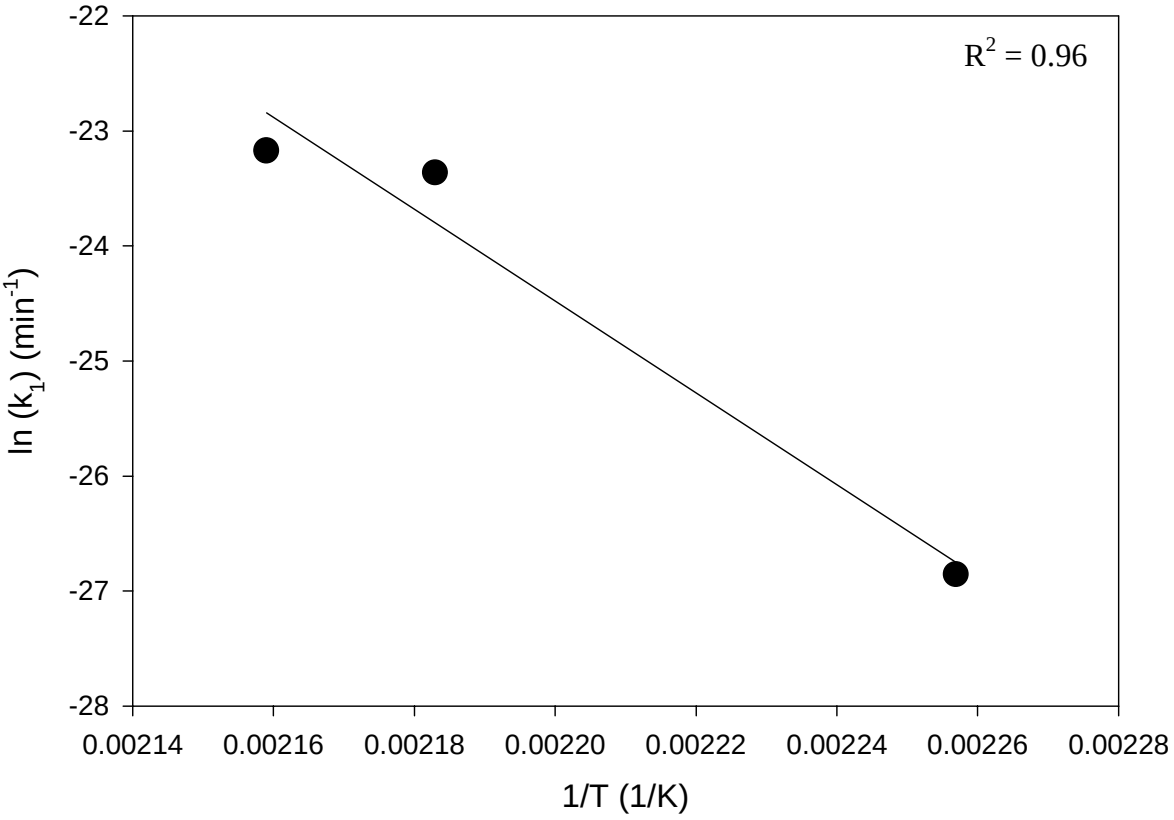

Figure 3.6: Plot of ln(k_1) vs. 1/T for temperatures between 170°C and 195°C for Fiberite 954-3 resin.

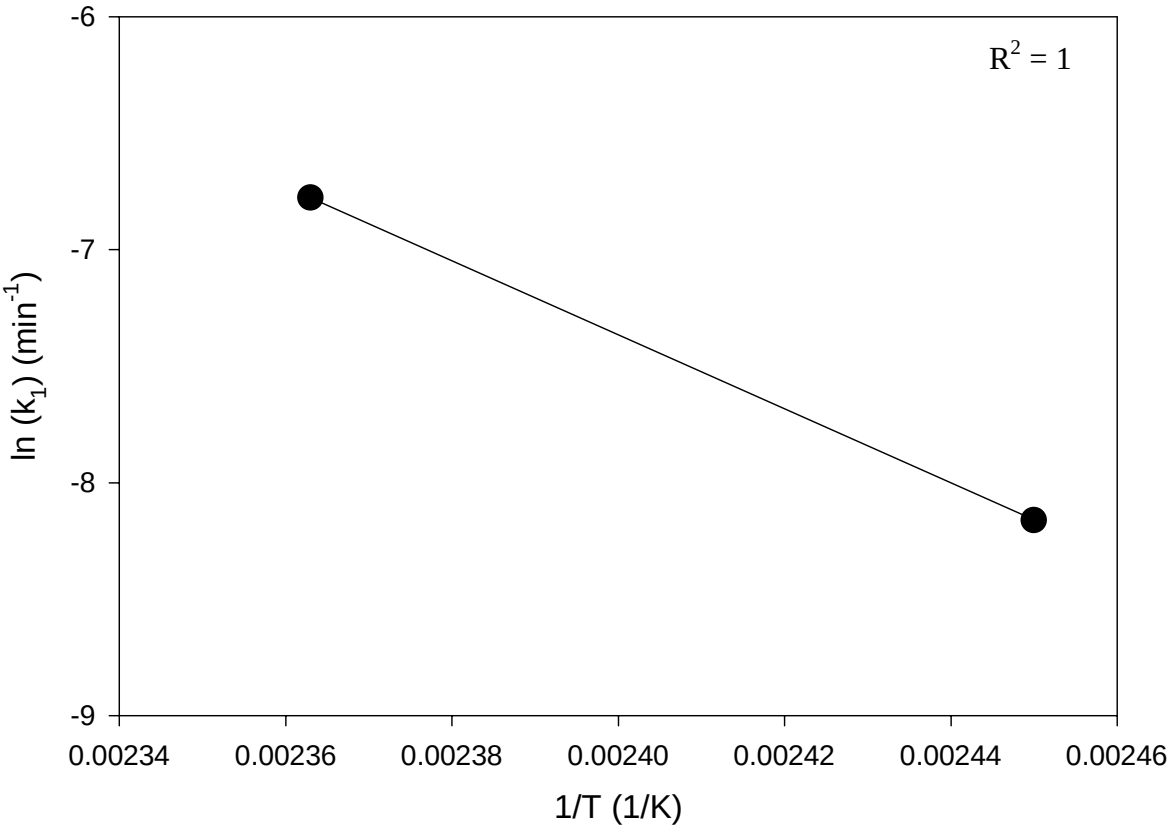

Figure 3.7: Plot of ln(k_1) vs. 1/T for temepratures between 135°C and 150°C for Fiberite 954-3 resin.

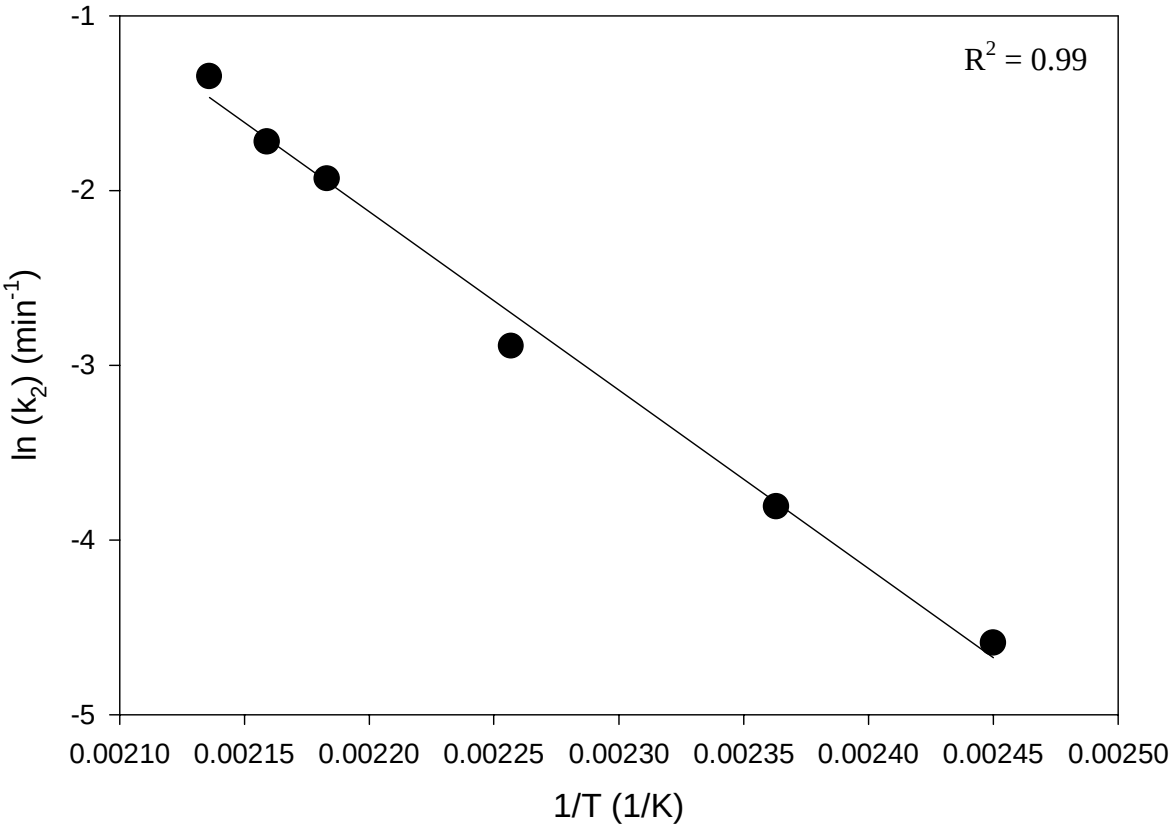

Figure 3.8: Plot of ln(k_2) vs. 1/T for Fiberite 954-3 resin.

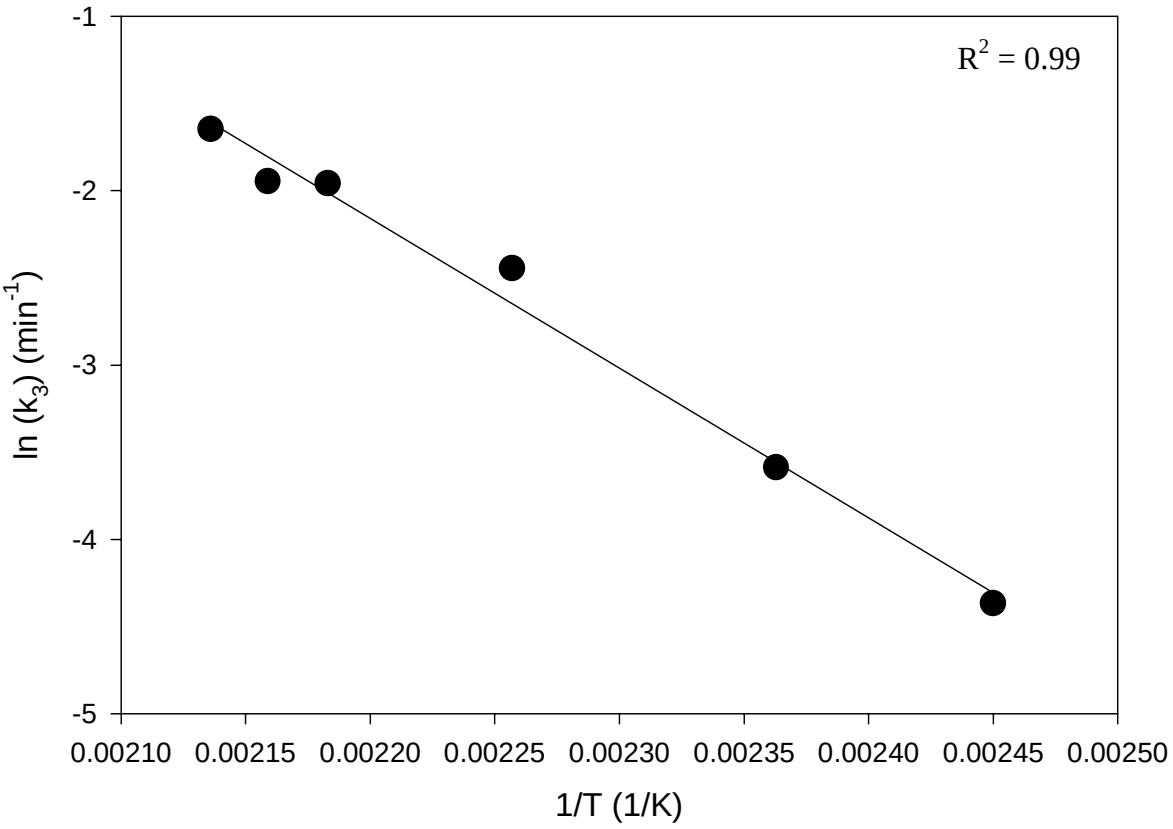

Figure 3.9: Plot of ln(k_3) vs. 1/T for Fiberite 954-3 resin.

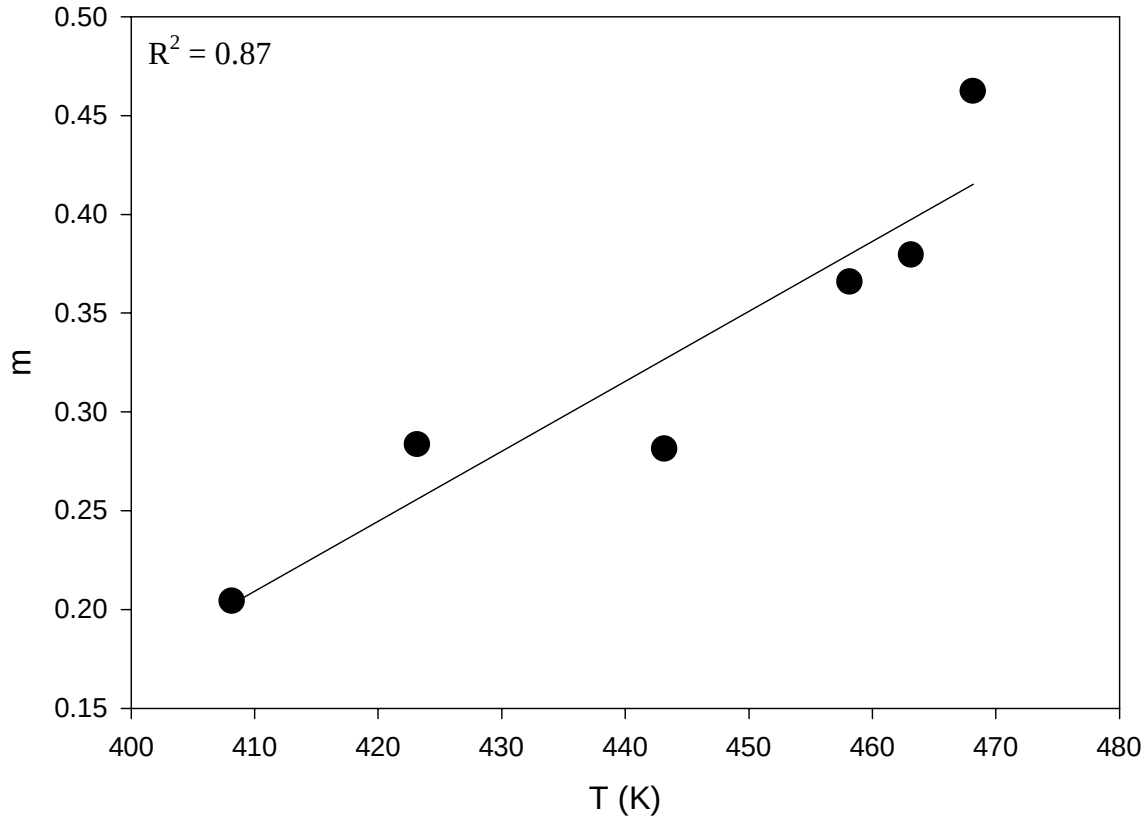

Figure 3.10: Kinetic exponent, m, as a function of temperature for Fiberite 954-3 resin.

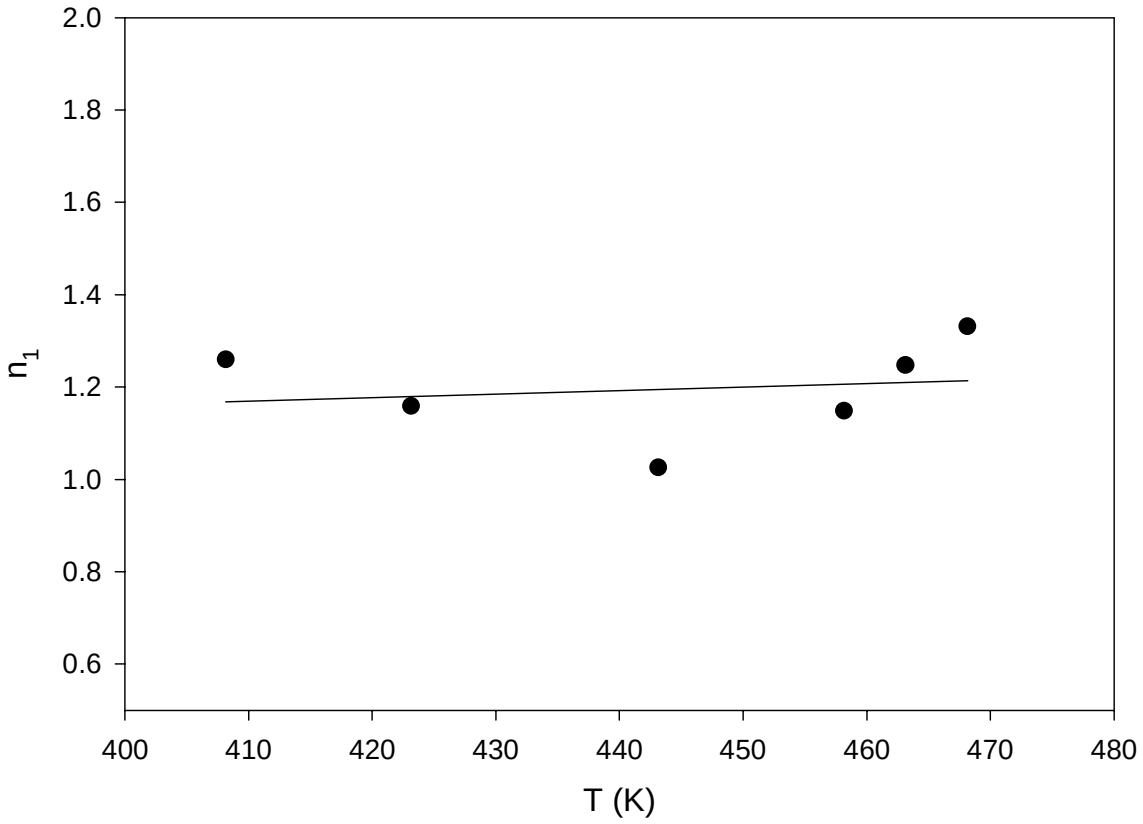

Figure 3.11: Kinetic exponent, n_1, as a function of temperature for Fiberite 954-3 resin.

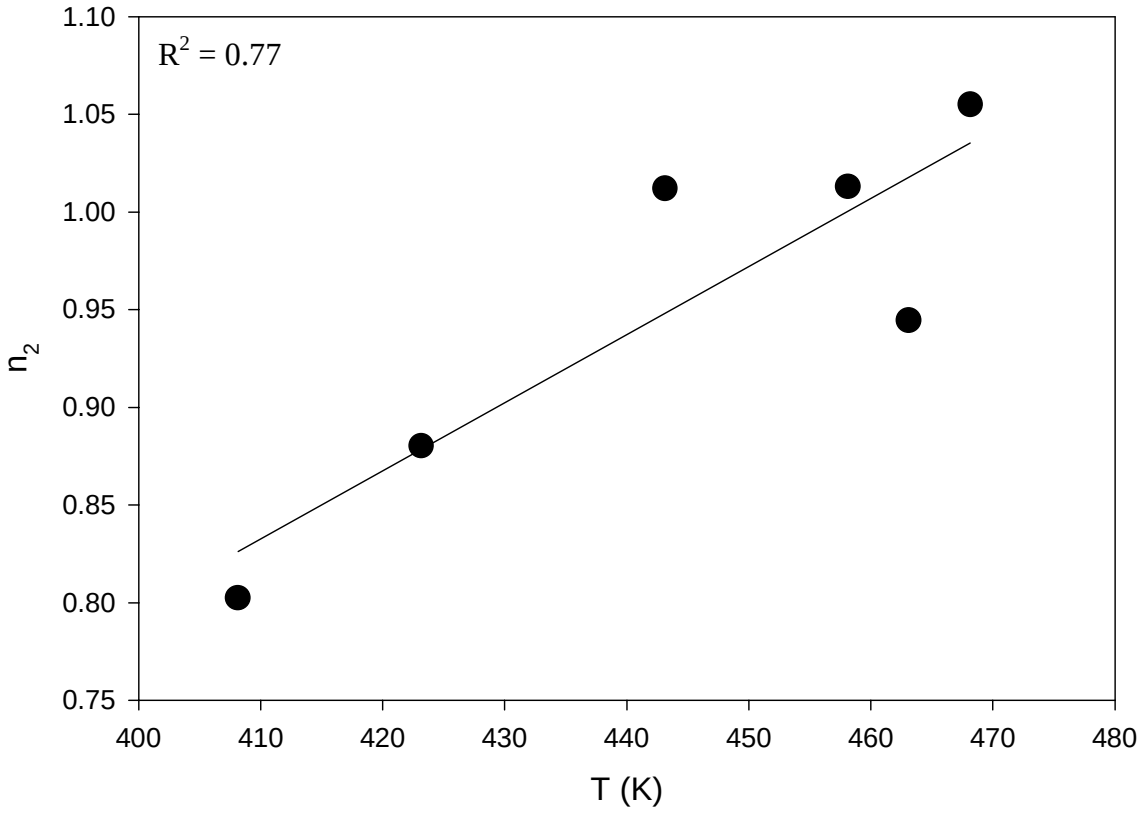

Figure 3.12: Kinetic exponent, n_2, as a function of temperature for Fiberite 954-3 resin.

The peak degree of cure, α_p, was also plotted as a function of temperature in Figure 3.13. The equation governing the fit to the α_p data is as follows

$$\alpha_p = 4.0 \times 10^{-3} (T) - 0.93 \qquad (3.11)$$

With the values of k_1, k_2, k_3, m, n_1, n_2 and α_p as functions of temperature an overall cure-kinetics model was determined. The temperatures used in the model were 195, 190, 185, 170, 150, and 135°C. Comparisons between the model predictions and data are shown in Figures 3.14 - 3.19. The 170°C model prediction slightly overpredicts the experimental data but the overall trend is very similar. From these figures, it can be seen that 954-3 cyanate ester resin never isothermally cures 100%. For this reason, a post-cure of about 220°C for one hour is recommended [11].

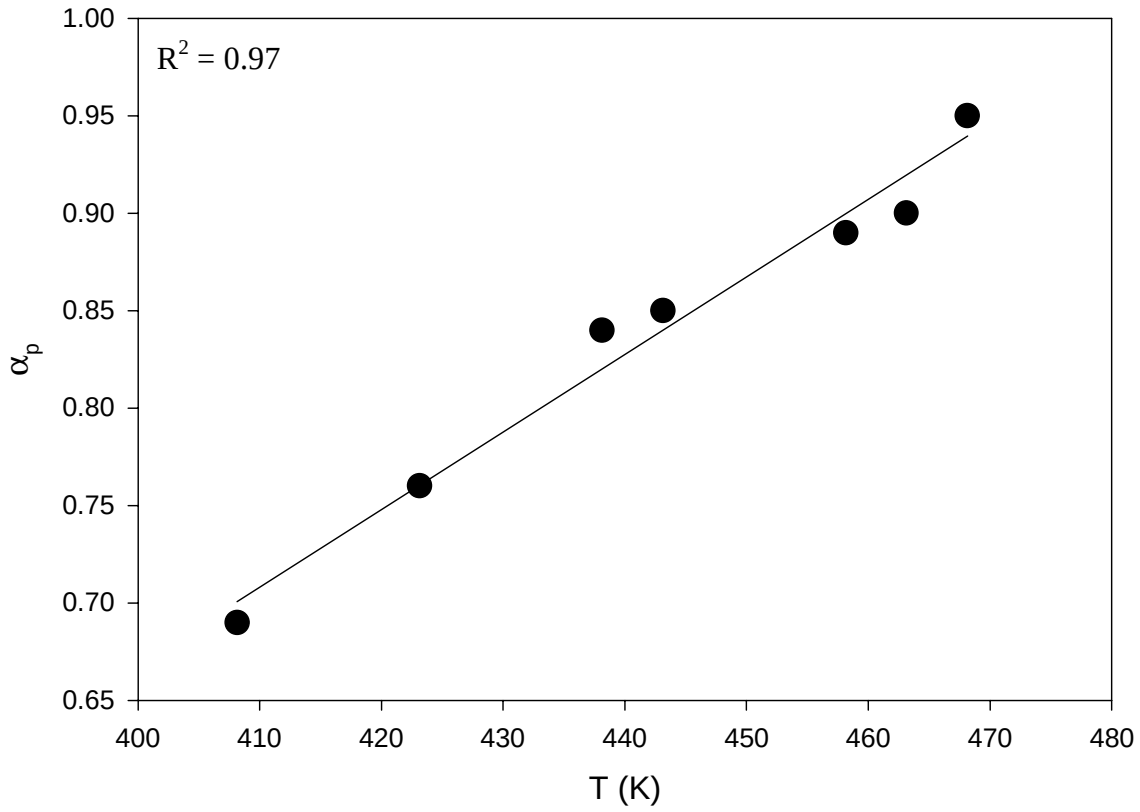

Figure 3.13: Plot of peak degree of cure vs. temperature for Fiberite 954-3 resin.

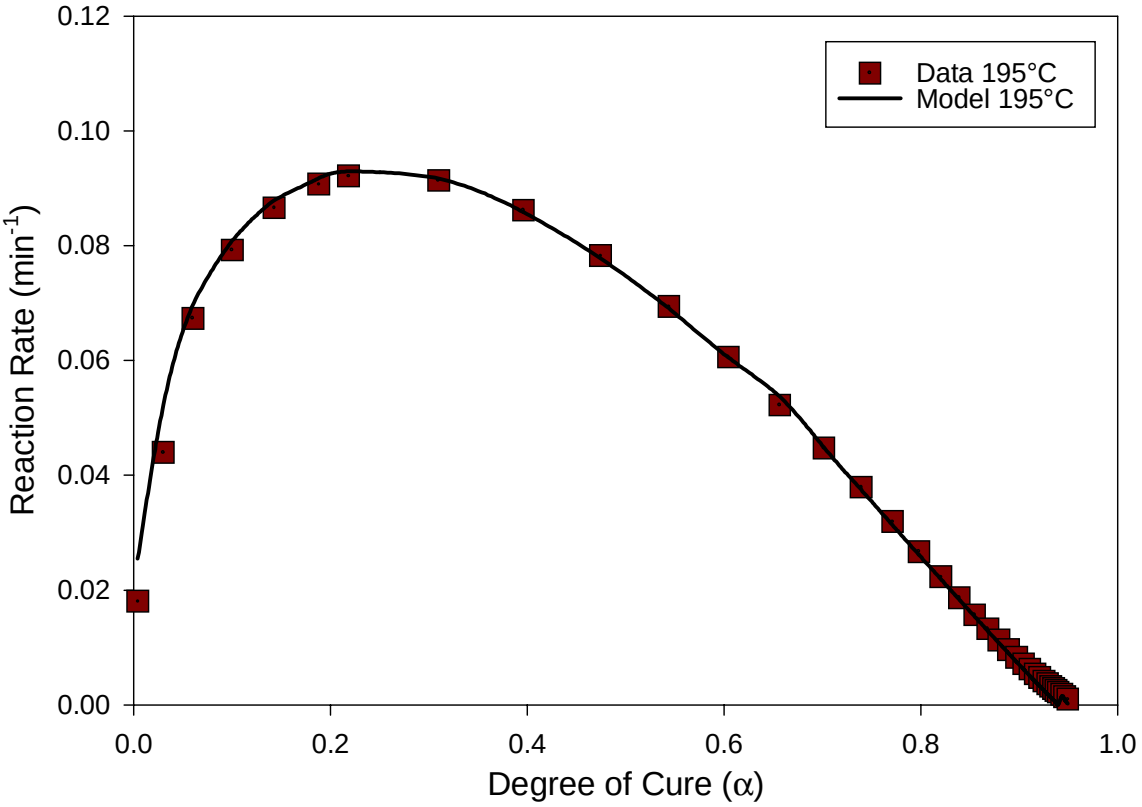

Figure 3.14: Comparison between experimental and model values for reaction rate as a function of degree of cure for 195°C.

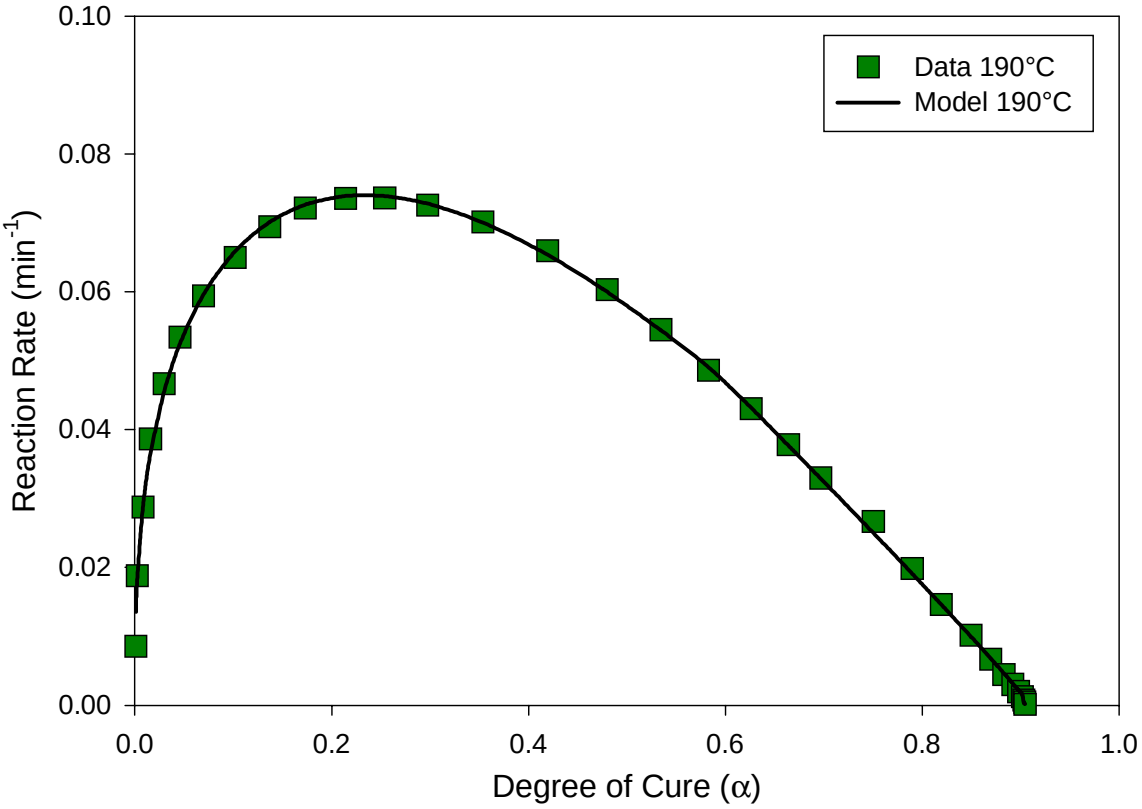

Figure 3.15: Comparison between experimental and model values for reaction rate as a function of degree of cure for 190°C.

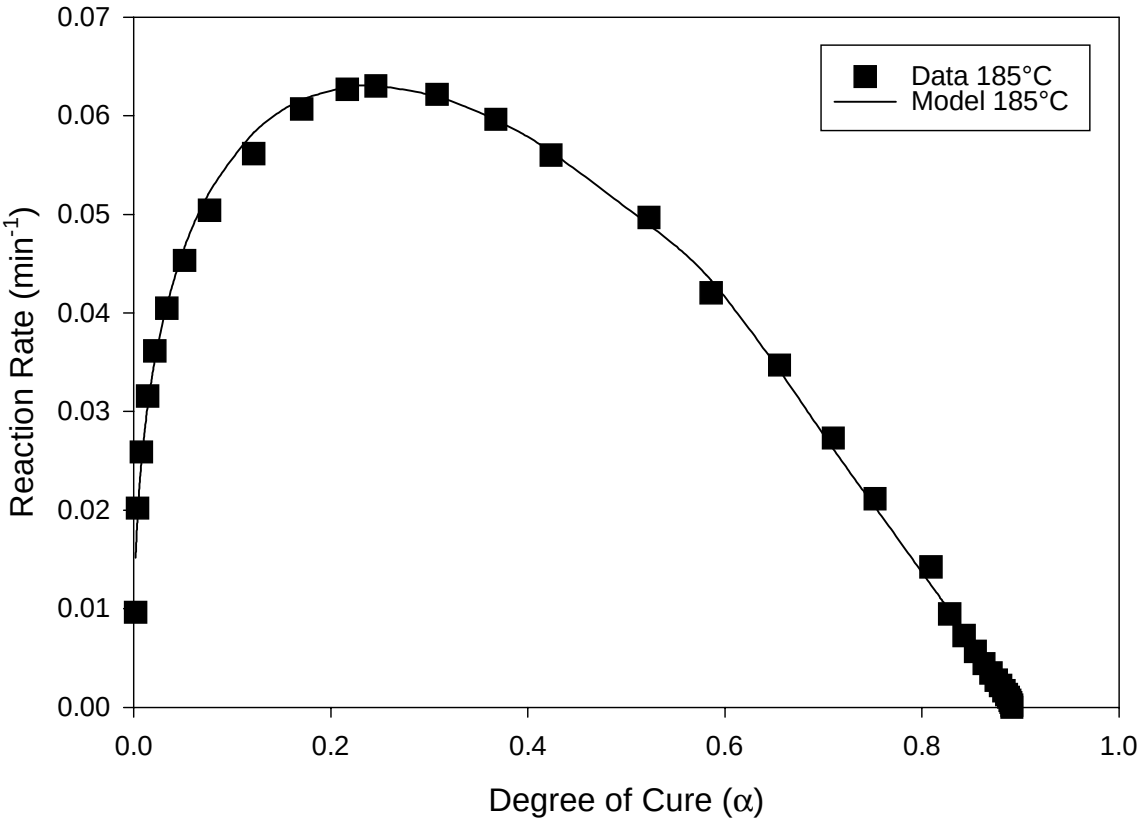

Figure 3.16: Comparison between experimental and model values for reaction rate as a function of degree of cure for 185°C.

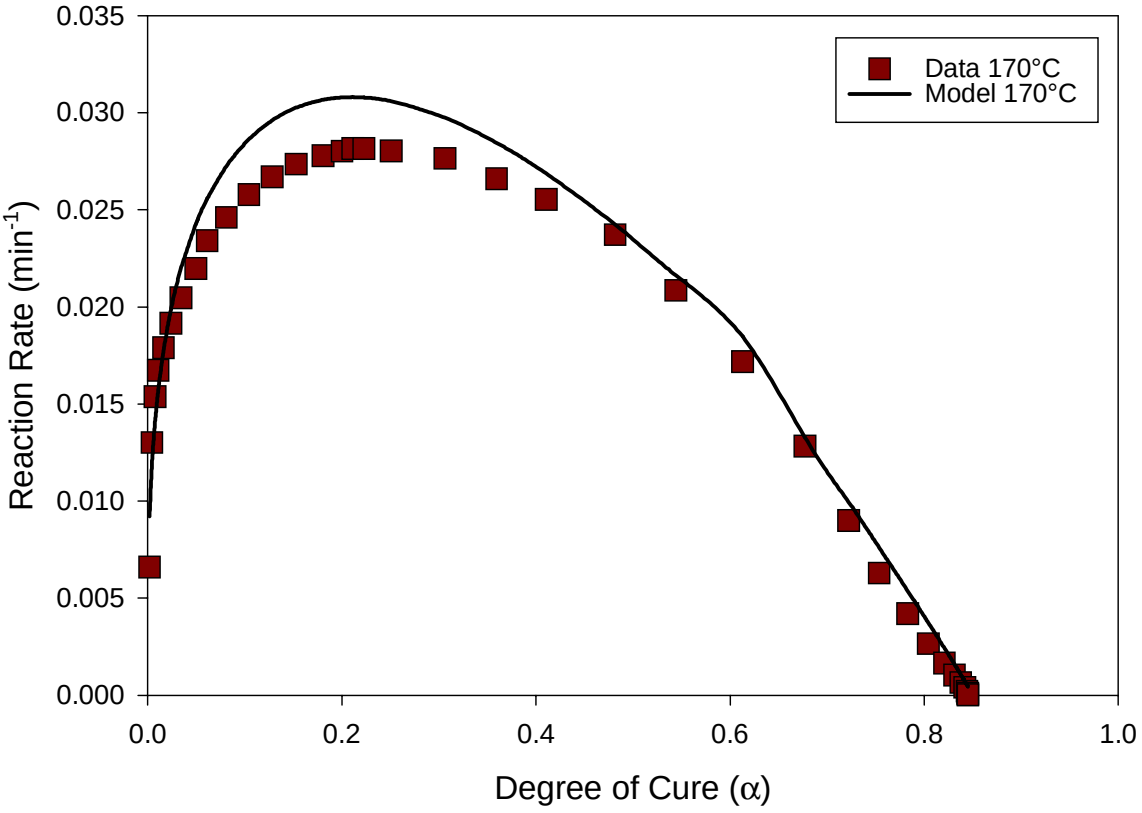

Figure 3.17: Comparison between experimental and model values for reaction rate as a function of degree of cure for 170°C.

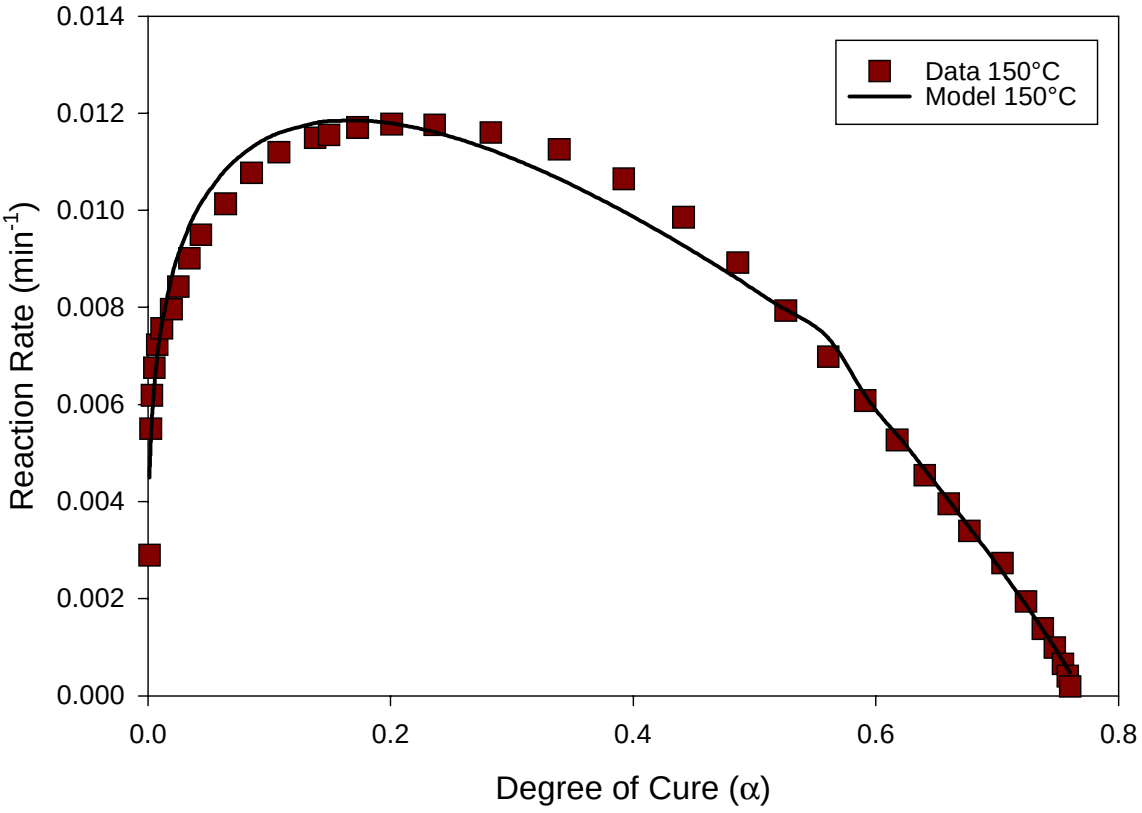

Figure 3.18: Comparison between experimental and model values for reaction rate as a function of degree of cure for 150°C.

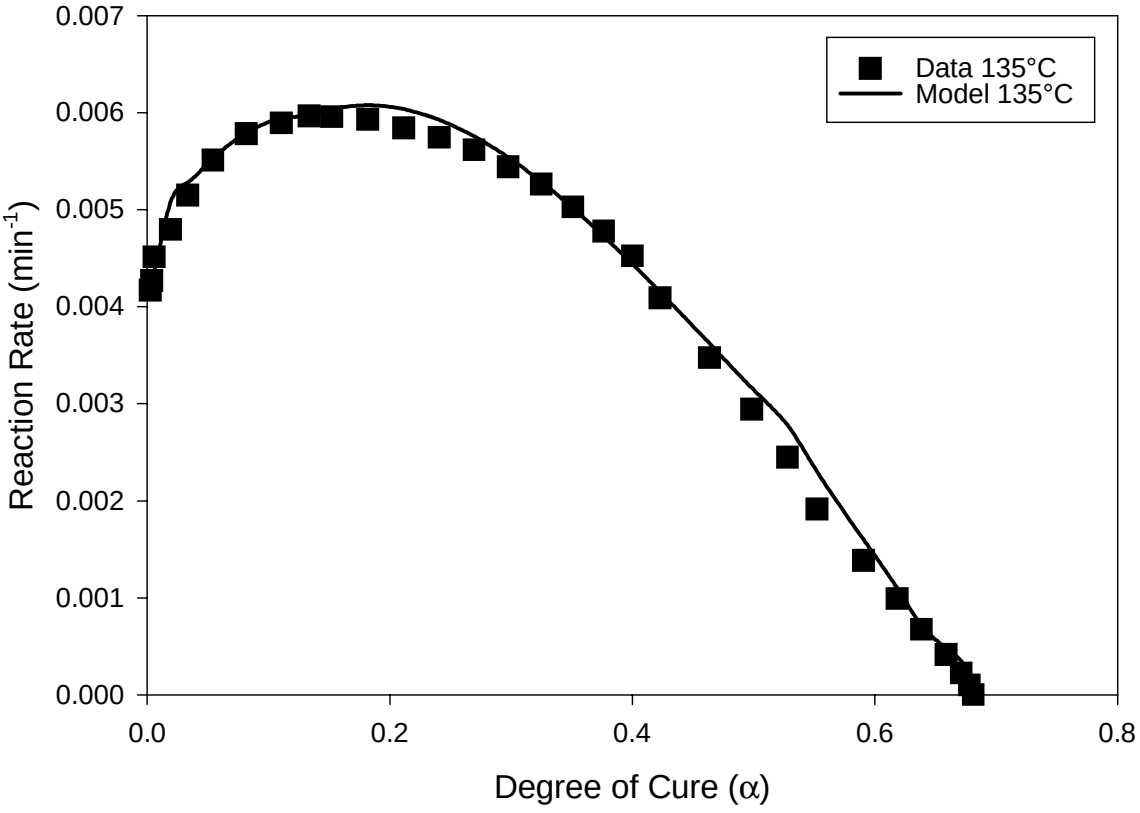

Figure 3.19: Comparison between experimental and model values for reaction rate as a function of degree of cure for 135°C.

3.3.2. 954-2A TOUGHENED CYANATE ESTER RESIN

The series of dynamic scans performed on 954-2a consisted of heating rates of 10, 7.5, 5, 4, and 2°C/min. The total heat of reaction, H_T, was determined to be 383 ± 14 J/g. Table 3.3 contains the five dynamic scans and their heats of reaction.

Table 3.3 - Heating rates and their respective heats of reaction for 954-2a.

Heating rate (°C/minute)	H_r (J/g)
10.0	391.4
7.5	395.0
5.0	392.6
4.0	370.9
2.0	364.1

From the dynamic scans, the isothermal scanning range was determined to be between 120°C and 180°C.

The isothermal DSC scans at 120, 130, 140, 150, 160, 170, and 180°C were used to determine the rate constants and kinetic exponents in the mathematical model described in Section 3.2. The wide range in temperatures required a separate fit to the kinetics data between 160 and 180°C and the kinetics data between 120 and 160°C.

3.3.2.1 HIGH TEMPERATURE MODEL

In the high temperature region (160 - 180°C), a linear least squares fit was used on the $\ln(k_i)$ vs. 1/T curve and the following equations were the result.

$$k_1 = \exp(-9.9 \times 10^3 (1/T) + 0.20)$$

$$k_2 = \exp(-1.3 \times 10^4 (1/T) + 29) \qquad (3.12)$$

$$k_3 = \exp(-1.1 \times 10^4 (1/T) + 22)$$

These plots are shown in Figures 3.20 - 3.22. Table 3.4 shows the pre-exponential constants, A_i, and the activation energies, E_i, for the high temperature region.

Table 3.4 - The pre-exponential constants (A_i) and the activation energies (E_i) for 954-2a - high temperature region.

	A_i (1/min)	E_i (J/mole)
k_1	1.2	8.2×10^4
k_2	3.2×10^{12}	1.1×10^5
k_3	3.8×10^9	9.0×10^4

Values of m and n_i were plotted against temperature and the following equations resulted,

$$m = 0.63 \text{ (average)}$$

$$n_1 = 0.02 (T) - 4.6 \qquad (3.13)$$

$$n_2 = 0.03 (T) - 9.4$$

where T is in Kelvin. Plots detailing these relationships are shown in Figures 3.23 -3.25.

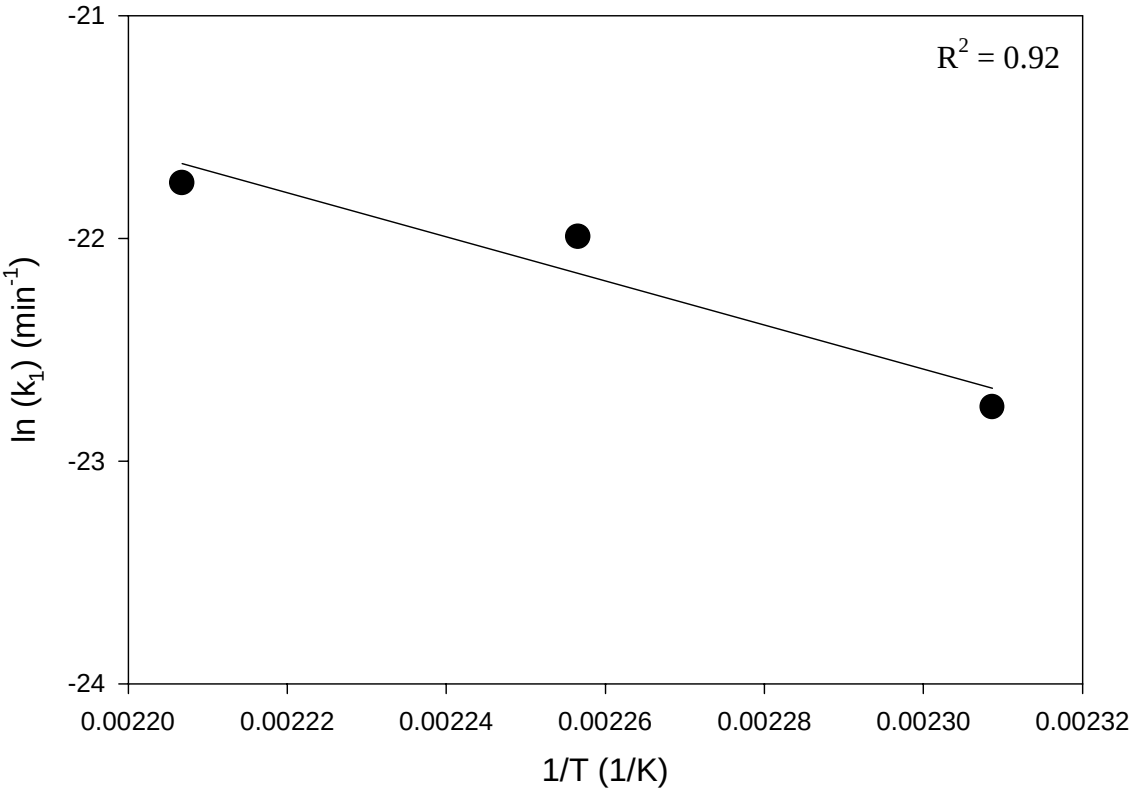

Figure 3.20: Plot of ln (k_1) vs. 1/T for temperatures between 160 and 180°C for Fiberite 954-2a resin.

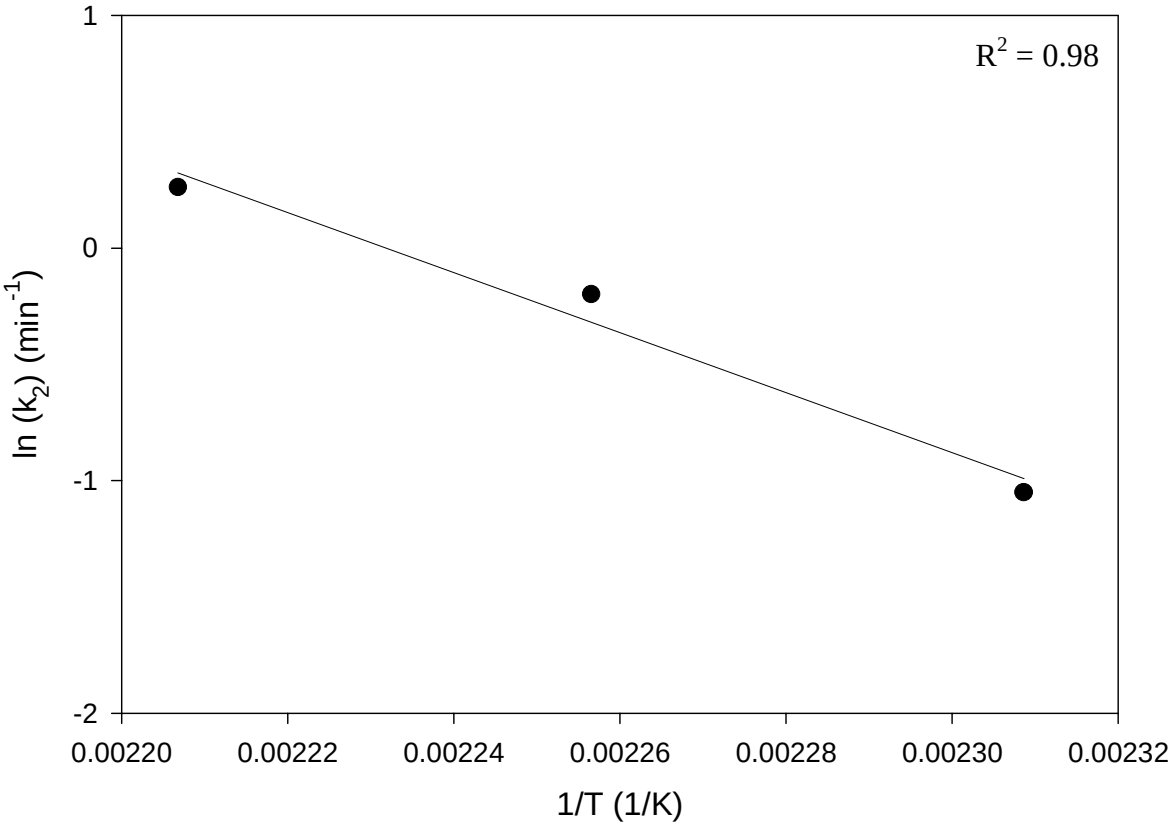

Figure 3.21: Plot of ln (k_2) vs. 1/T for temperatures between 160 and 180°C for Fiberite 954-2a resin.

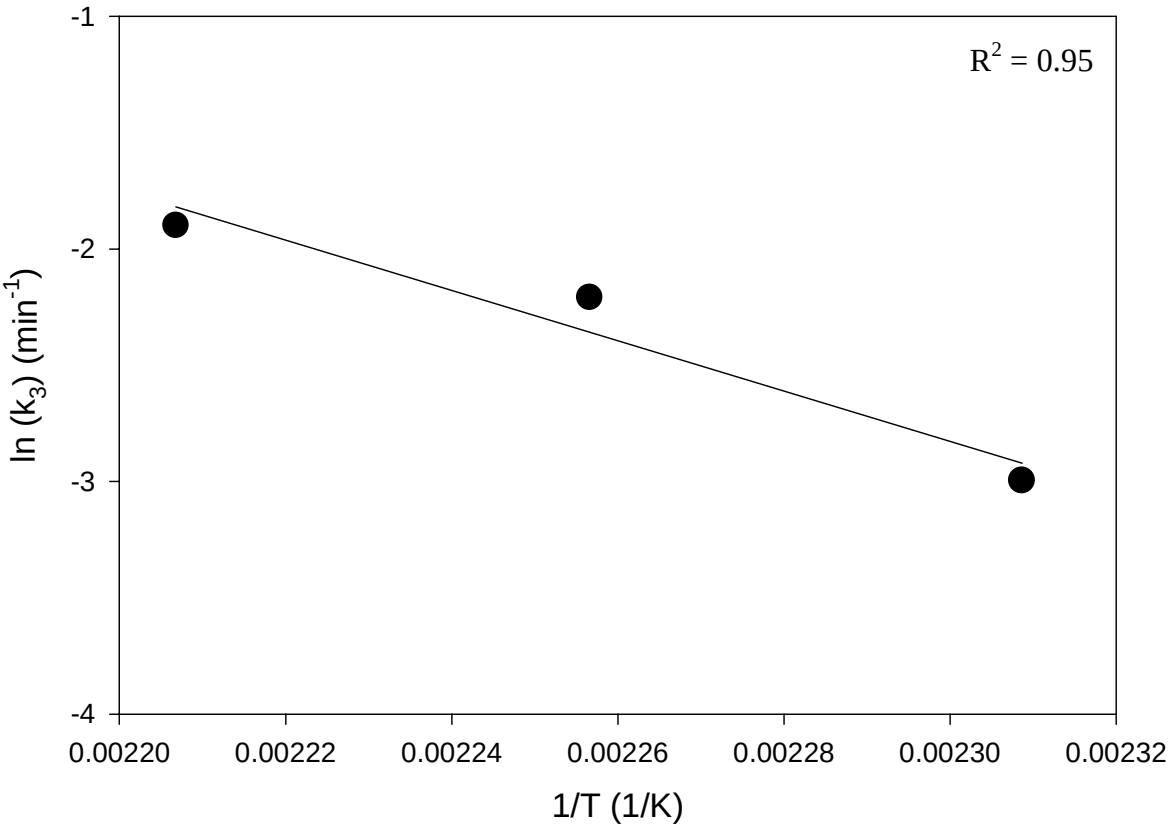

Figure 3.22: Plot of ln (k_3) vs. 1/T for temperatures between 160 and 180°C for Fiberite 954-2a resin.

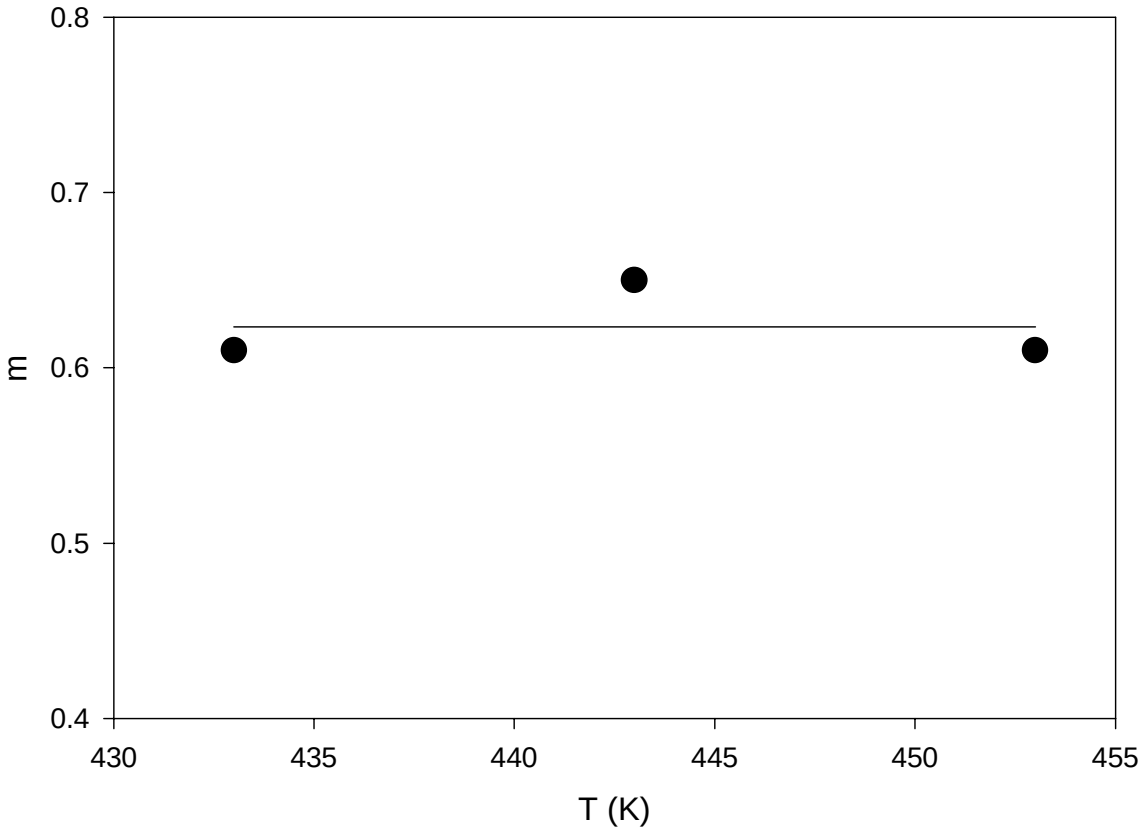

Figure 3.23: Kinetic exponent, m, as a function of temperature between 160 and 180°C for Fiberite 954-2a resin.

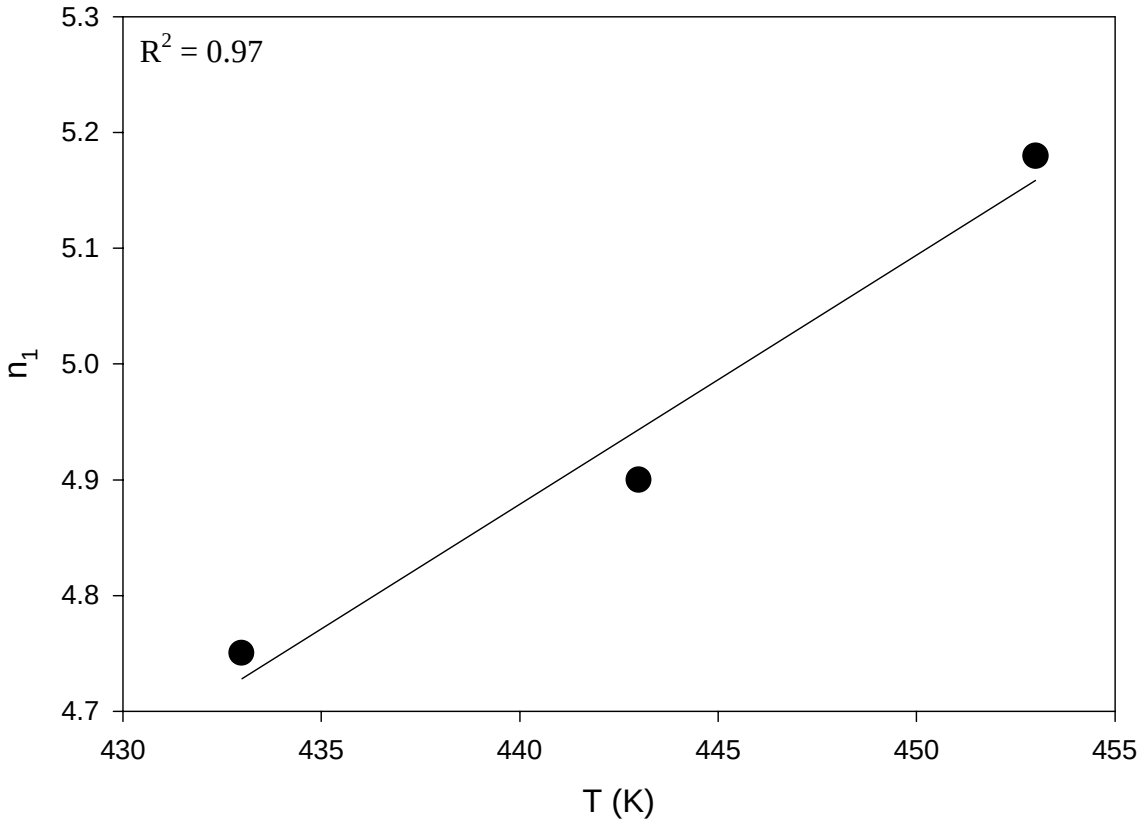

Figure 3.24: Kinetic exponent, n_1, as a function of temperature between 160 and 180°C for Fiberite 954-2a resin.

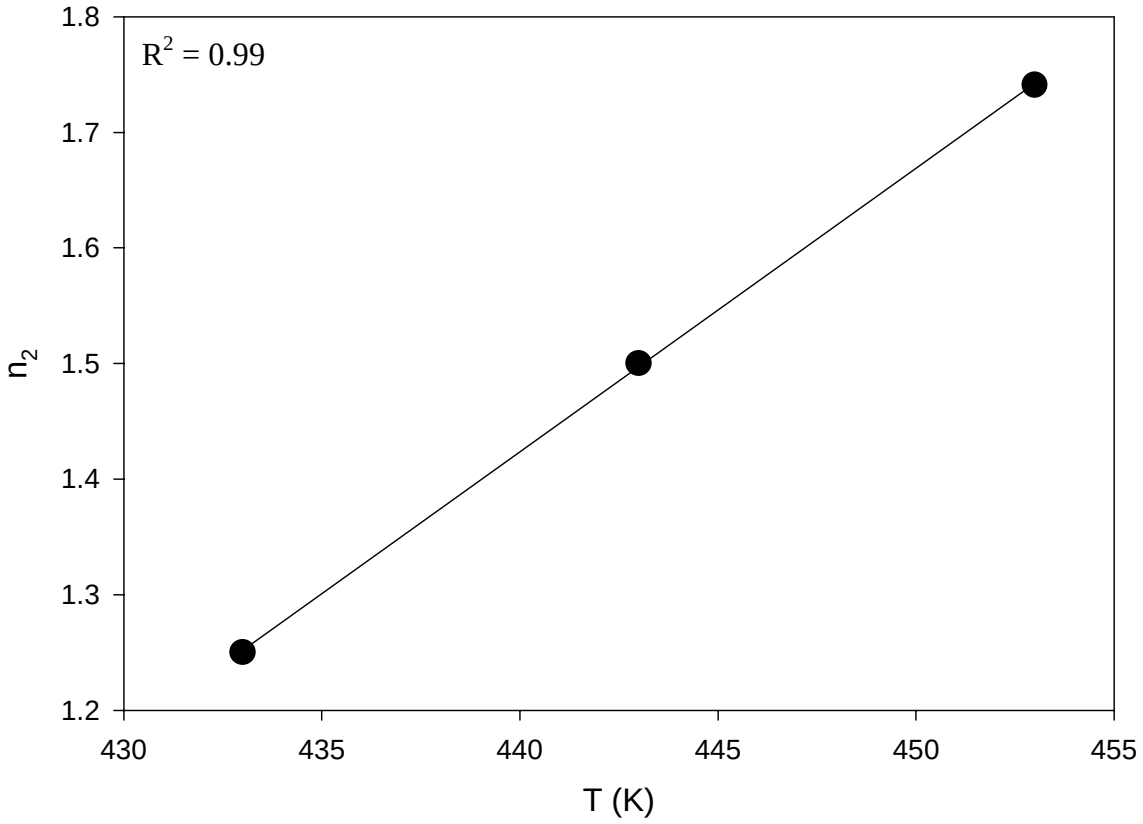

Figure 3.25: Kinetic exponent, n_2, as a function of temperature between 160 and 180°C for Fiberite 954-2a resin.

3.3.2.2 LOW TEMPERATURE MODEL

Within our low temperature testing region (120 - 160°C), a linear least squares fit was used to determine the slope and intercept of the Arrhenius plots found in Figures 3.26 - 3.28. The following equations were the result

$$k_1 = \exp\left(-5.2 \times 10^3 \, (1/T) + 7.3\right)$$

$$k_2 = \exp\left(-61 \times 10^3 \, (1/T) + 13\right) \qquad (3.14)$$

$$k_3 = \exp\left(-4.8 \times 10^3 \, (1/T) + 8.0\right)$$

Table 3.5 shows the pre-exponential constants and the activation energies for the low temperature region of 954-2a toughened cyanate ester resin.

Table 3.5 - The pre-exponential constants (A_i) and the activation energies (E_i) for 954-2a - low temperature region.

	A_i (1/min)	E_i (Activation Energy)
k_1	1.5×10^3	4.3×10^4
k_2	3.7×10^5	5.1×10^4
k_3	2.9×10^3	4.0×10^4

Values of m and n_i were plotted against temperature in Figures 3.29 - 3.31 and the following equations were the result.

$$m = -1.5 \times 10^{-2} \, (T) + 6.7$$

$$n_1 = 3.5 \times 10^{-2} \, (T) - 11 \qquad (3.15)$$

$$n_2 = 8.2 \times 10^{-3} \, (T) - 2.4$$

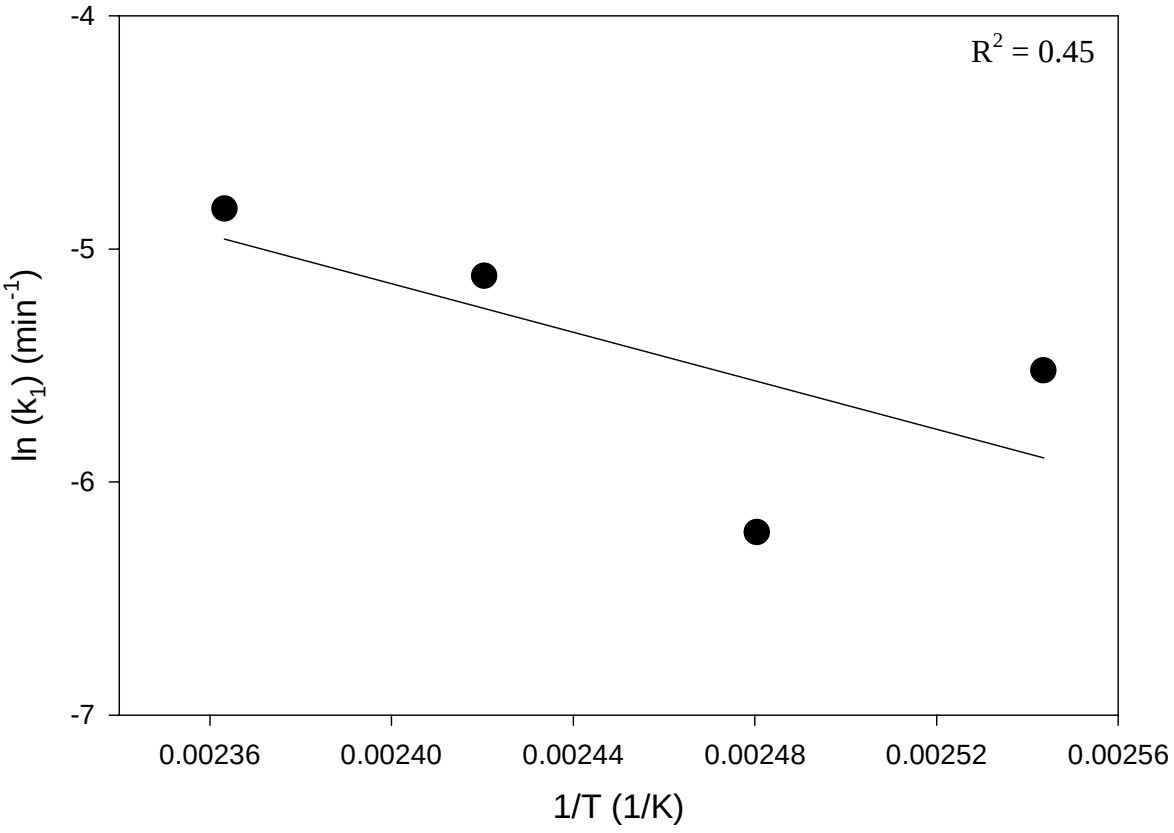

Figure 3.26: Plot of ln (k_1) vs. 1/T for temperatures between 120 and 160°C for Fiberite 954-2a resin.

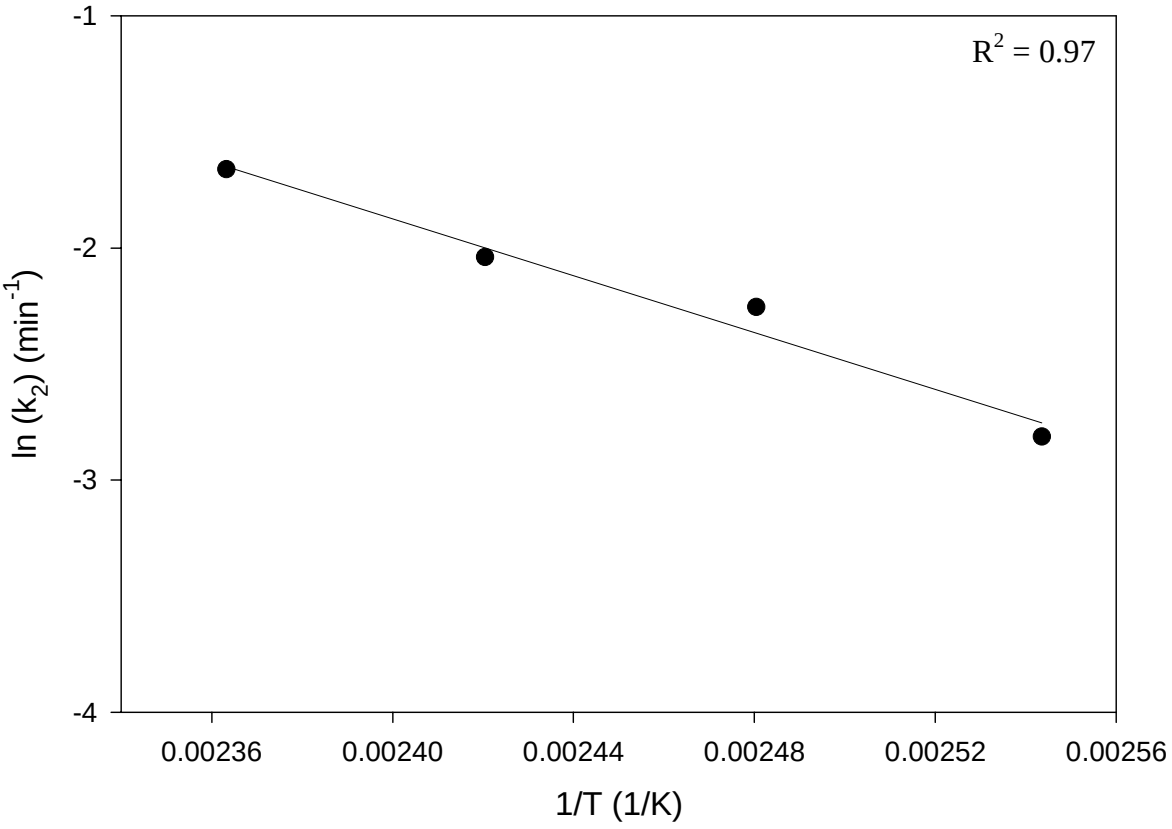

Figure 3.27: Plot of ln (k_2) vs. 1/T for temperatures between 120 and 160°C for Fiberite 954-2a resin.

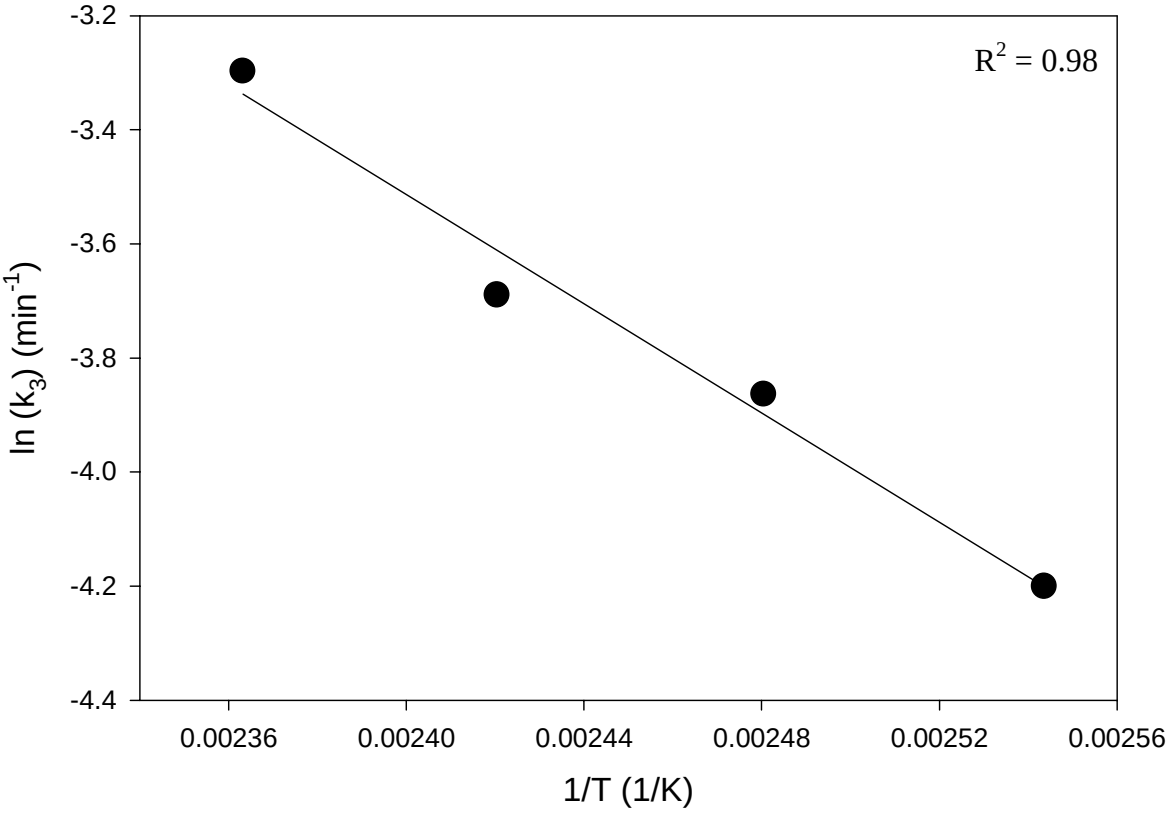

Figure 3.28: Plot of ln (k_3) vs. 1/T for temperatures between 120 and 160°C for Fiberite 954-2a resin.

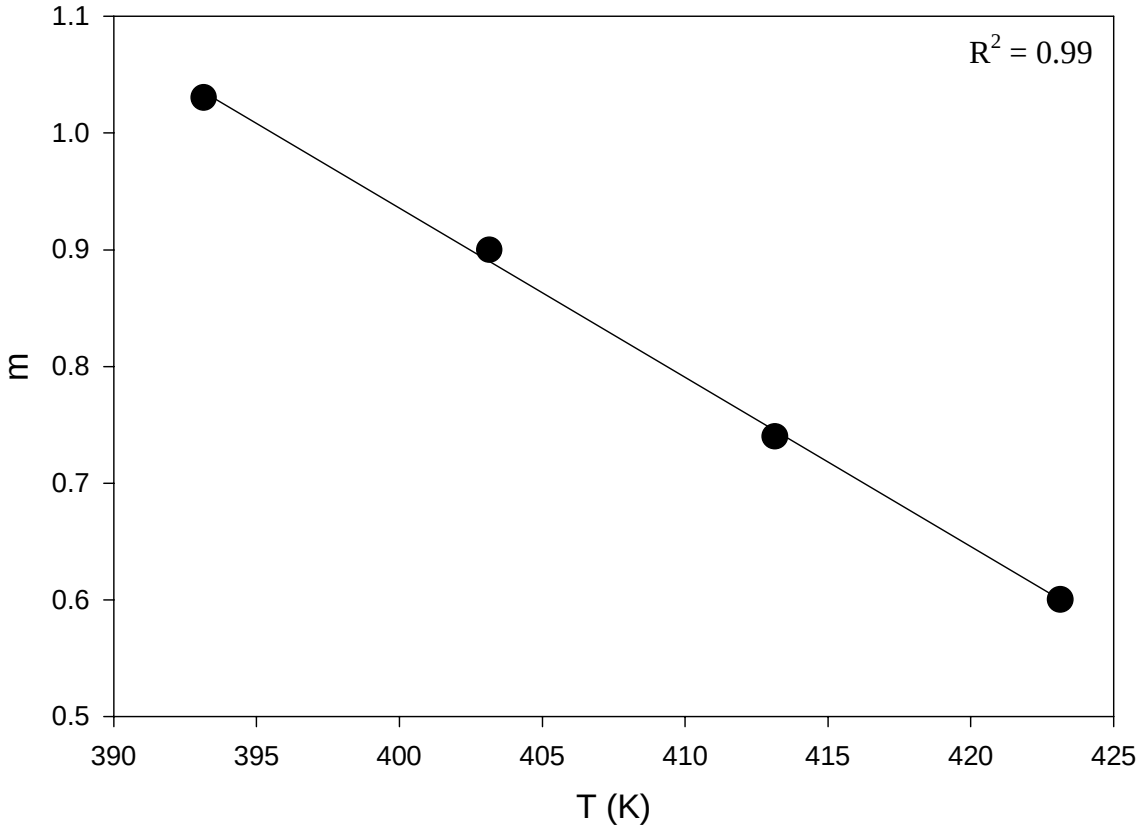

Figure 3.29: Kinetic exponent, m, as a function of temperature between 120 and 160°C for Fiberite 954-2a resin.

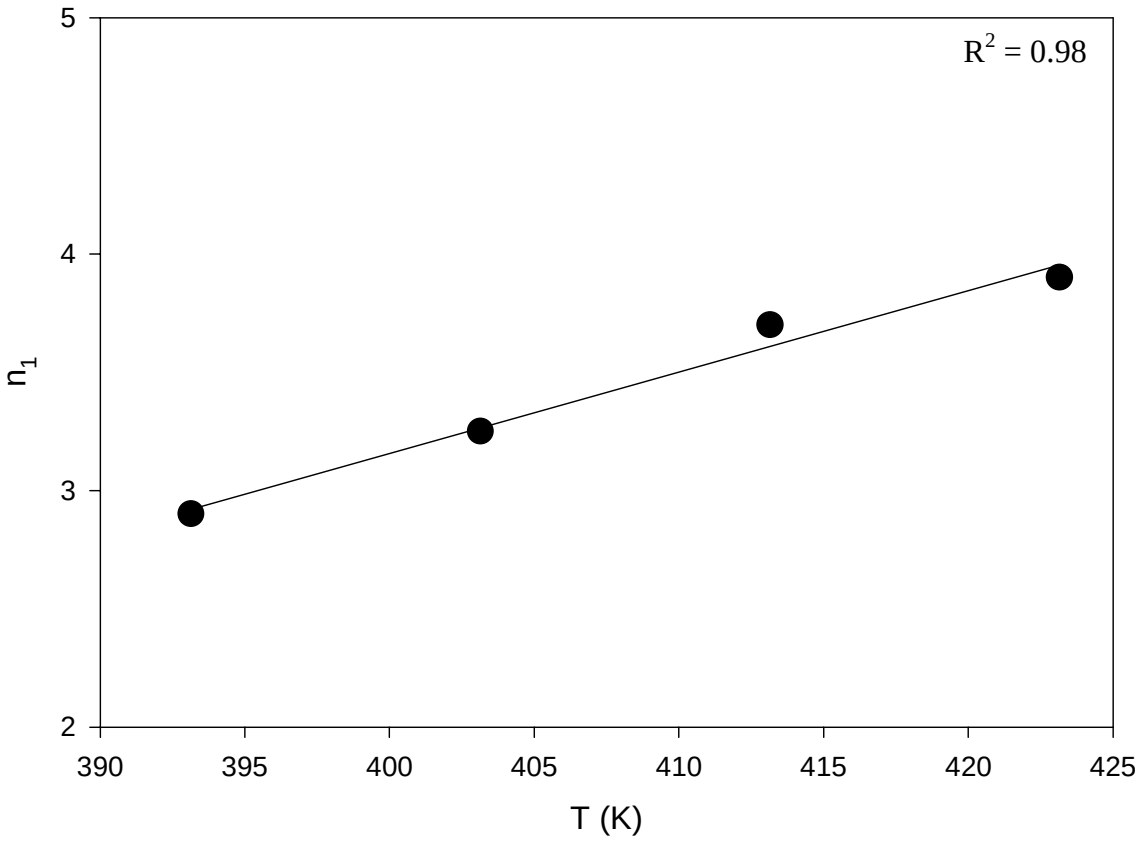

Figure 3.30: Kinetic exponent, n_1, as a function of temperature between 120 and 160°C for Fiberite 954-2a resin.

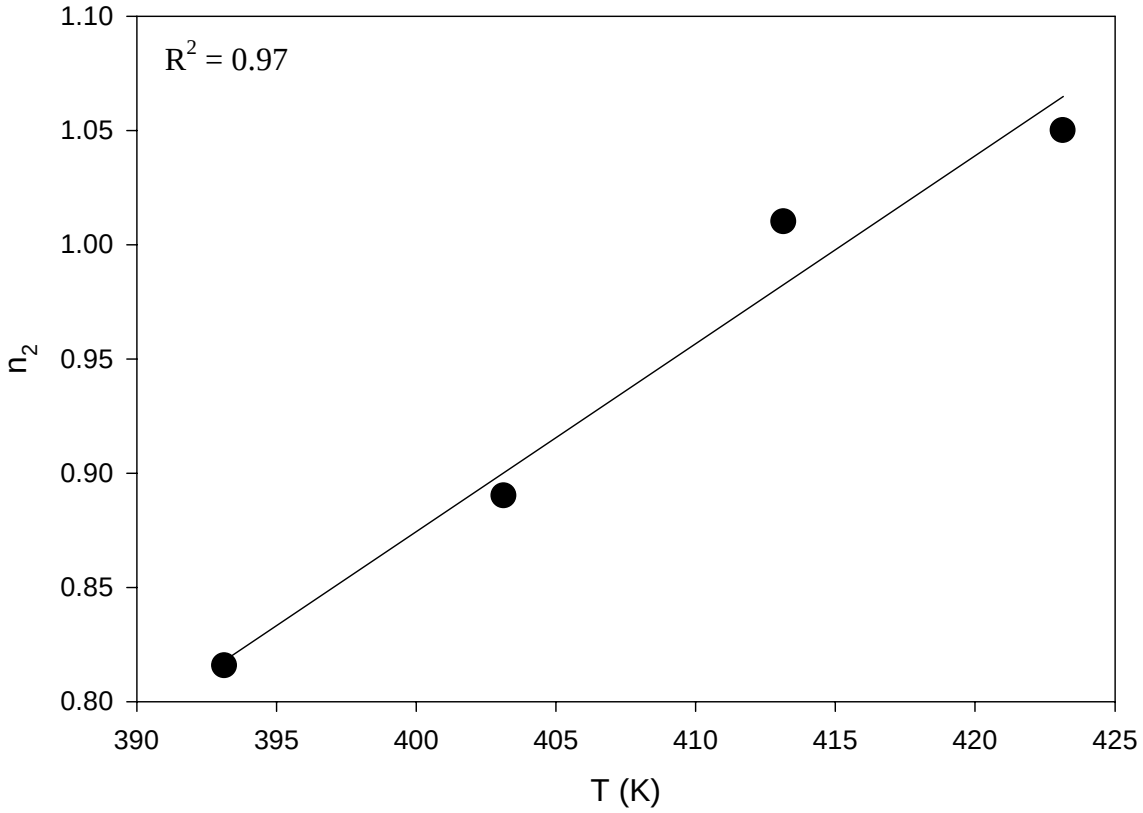

Figure 3.31: Kinetic exponent, n_2, as a function of temperature between 120 and 160°C for Fiberite 954-2a resin.

α_p is plotted a function of temperature in Figure 3.32 and the following equation governs the fit.

$$\alpha_p = 3.3 \times 10^{-3} (T) - 0.57 \qquad (3.16)$$

By determining the Arrhenius constants and the kinetic exponents as functions of temperature in the high and low temperature regions as well as the peak degree of cure (α_p), verification of the model was possible. Figures 3.33 - 3.39 show comparisons between experimental and model values for $d\alpha/dt$ as a function of α. The proposed model proved to be an accurate representation of the experimental data over the entire range of temperatures.

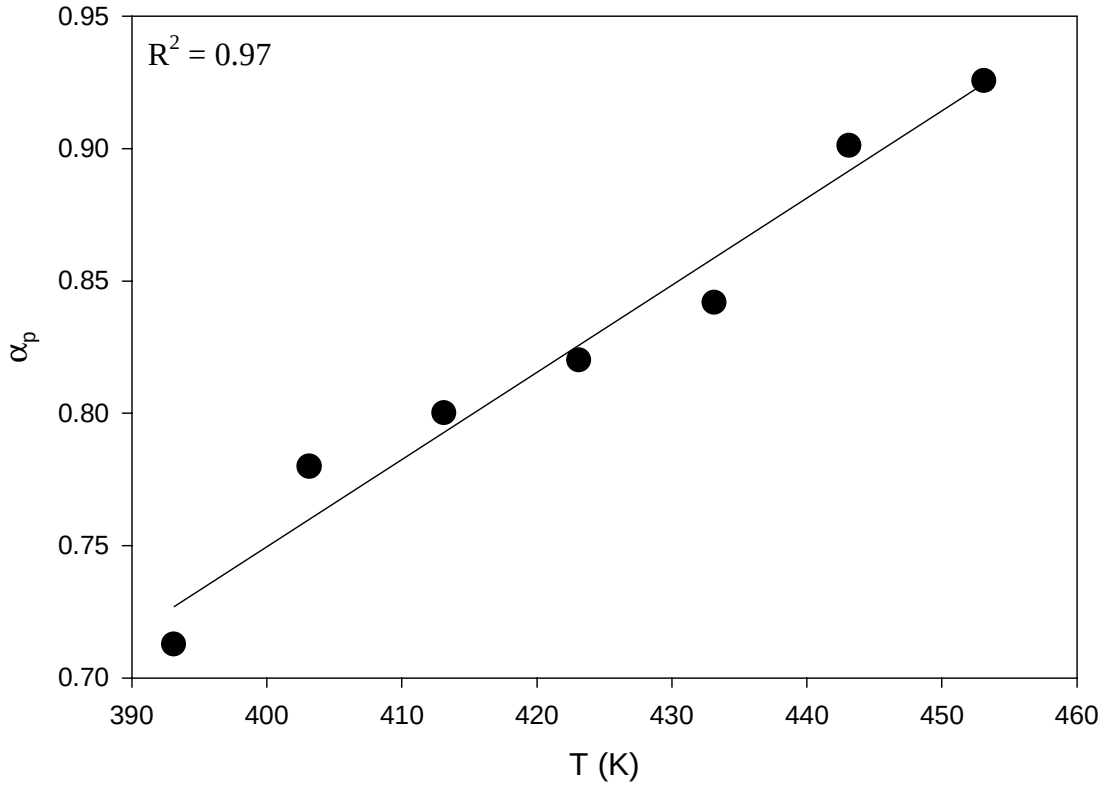

Figure 3.32: Plot of peak degree of cure vs. temperature for Fiberite 954-2a resin.

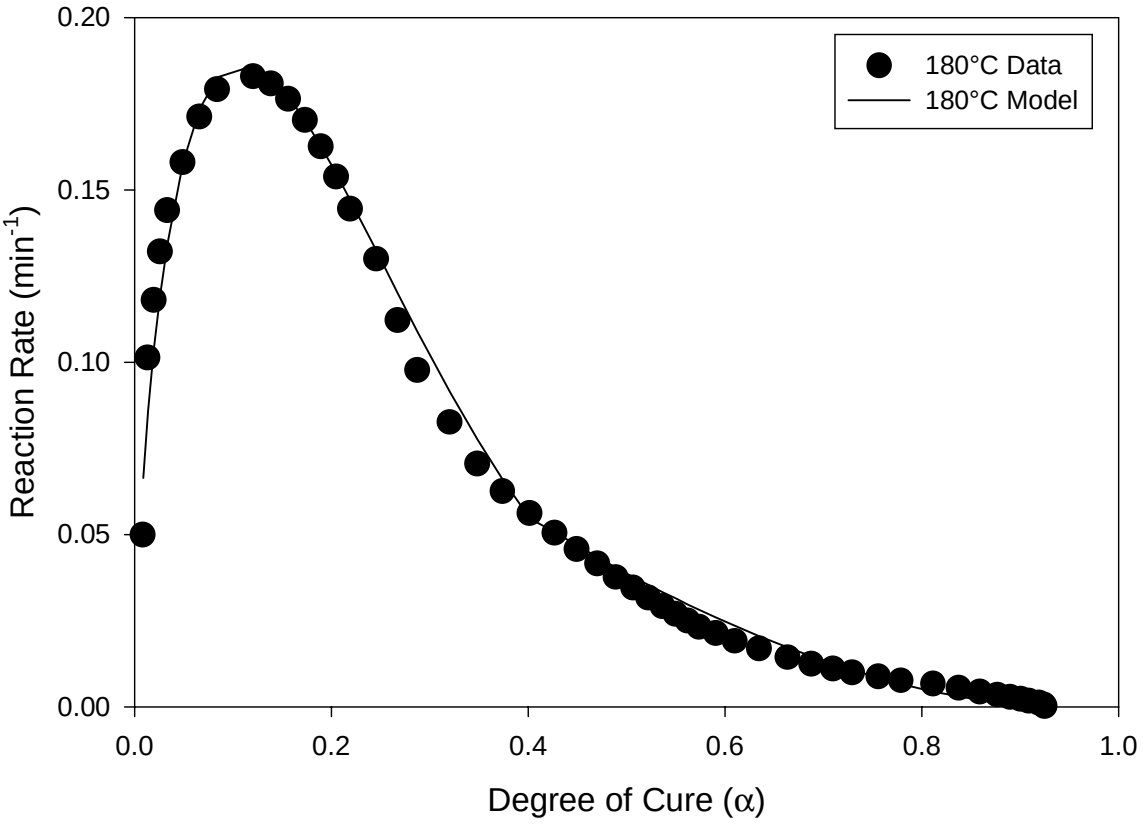

Figure 3.33: Comparison between experimental and model values for reaction rate as a function of degree of cure for 180°C.

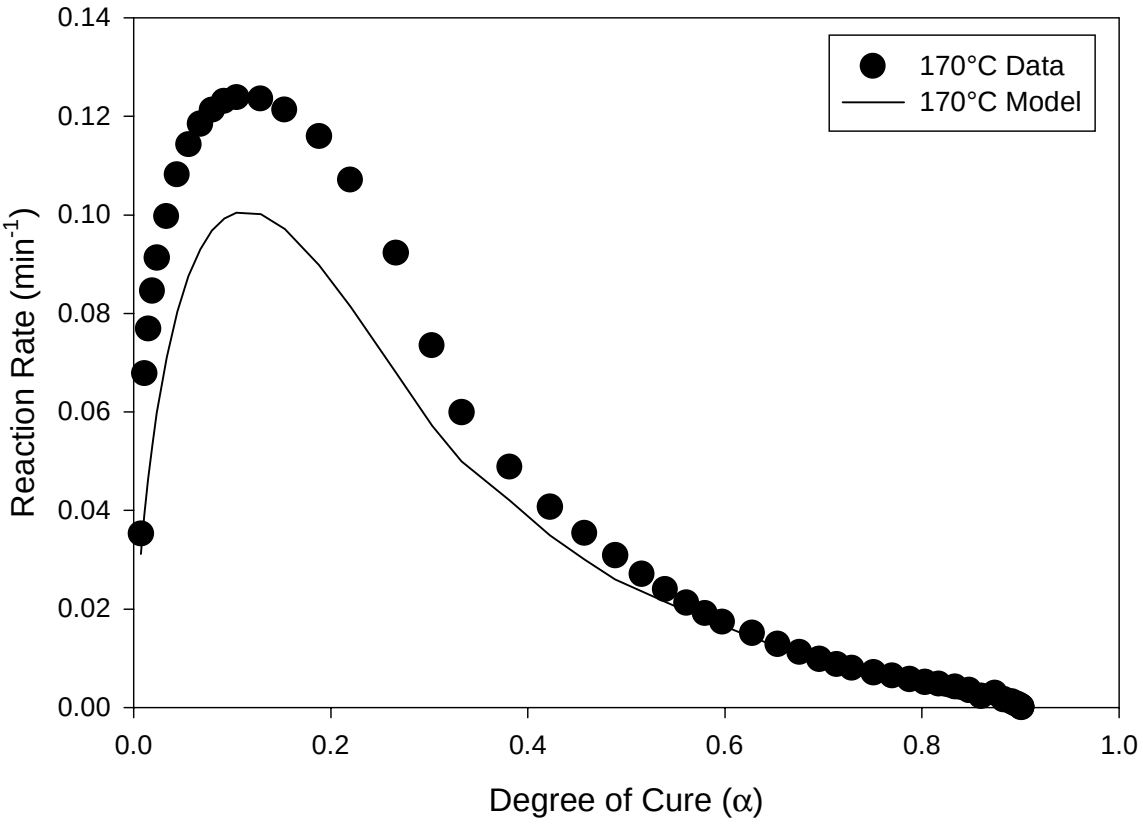

Figure 3.34: Comparison between experimental and model values for reaction rate as a function of degree of cure for 170°C.

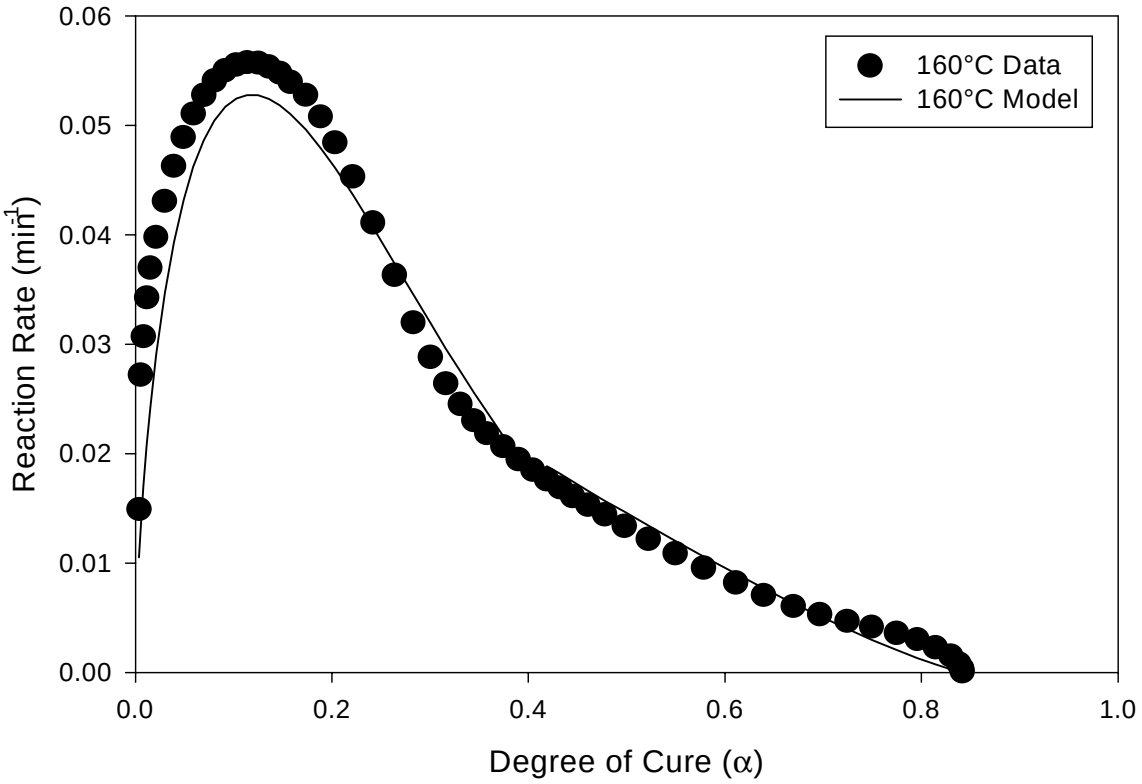

Figure 3.35: Comparison between experimental and model values for reaction rate as a function of degree of cure for 160°C.

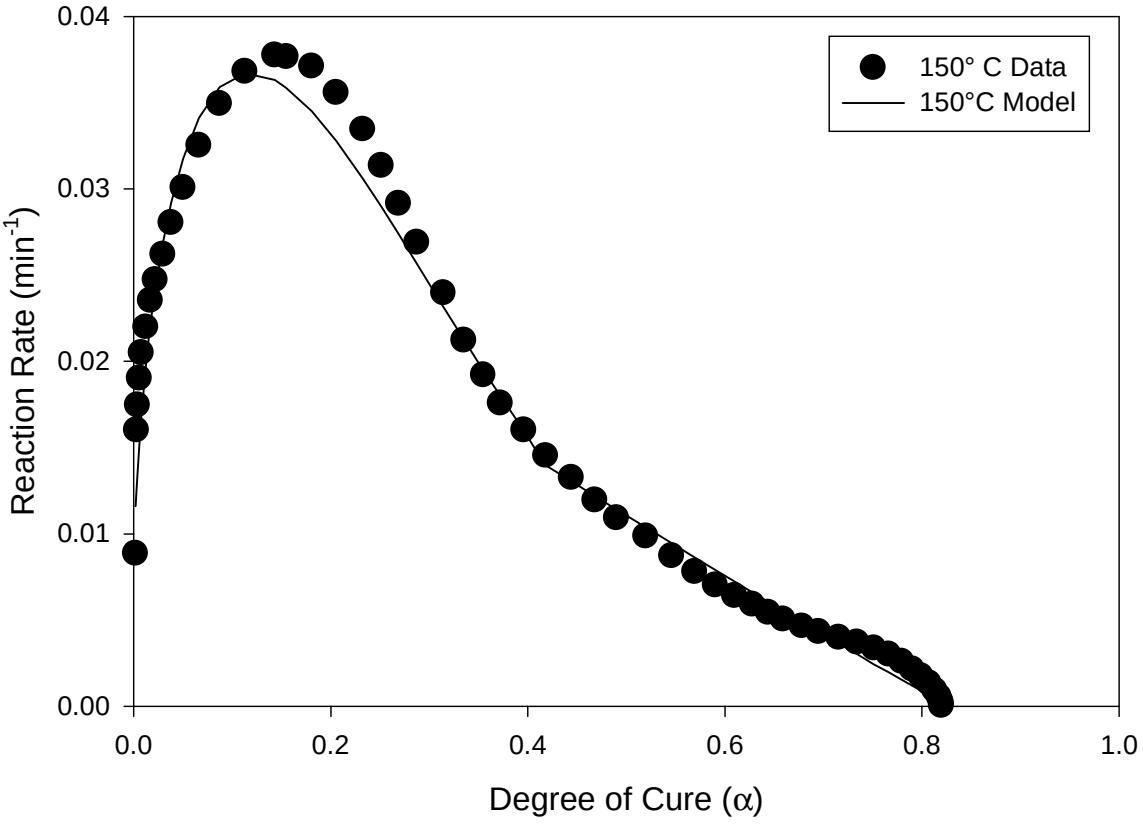

Figure 3.36: Comparison between experimental and model values for reaction rate as a function of degree of cure for 150°C.

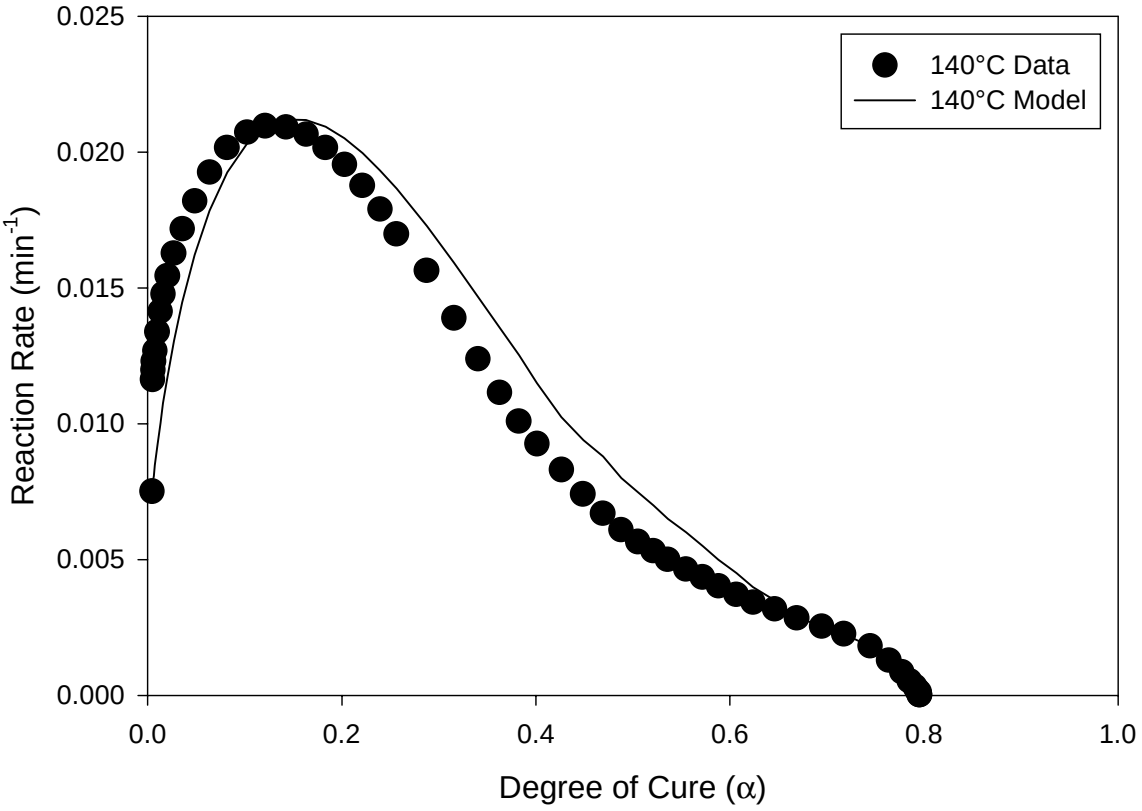

Figure 3.37: Comparison between experimental and model values for reaction rate as a function of degree of cure for 140°C.

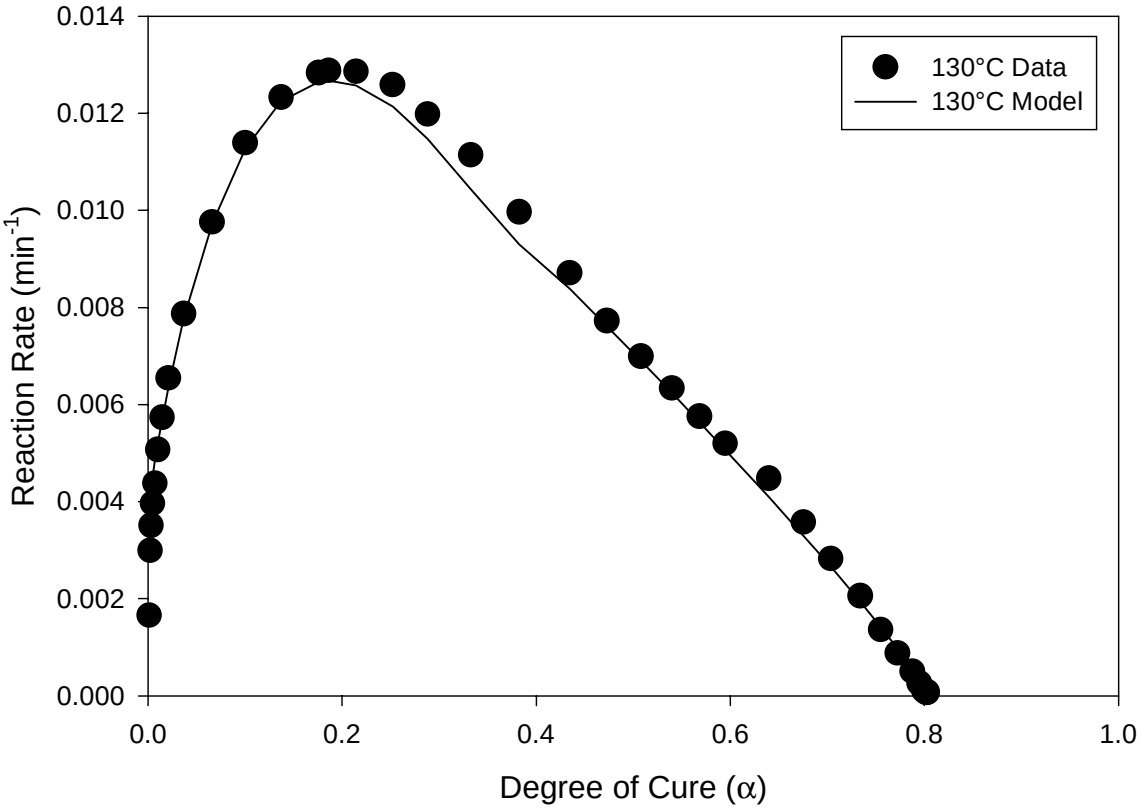

Figure 3.38: Comparison between experimental and model values for reaction rate as a function of degree of cure for 130°C.

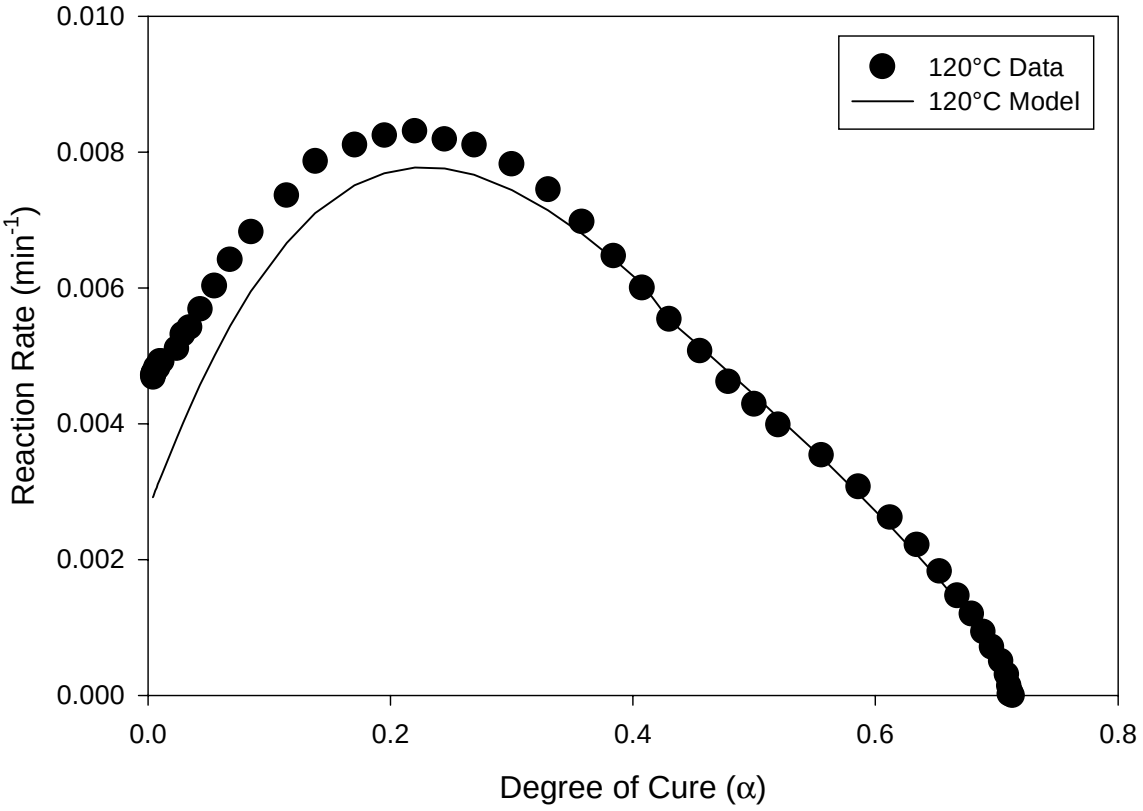

Figure 3.39: Comparison between experimental and model values for reaction rate as a function of degree of cure for 120°C.

CHAPTER 4: VISCOSITY CHARACTERIZATION

4.0 VISCOSITY CHARACTERIZATION

Just as it is critical to have an accurate kinetics model to predict the cure behavior of the resin after infiltration, it is equally important to have a viscosity model to predict the viscosity behavior during infiltration. As the resin infiltrates the preform it continues to flow up to a point. This point, the degree of cure at gel, α_g [20], is characterized by a dramatic increase in viscosity resulting in the end of resin infiltration. In order to determine the time it takes for the resin to reach this point without a trial and error method, a viscosity model was proposed. The viscosity model was set up to determine viscosity as a function of time or degree of cure at a specified temperature. This chapter will cover the details of the viscosity measurements and the rheological models for both cyanate ester resin systems.

4.1. EXPERIMENTAL PROCEDURE

Viscosity measurements were taken on the two resins described earlier, 954-3 and 954-2a. A Brookfield Model DV-III programmable rheometer in conjunction with a Brookfield thermosel and a Brookfield programmable temperature controller were used for the viscosity testing. Two spindles were used in the testing and their pertinent information is presented in Table 4.1.

Table 4.1 - Spindles used in the viscosity testing of two cyanate ester resins [21].

Spindle	Viscosity range (Pa-s)	Shear rate	sample volume (ml)
SC4-21	0.020 - 500	0.93 x rpm	8.0
SC4-27	0.10 - 2,500	0.34 x rpm	10.5

The rheometer measures viscosity as a function of time at a fixed temperature and rpm. The temperatures used for the viscosity testing were the same temperatures used in the DSC testing. By referring to the Fiberite data sheets [11] an approximate viscosity range was determined enabling the selection of the correct spindle. Table 4.1 was then referenced to determine the resin sample size needed for each spindle.

The resin was removed from the freezer, weighed, and then crushed. The 954-2a resin system was degassed for 45 minutes at 70°C. The resin was put into a disposable aluminum tube and inserted into the pre-heated thermosel. The spindle was pre-heated under hot water, dried and attached to the rheometer. Pre-heating raised the spindle temperature closer to that of the heated resin. The spindle was lowered into the thermosel until it was completely covered by the resin. The first few minutes of data acquisition were ignored because the spindle had not yet reached the resin temperature. The invalid data were characterized by a gradual decrease in viscosity eventually reaching a minimum. Data acquisition commenced when this minimum viscosity was reached. The test measured viscosity as a function of time, and continued until a sharp increase in viscosity was noted and a torque of about 80% of maximum was reached. This procedure was followed for both resins at all of the pre-selected temperatures.

Prior to fitting the viscosity data to a model, a conversion from viscosity versus time to viscosity versus degree of cure was required. In order to do this, the DSC data

and rheometry data were analyzed simultaneously at a common temperature. By selecting specific times, viscosity was able to be determined as a function of degree of cure. Once this conversion was completed at several temperatures, model fitting was possible.

4.2. MODEL EQUATIONS

The data were then fit to an empirical chemorheological model proposed by Castro and Macosko [20]. Equation 4.1 shows the form of the model which correlates the resin viscosity to both, temperature and degree of cure,

$$\mu(\alpha, T) = \mu_0 \left(\frac{\alpha_g}{\alpha_g - \alpha} \right)^{f(\alpha)} \qquad (4.1)$$

where μ_0 is the viscosity at time equal to zero, α is the degree of cure, α_g is the degree of cure at gel, and $f(\alpha) = A + B\alpha$ [20].

The initial viscosity term, μ_0 is expressed in terms of temperature by an Arrhenius type expression,

$$\mu_0 = A_\mu e^{\left(\frac{E_\mu}{RT}\right)} \qquad (4.2)$$

where A_μ is a pre-exponential constant, E_μ is the activation energy, R is the universal gas constant, and T is the temperature in Kelvin. These parameters were determined by constructing an Arrhenius plot of the natural log of initial viscosity versus inverse temperature where the natural log of the y-intercept is equal to A_μ and the slope is E_μ/R.

4.3. RESULTS AND DISCUSSION

The results of the viscosity testing are presented in two sections. The first set of results contains the rheometry data, Arrhenius plots, and comparisons between the model predicted and experimental data for the 954-3 resin. Section 4.3.2 will present similar results but for the 954-2a toughened cyanate ester resin system.

4.3.1. 954-3 CYANATE ESTER RESIN

Isothermal rheometry tests were performed at 100, 120, 130, 140, 150, 160, 170, and 185°C. The raw data of viscosity as a function of time are presented in Figure 4.1. Each run showed a characteristic dramatic increase in viscosity at a certain time except for the 100°C test. Apparently 954-3 does not cure to any extent at 100°C even after three hours of testing.

Figure 4.2 is the Arrhenius plot of the $\ln(\mu_0)$ versus 1/T. From the plot, E_μ and A_μ were determined using a least squares linear regression fit of the following form,

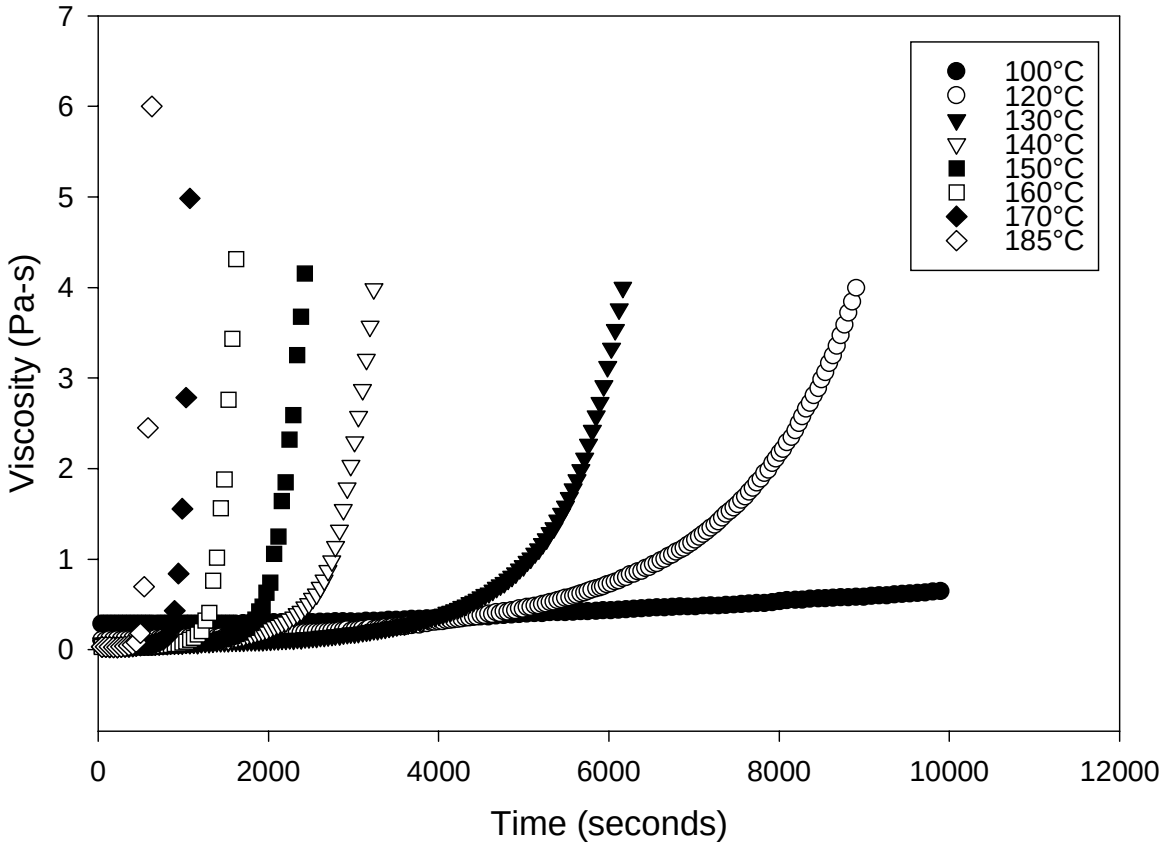

Figure 4.1: Measured viscosity as a function of time at different isothermal temperatures for the 954-3 cyanate ester resin system.

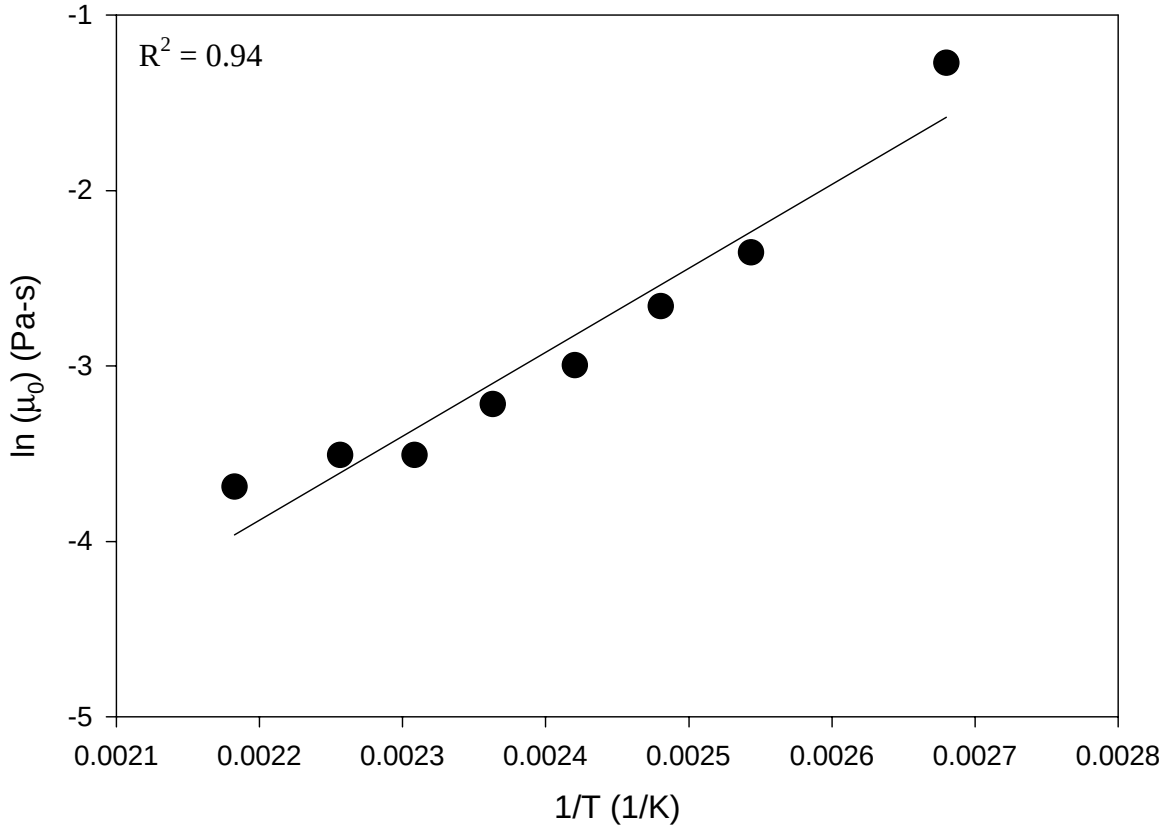

Figure 4.2: Arrhenius plot showing the temperature dependence of initial viscosity for 954-3.

$$\ln(\mu_0) = 4787\left(\frac{1}{T}\right) - 14.41 \qquad (4.3)$$

The degree of cure at gel, α_g, was determined by analyzing the plots of μ vs. α for the different temperatures, and selecting the degree of cure where viscosity was increasing very rapidly. Figure 4.3 shows a plot of α_g as a function of temperature for 954-3. The degree of cure at gel, α_g, fits the following linear equation.

$$\alpha_g = 2.51 \times 10^{-3} (T) - 0.62 \qquad (4.4)$$

By using the equations for μ_0 and α_g as well as Equation 4.1, SigmaPlot's non-linear multiple regression algorithm was utilized and values of A and B were determined [19]. The values of A and B were plotted as functions of temperature in Figures 4.4 and 4.5, respectively. The least squares linear regression fits to the data are as follows

$$A = -6.36 \times 10^{-3} (T) + 1.51 \qquad (4.5)$$

$$B = -6.36 \times 10^{-2} (T) + 37.10$$

The temperatures used for the model fits were 140, 150, 170, and 185°C. Plots comparing the measured data and the model generated viscosity-degree of cure profiles for each of the isothermal temperatures are shown in Figures 4.6-4.9. Overall, the model nicely predicted the values and the trend of the viscosity versus degree of cure curves.

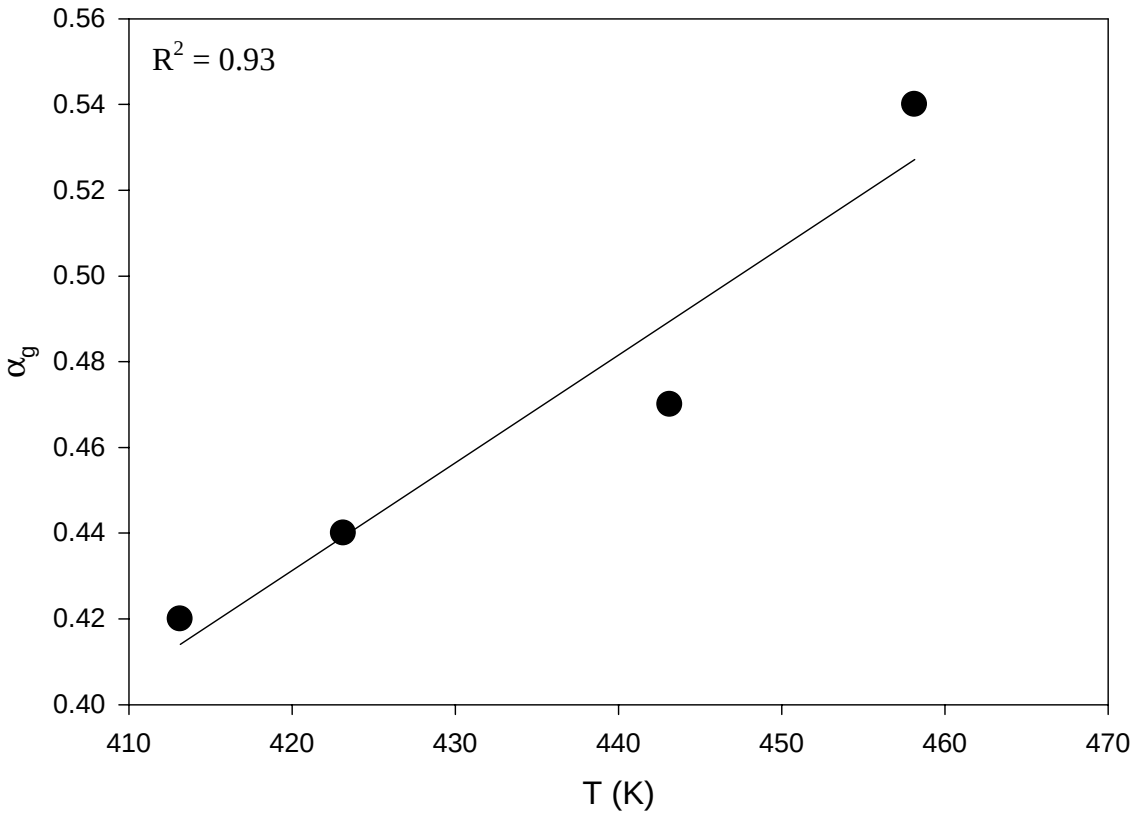

Figure 4.3: Temperature dependence of the degree of cure at gel for 954-3.

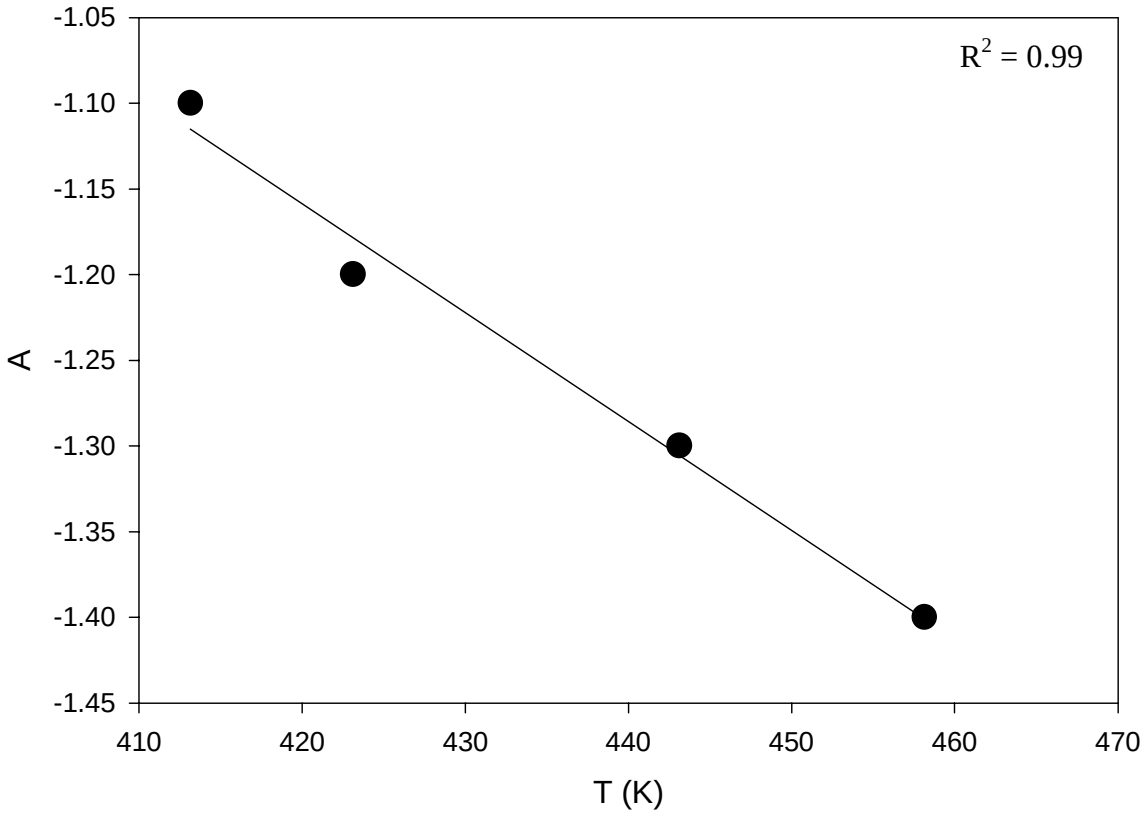

Figure 4.4: Model parameter, A, as a function of temperature for 954-3.

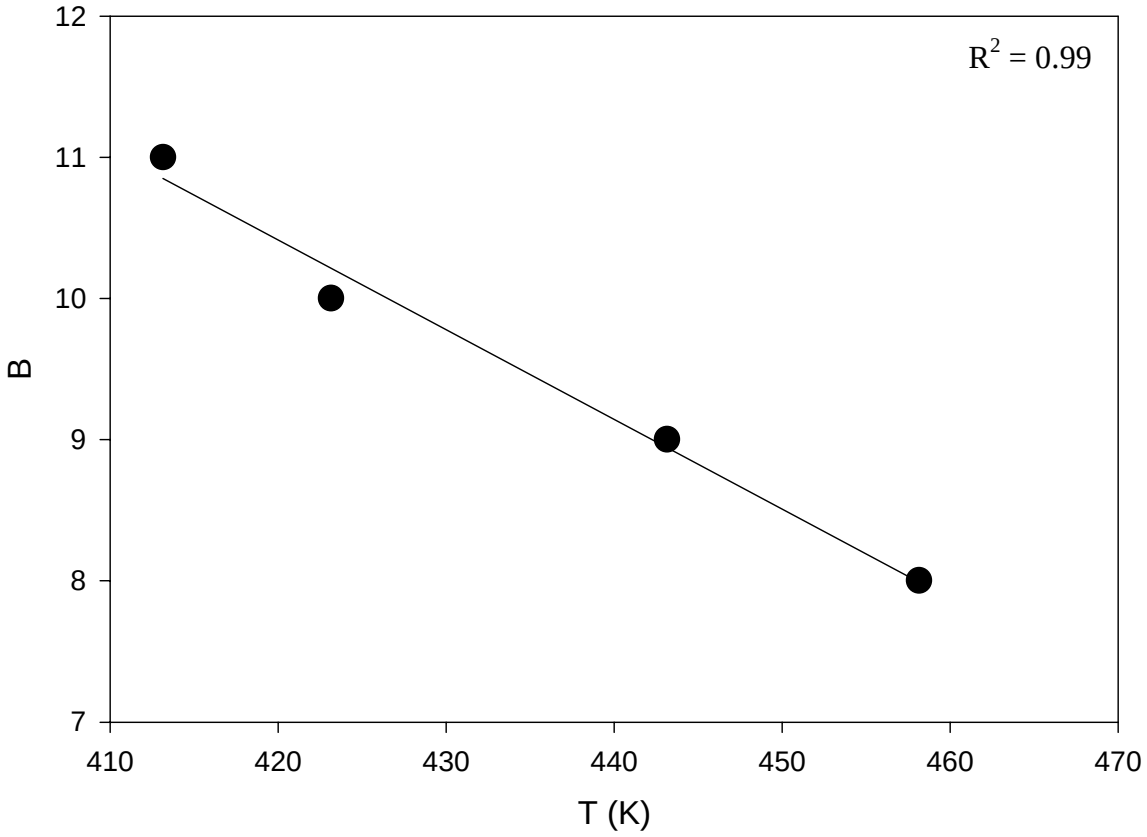

Figure 4.5: Model parameter, B, as a function of temperature for 954-3.

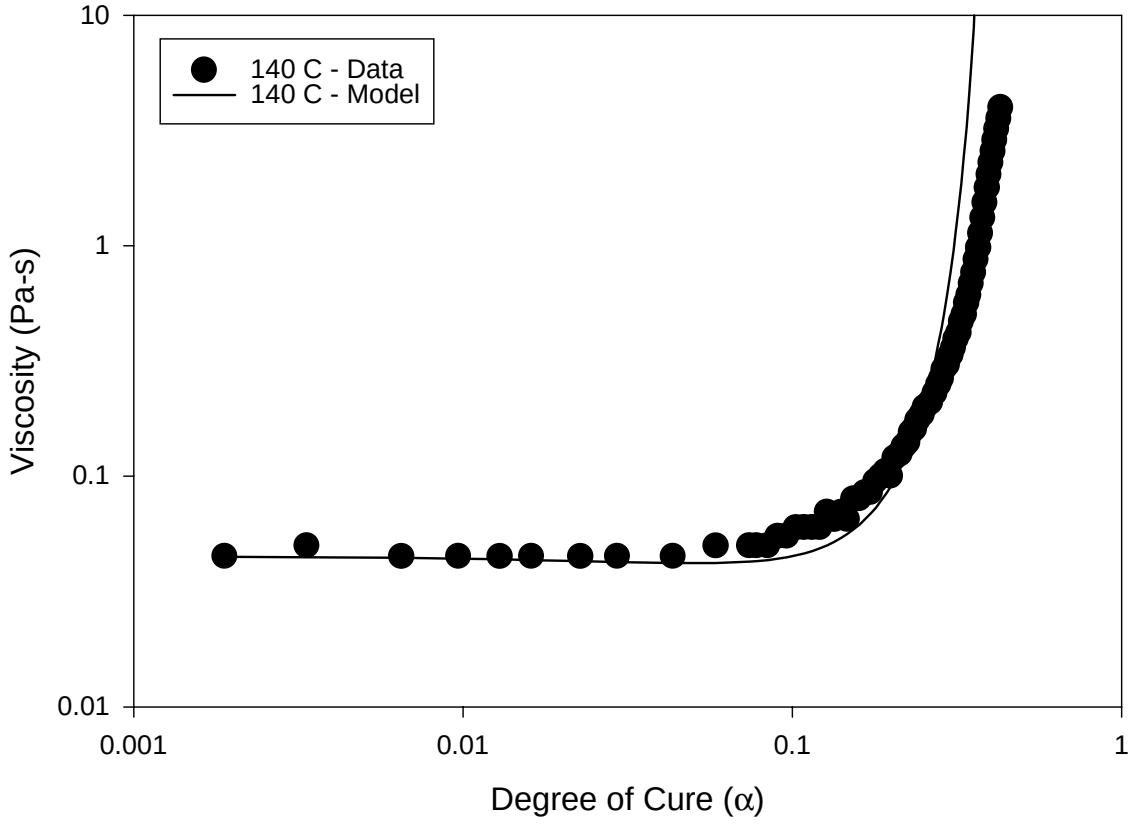

Figure 4.6: Comparison of measured and model predicted viscosity as a function of time at 140°C for 954-3 cyanate ester resin.

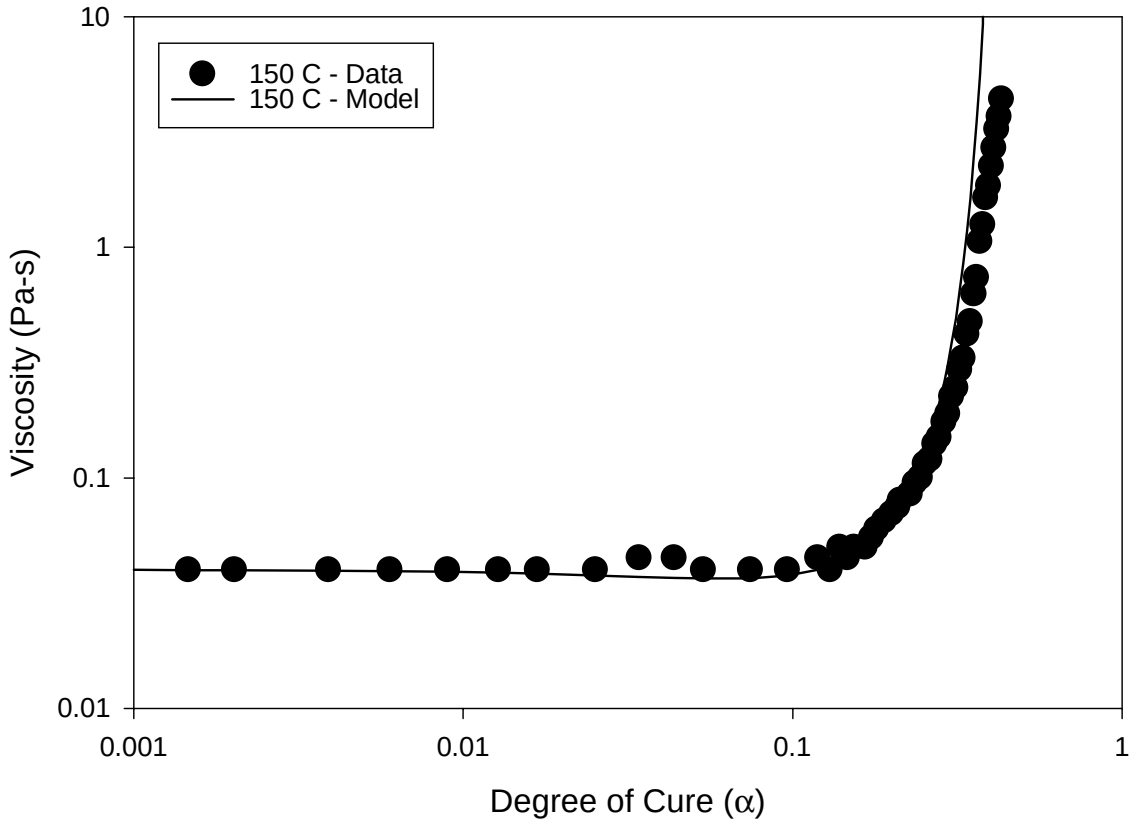

Figure 4.7: Comparison of measured and model predicted viscosity as a function of time at 150°C for 954-3 cyanate ester resin.

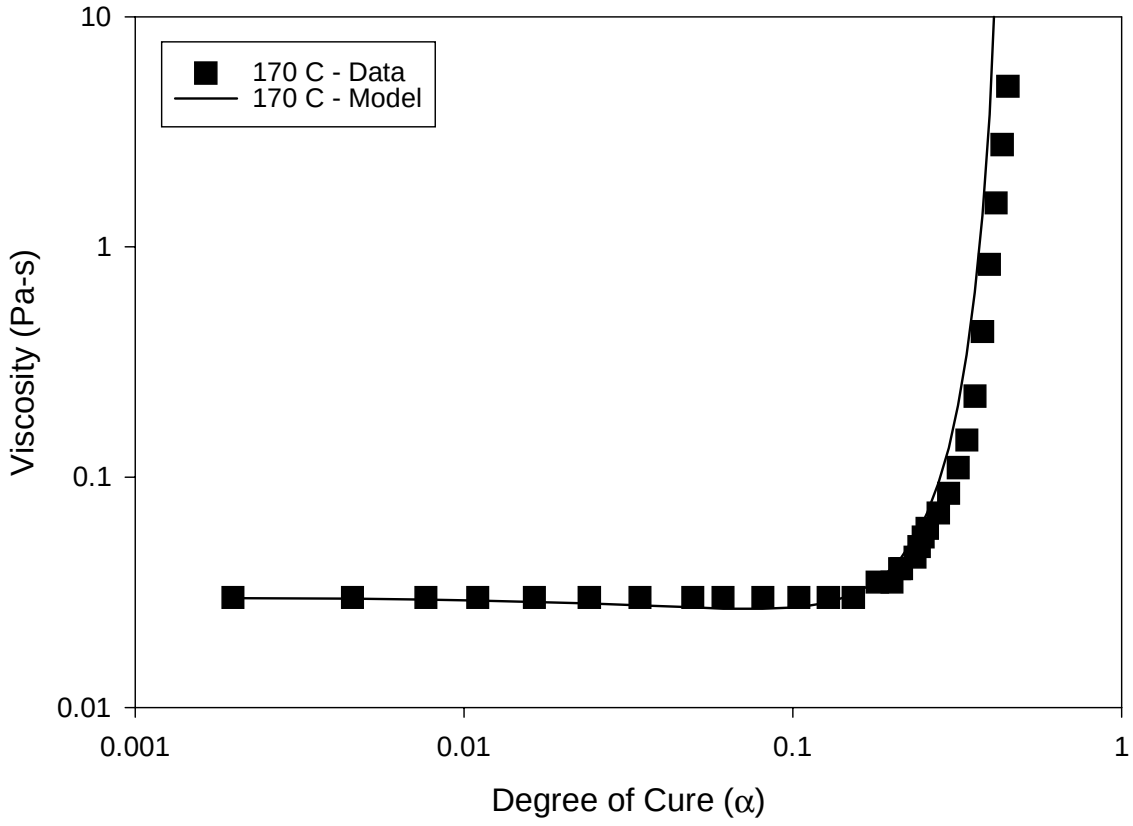

Figure 4.8: Comparison of measured and model predicted viscosity as a function of time at 170°C for 954-3 cyanate ester resin.

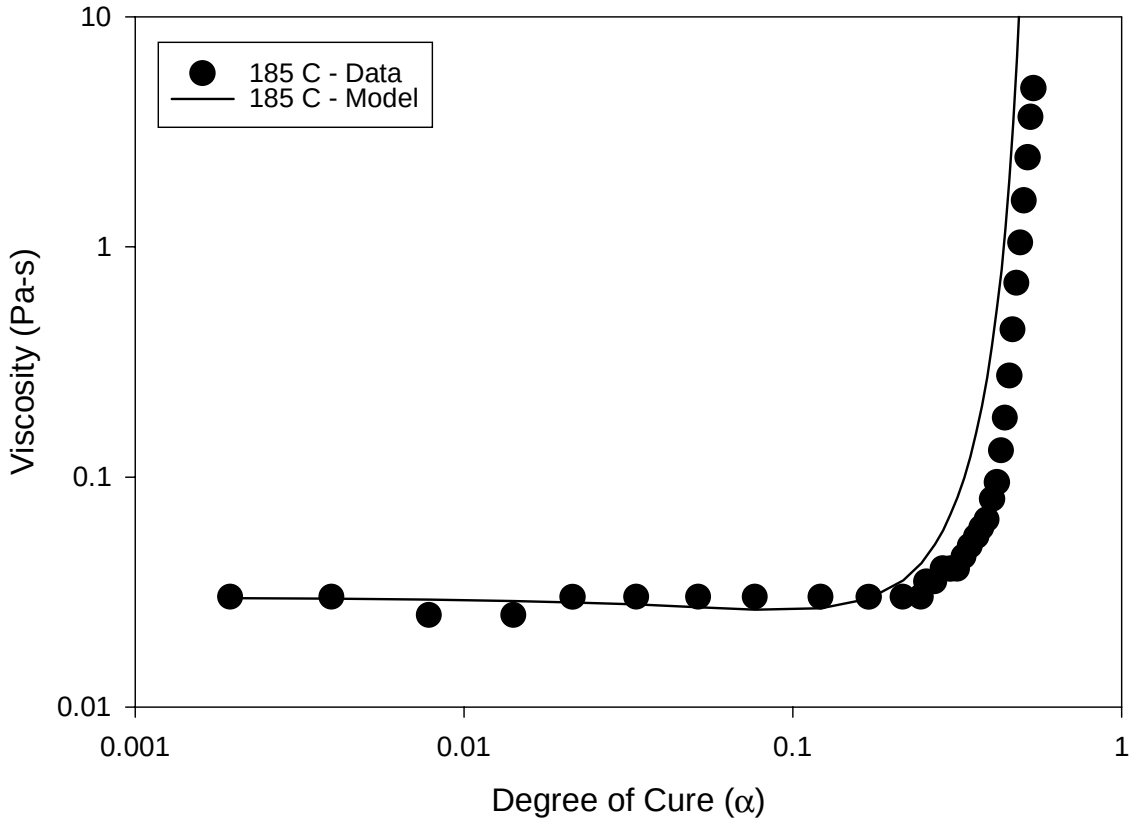

Figure 4.9: Comparison of measured and model predicted viscosity as a function of time at 185°C for 954-3 cyanate ester resin.

4.3.2. 954-2A TOUGHENED CYANATE ESTER RESIN

The isothermal temperatures used for the viscosity measurements were dictated by the behavior of the resin. Since this resin cured much quicker than 954-3, a lower temperature range was used. Isothermal viscosity testing was performed between 100°C and 150°C, but only 120°C - 150°C were used for the mathematical fits. Figure 4.10 shows the much shorter times to gel and the high initial viscosities for the 954-2a cyanate ester resin system as opposed to the 954-3. The temperature dependence of initial viscosity, μ_0, was determined by plotting the natural log of initial viscosity as a function of inverse temperature, and fitting the data with a least squares linear regression fit. The plot is shown in Figure 4.11, and the following equation is representative of the curve fit,

$$\ln(\mu_0) = 5810\left(\frac{1}{T}\right) - 5.55 \qquad (4.6)$$

where T is in Kelvin.

α_g was determined from the viscosity versus degree of cure graphs and plotted as a function of temperature in Figure 4.12. Equation 4.7 is the equation of the least squares fit for α_g versus T.

$$\alpha_g = 4.90 \times 10^{-3} (T) - 1.69 \qquad (4.7)$$

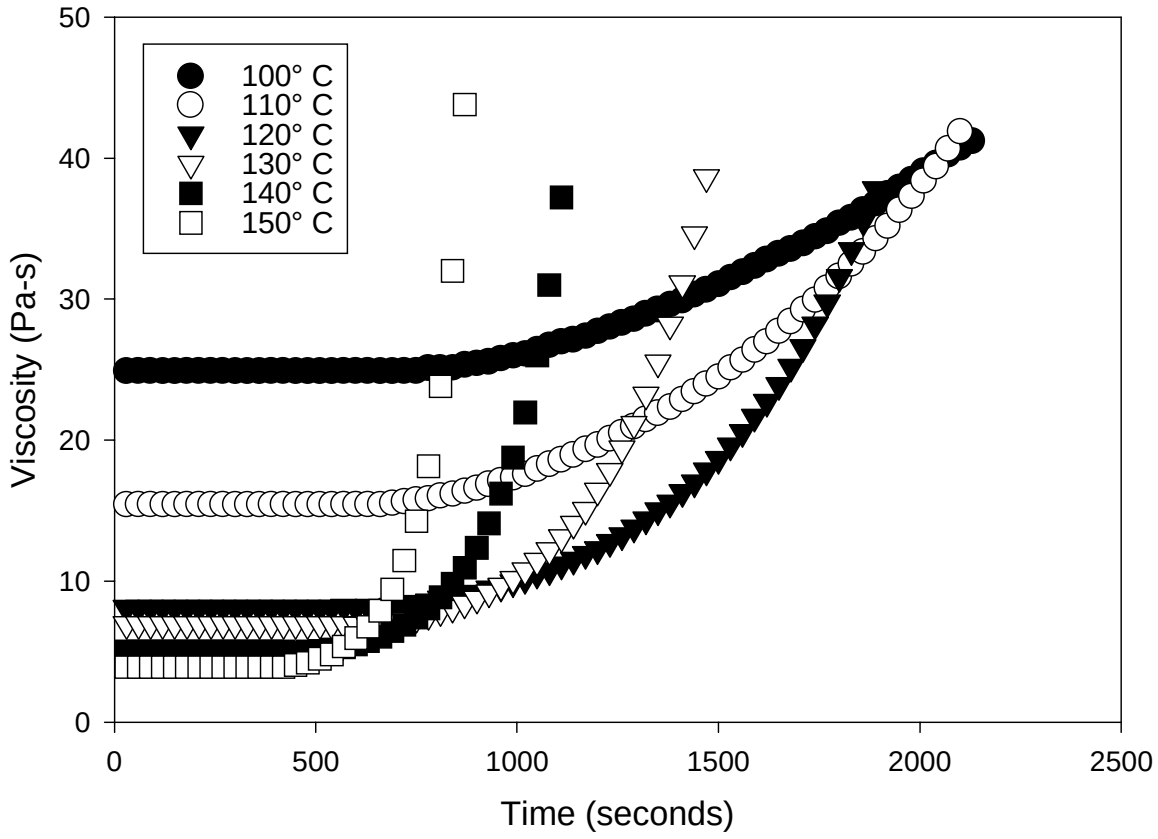

Figure 4.10: Measured viscosity as a function of time at different isothermal temperatures for the toughened cyanate ester resin system.

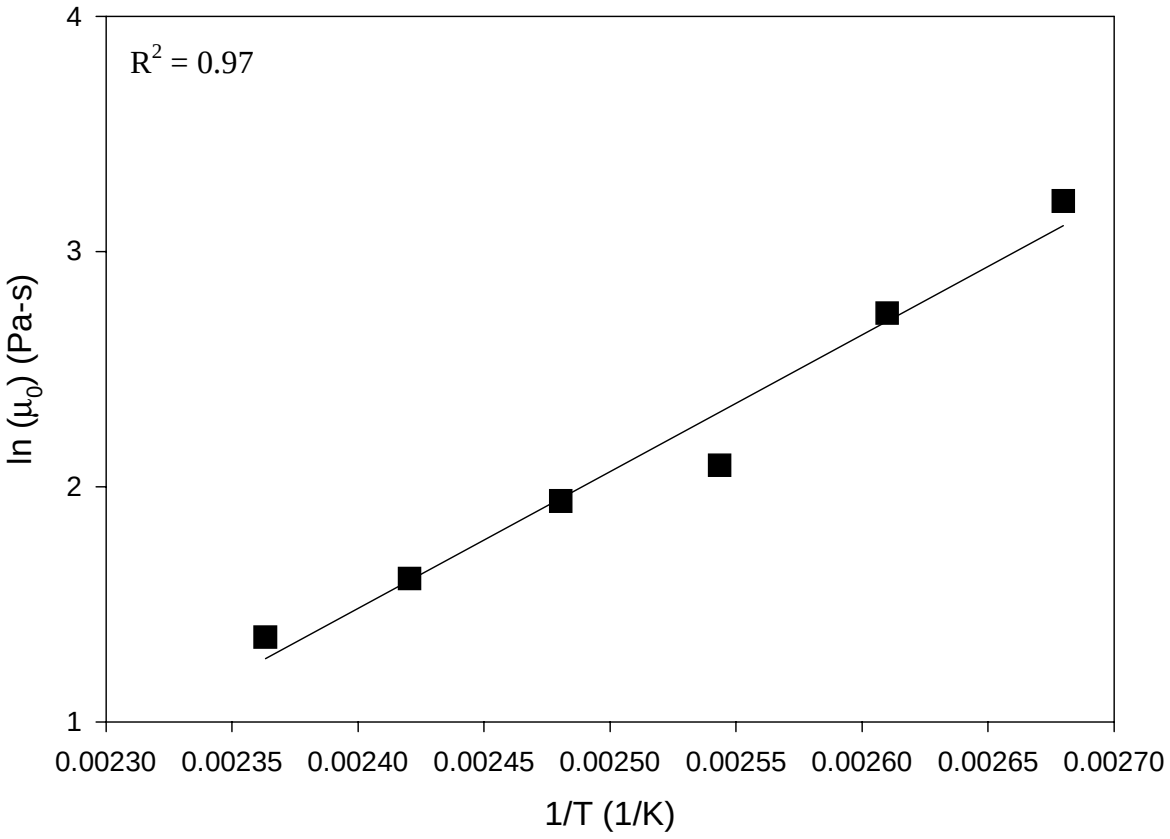

Figure 4.11: Arrhenius plot showing the temperature dependence of initial viscosity for 954-2a.

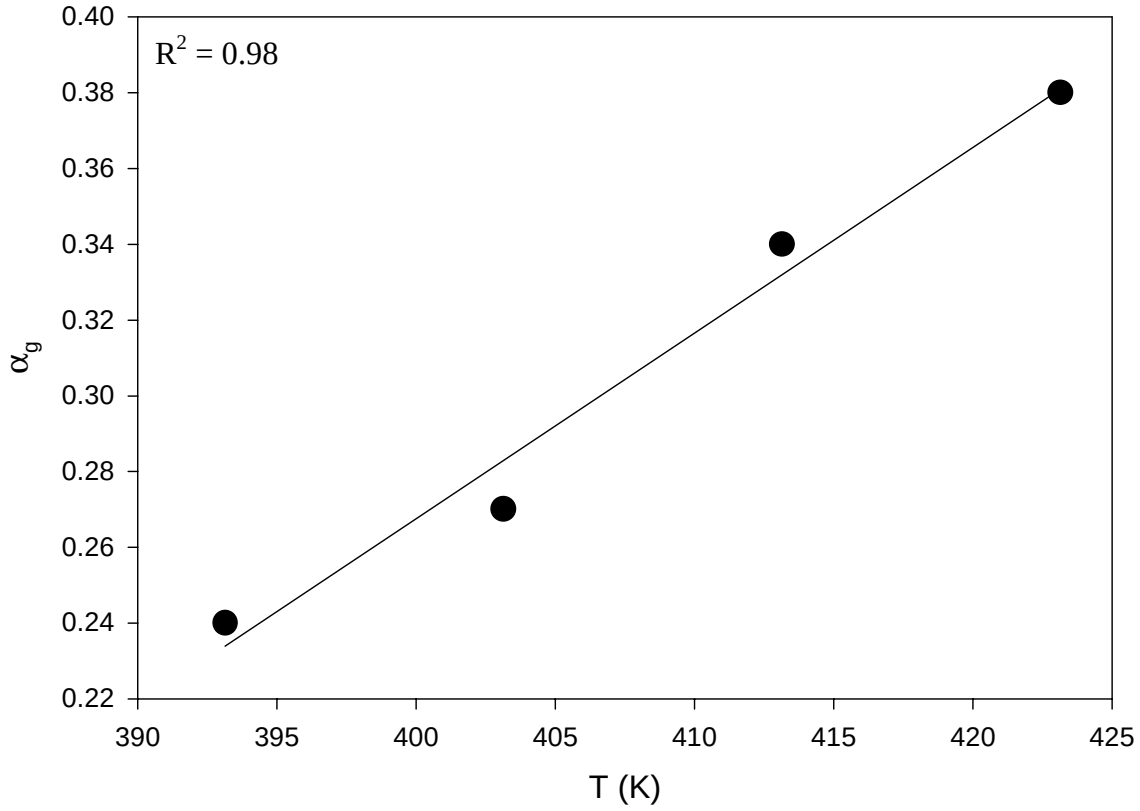

Figure 4.12: Temperature dependence of the degree of cure at gel for 954-2a.

Once μ_0 and α_g were determined as functions of temperature, values of A and B were produced by SigmaPlot and plotted as functions of temperature in Figures 4.13 and 4.14. The least squares fits from those curves resulted in the following equations.

$$A = -0.23\,(T) + 8.98 \qquad (4.8)$$

$$B = 0.039\,(T) - 12.09$$

With all of the temperature dependent parameters determined for the 954-2a toughened cyanate ester resin system, comparisons between model predicted viscosities and test data are shown in Figures 4.15 - 4.18.

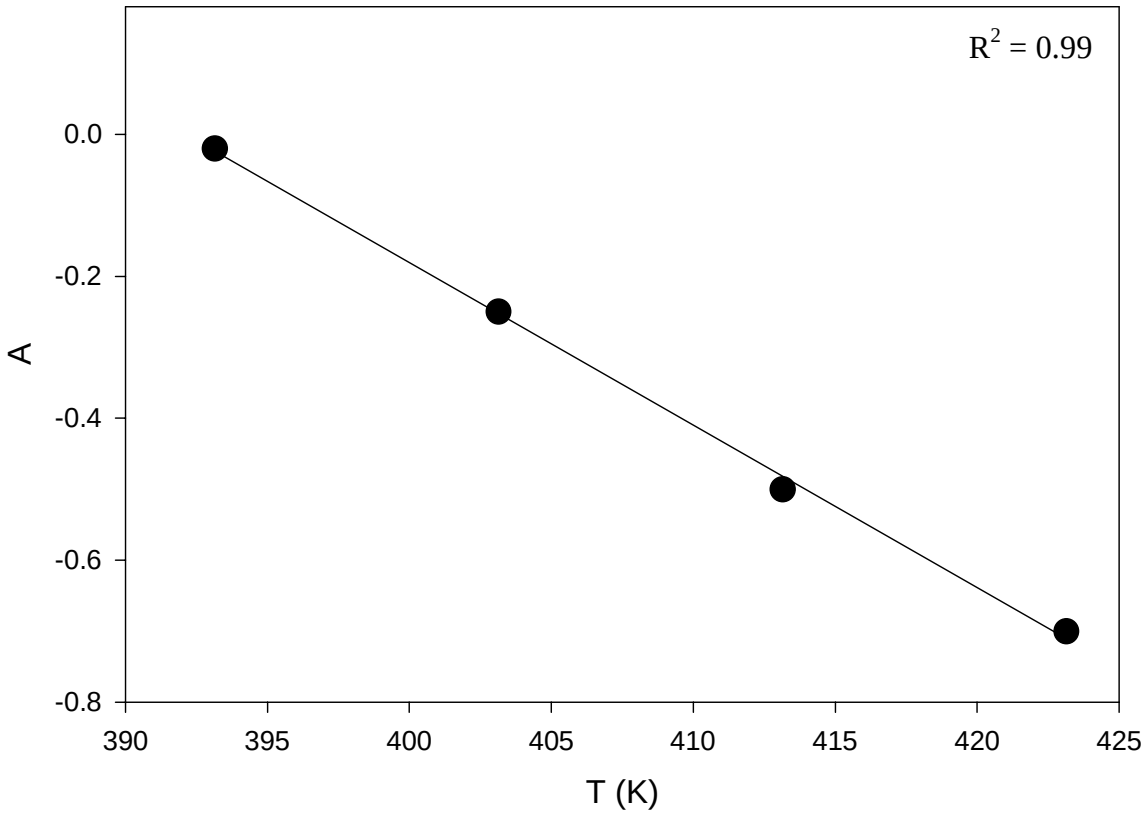

Figure 4.13: Model parameter, A, as a function of temperature for 954-2a.

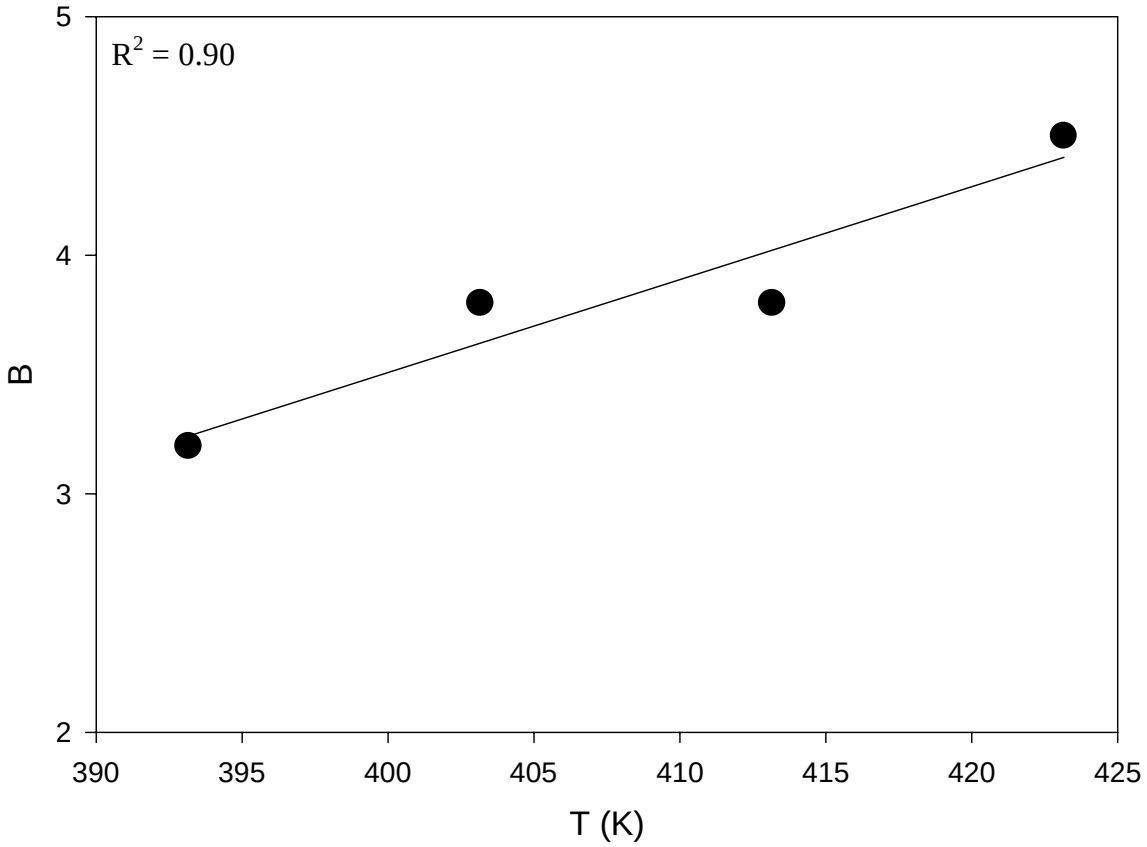

Figure 4.14: Model parameter, B, as a function of temperature for 954-2a.

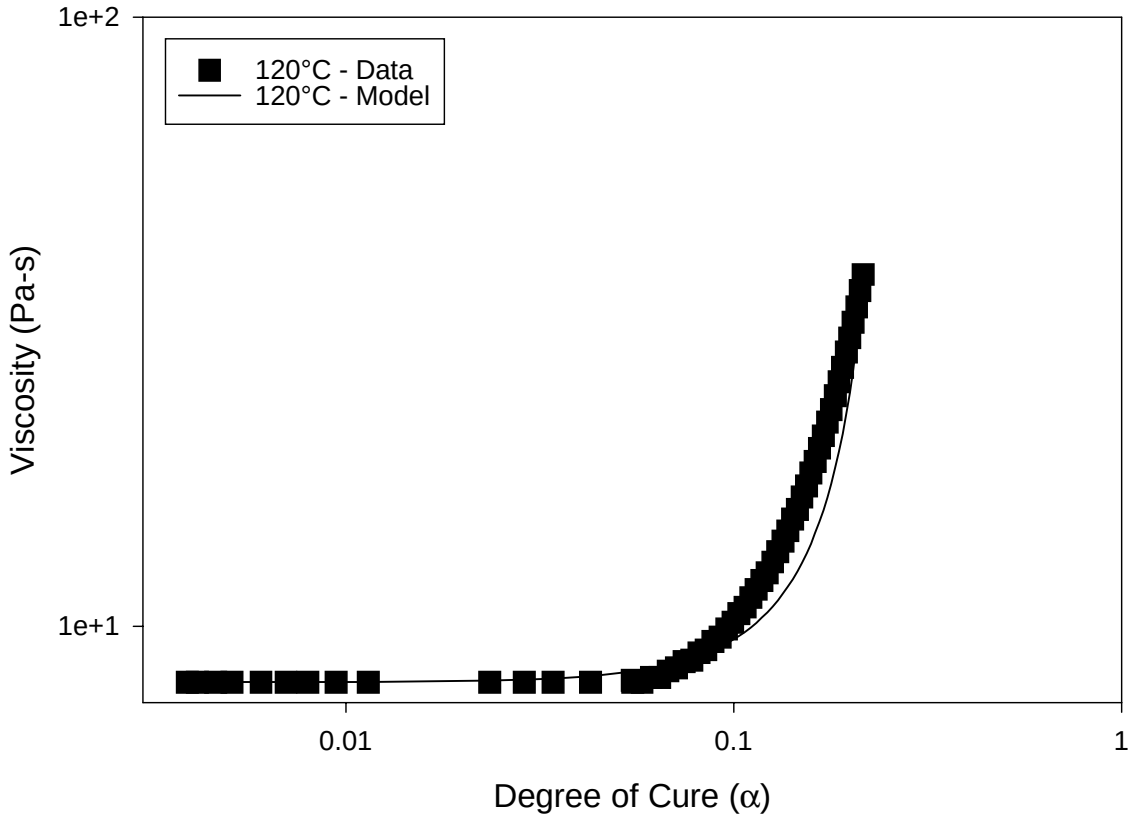

Figure 4.15: Comparison of measured and model predicted viscosity as a function of time at 120°C for 954-2a toughened cyanate ester resin.

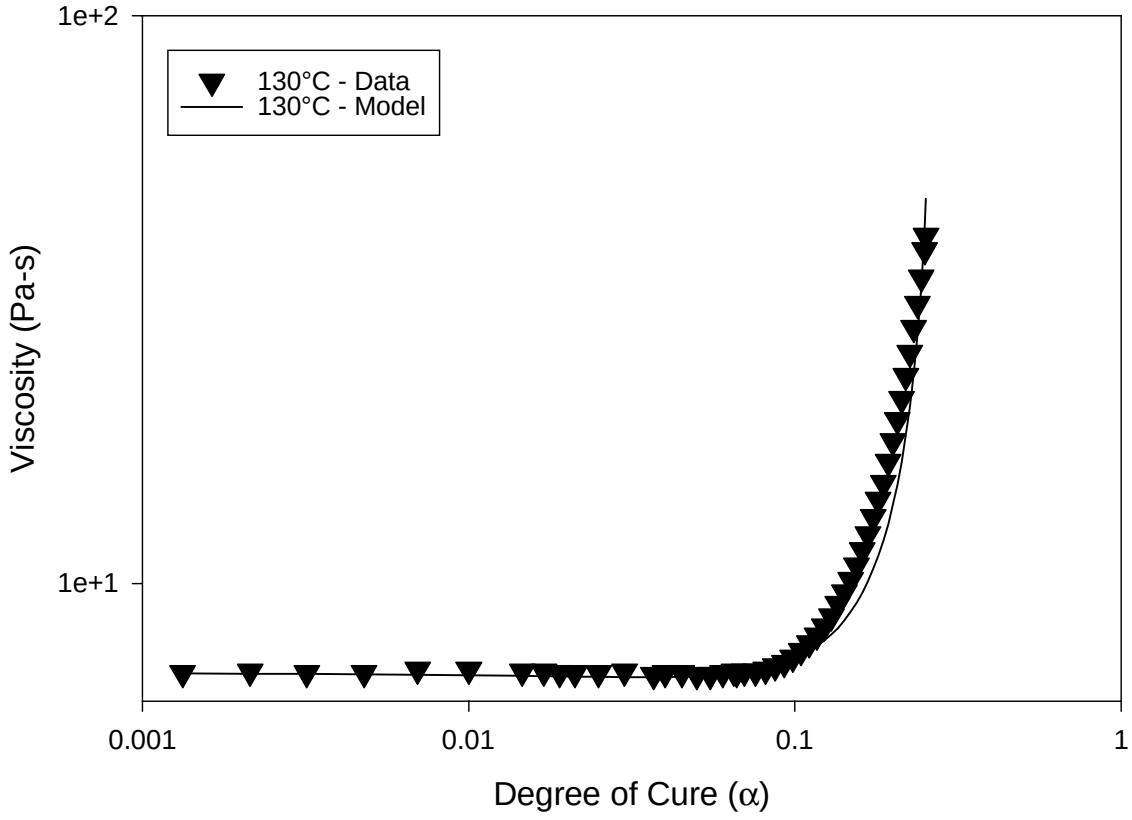

Figure 4.16: Comparison of measured and model predicted viscosity as a function of time at 130°C for 954-2a toughened cyanate ester resin.

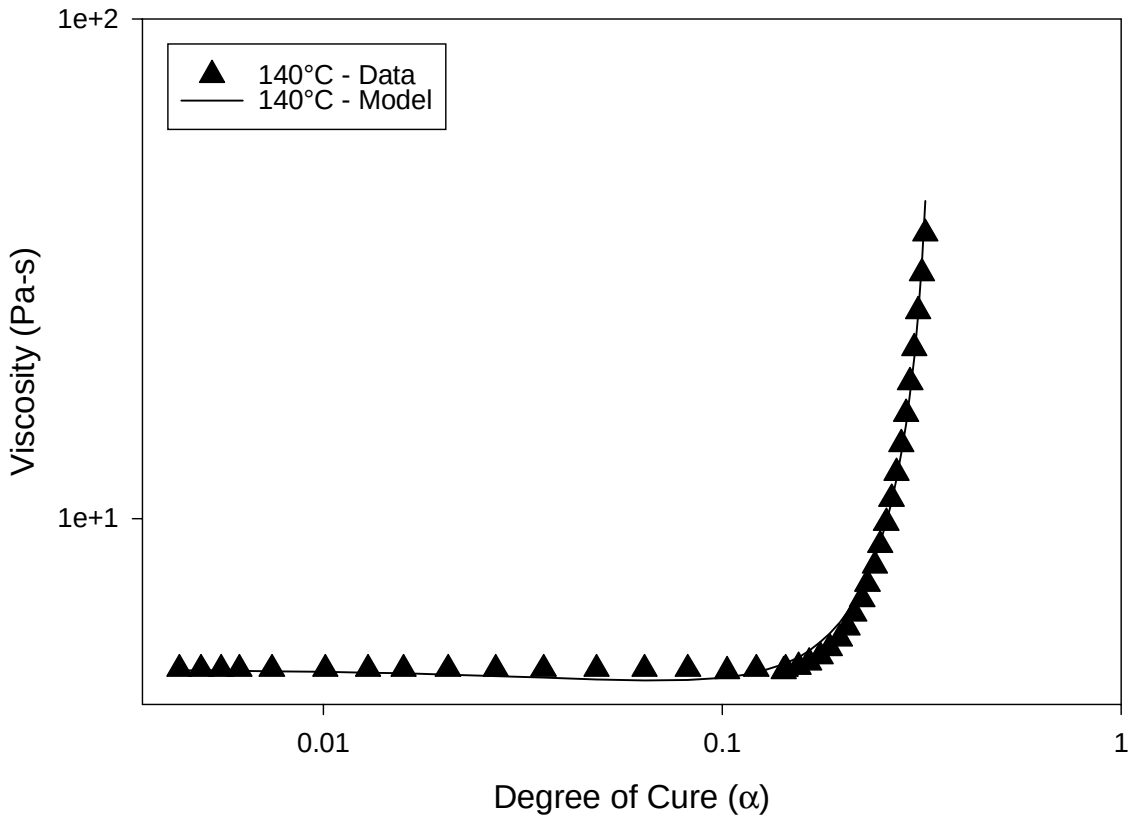

Figure 4.17: Comparison of measured and model predicted viscosity as a function of time at 140°C for 954-2a toughened cyanate ester resin.

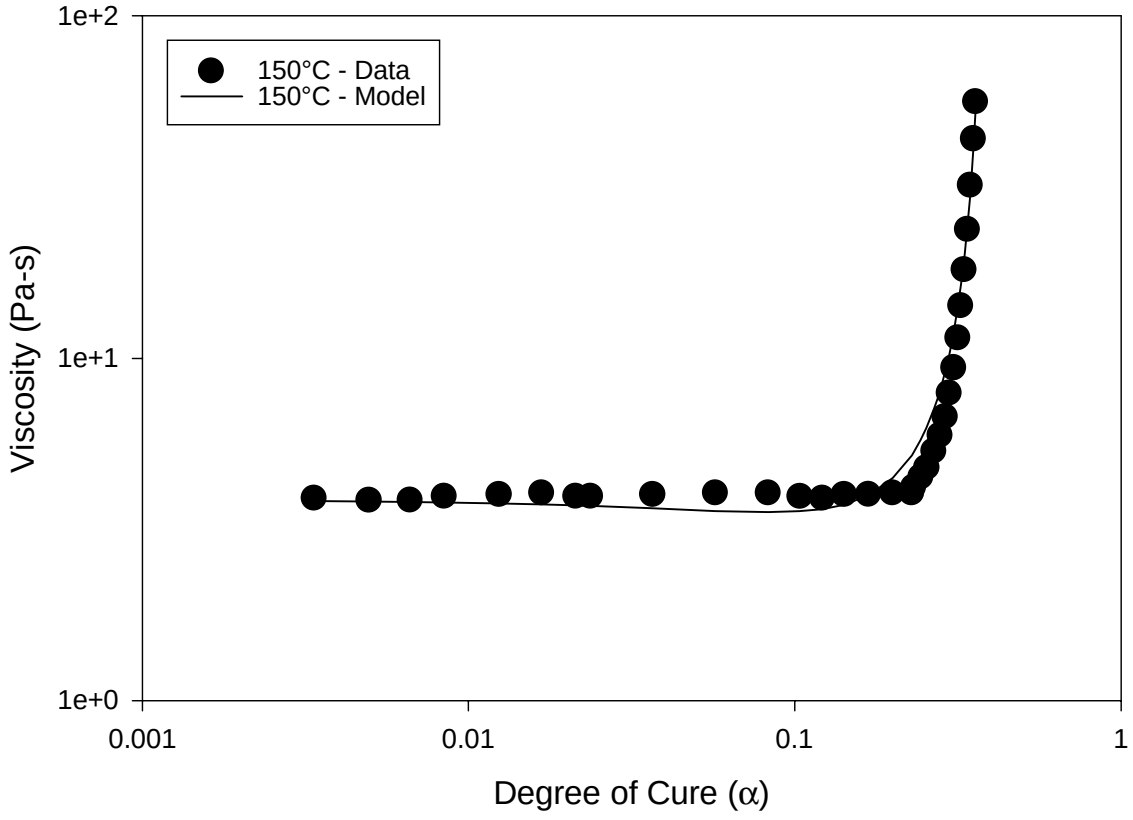

Figure 4.18: Comparison of measured and model predicted viscosity as a function of time at 150°C for 954-2a toughened cyanate ester resin.

4.4. CONCLUSIONS

Good agreement between the measured and the model predicted viscosities was seen, however, the limitations of this model must be recognized. One thing the model does not take into consideration is the initial state of cure of the resin. Unless the initial state of cure is determined experimentally, caution should be exercised in using such a model for process simulation. The state of cure of the resin system at the time of manufacture must be identical to that used in the viscosity measurements. For instance, if a resin has been exposed to moderate temperatures (≈ 25°C) for extended periods of time, some cure could have taken place. As a result, the degree of cure at gel of the resin may be partially or significantly reduced. Failure to ensure that no cure has taken place can lead to significant discrepancy between predicted and actual behavior.

CHAPTER 5: PERMEABILITY AND COMPACTION

5.0 PERMEABILITY AND COMPACTION

During the resin film infusion process, a hot-melt thermosetting resin flows up through the layers of the compacted fabric. Compaction characteristics of the fabric preform determine the compaction load required to reach a specified fiber volume fraction. The permeability of the fabric determines how easily the resin will flow at that fiber volume fraction. When the fabric characteristics are coupled with the resin properties discussed earlier, a complete understanding of the resin infiltration process is achieved.

5.1. LITERATURE REVIEW

5.1.1. COMPACTION

Compaction testing involves applying a load to compact a dry fabric or preform and measuring the resulting fiber volume fraction. This is the first test performed on a fabric because it determines the initial fiber volume fraction and the amount of load that must be applied on the preform to achieve a certain fiber volume fraction.

Extensive work has been published by Batch and Cuminsky [22] in the area of multilayer compaction. They have found that a random fiber mat is easily compressible and has a larger thickness change during mold closing than a unidirectional fabric. The

fiber volume fraction varies depending upon the fiber type, the weave type, and the fiber areal weight. In multilayered composites, each layer compresses under the same pressure, hence the change in layer thickness during mold closing decreases as void volume decreases, requiring substantially more compaction force to compress a reinforcement to high fiber volume fractions.

5.1.2. PERMEABILITY

Permeability is the ease with which a fluid moves through a porous medium. The permeability of the medium is directly related to the fiber volume fraction of the medium. The following section details the various governing relationships that are used in the study of permeability, and the relation between permeability and fiber volume fraction.

The most commonly used description of the flow of a Newtonian fluid through a porous medium is that proposed by Darcy [23]. In one-dimensional form, the law states that the flow rate (Q) through a constant area specimen is proportional to its cross sectional area (A) and the pressure drop across the specimen (ΔP) while being inversely proportional to the viscosity of the fluid (μ) and the length (L). Darcy's model equation also known as Darcy's law is written as follows

$$Q = \frac{SA}{\mu}\frac{\Delta P}{L} \qquad (5.1)$$

where S is the permeability of the porous medium.

There has however been some debate in the past couple of years on the validity of Darcy's law. Gauvin and Chibani [24] have reported experimental RTM results, where flow was not linearly proportional to the pressure gradient. They assume that the reason for the discrepancies is that the resin does not behave like a Newtonian fluid. Molnar, Trevino and Lee [25] have also reported similar results while Fracchia and Tucker [26] and Gebart, Strombeck and Lundemo [27] have reported excellent agreement between experiments and Darcy's law.

The permeability of the fabric preform is one of the most important parameters in the RFI process. E. Galli [28] has defined permeability as "that property of a porous material which characterizes the ease with which a fluid may be made to flow through the material by an applied pressure gradient." Permeability is a tensor quantity which may vary by direction within a given medium.

In composites manufacturing it is necessary to know the influence of fiber volume fraction on preform permeability because the fiber volume fraction (ν_f) is what determines the mechanical properties of the final product. Many models have been suggested to relate the permeability, S, of the preform to its fiber volume fraction, ν_f, and average fiber diameter, D_f. The most widely used are conduit flow models of which the one generally accepted is the Kozeny-Carman equation [29].

$$S = \frac{D_f^{\,2}}{16C}\frac{(1-v_f)^3}{v_f^{\,2}} \qquad (5.2)$$

where C is the Kozeny constant which accounts for tortuosity and pore nonuniformity. However, the predictive capability of the Kozeny-Carman equation is severely limited. Because idealized structures are assumed and the model depends only on the fiber diameter and fiber volume fraction, they are strictly applicable to uniform or narrow distributions of fiber volume.

Recently, Skartsis, Kardos, and Khomami [30] reviewed theoretical and experimental studies concerned with resin flow through porous media. They concluded that the Kozeny-Carman equation does not accurately describe the permeability behavior even though the flow might be Newtonian and at low Reynolds numbers. They noted several cases where the assumptions behind the Kozeny Carman equation were not justified. However, for perfectly spaced and aligned cylinder arrays, the theoretical models satisfactorily described transverse permeability behavior only for fiber volume fractions below 0.4.

Gutkowski et al. [31, 32] proposed modifying the Kozeny-Carman equation for unidirectional reinforcements with different Kozeny constants in different directions. The Kozeny-Carman equation then has the form,

$$S_{ii} = \frac{D_f^{\,2}}{\kappa_{ii}}\frac{(1-v_f)^3}{v_f^{\,2}} \qquad (5.3)$$

where κ_{ii} is the Kozeny constant in different directions.

Gebart [27] has presented models for through-the-thickness permeability which are dependent on the fiber packing in the preform. In the model, the flow resistance is assumed to be a result of the pressure drop across the gaps between individual fibers. For a preform composed of aligned, quadrilaterally packed fibers, the equation is written as

$$S_z = \frac{16}{9\pi\sqrt{2}}\left(\sqrt{\frac{v_{f\,\max}}{v_f}-1}\right)^{\frac{5}{2}} R^2 \qquad (5.4)$$

where v_{fmax} is the maximum fiber volume fraction, $\pi/4$ (0.785) [27], and R is the fiber radius.

For hexagonal fiber bed packing, the relationship between fiber volume fraction and permeability may be written as

$$S_z = \frac{16}{9\pi\sqrt{6}}\left(\sqrt{\frac{v_{f\,\max}}{v_f}-1}\right)^{\frac{5}{2}} R^2 \qquad (5.5)$$

where v_{fmax} in this case is $\pi/(2\sqrt{3})$ (0.907) [27].

Because most preforms are not made up of either quadrilateral or hexagon fiber packing arrangement, but rather are random in nature, the following equation was suggested to relate through-the-thickness permeability and fiber volume fraction,

$$S_z = C\left(\sqrt{\frac{v_{f\,\max}}{v_f} - 1}\right)^{\frac{5}{2}} R^2 \qquad (5.6)$$

where the constant C depends on fiber arrangement and can be determined experimentally.

During the resin film infusion process a significant portion of the resin flow is through the thickness of the fabric. Molnar, Trevino, and Lee [25] looked at through-the-thickness permeability behavior for random and unidirectional mats. For a pure unidirectional mat, the close packing of the individual layers was found to greatly reduce the permeability. However, by adding random mats with higher permeability, the fluid was able to quickly reach the unidirectional layers. Once this layer was saturated, the flow was able to progress through the preform**.**

Loos and Hammond [33] characterized the through the thickness permeability behavior for a TTI IM7/8HS fabric. It was shown that permeability decreased as a function of fiber volume fraction faster for the 8HS than for other woven fabrics. This was attributed to the complicated eight harness satin weave pattern. Due to the complexity of the weave, the flow paths in the preform are more convoluted and the fluid has a harder time passing through the preform. Also, as the complex weave of the

preform is compressed, the flow paths close off at a faster rate, resulting in a faster decrease in permeability.

Loos and Wiedeman [34] also characterized the through the thickness permeability behavior for a TTI IM7/8HS fabric. It was shown that sample thickness had a negligible effect on the through-the-thickness permeability behavior. The permeability behavior of the TTI IM7/8HS fabric was shown to be very similar to that of a knitted Hexcel 8HS fabric. This similarity was due to both preforms being composed of fibers perpendicular to the flow direction with the rate of flow controlled by both the fiber bed packing arrangement and the gap distance between the individual fibers.

Permeability of porous materials depends very strongly on the morphological structure. Due to the complexity of the fiber architectures and the lack of an adequate mathematical model, many researchers continue to determine permeabilities experimentally.

5.2. EXPERIMENTAL PROCEDURE

Compaction and through the thickness permeability tests were performed on the Amoco EWC-600X 8HS graphite fabric. This section will describe the experimental procedures that were followed during the testing.

5.2.1. TEST FIXTURE

This section describes the stainless steel test fixture used for both through-the-thickness permeability testing and compaction testing. The fixture, shown in Figure 5.1, has a 5.08 cm x 5.08 cm cavity. The holes in the cavity are approximately 0.476 cm in diameter and spaced 0.635 cm apart [34]. The oil enters the cavity through a porous plate in the base and leaves through a similar porous plate mounted in the piston after traversing through the thickness of the preform. An Omega PX102-050GV 50 psi pressure transducer was used to measure the pressure drop across the preform. The load was transferred from the load frame to the fixture via a steel ball which represents a point load. An O-ring groove circumnavigates the piston and is used during the permeability testing.

5.2.2. SAMPLE PREPARATION

Each test sample consisted of 10 plies of 5.08 cm x 5.08 cm EWC-600X 8HS fabric. Samples were held in place with a steel pattern and cut with a utility knife. Each group of ten plies was weighed and placed into the fixture for testing. The areal weight, ξ, was determined for each group of ten plies by the following equation.

$$\xi = W_T / A \qquad (5.7)$$

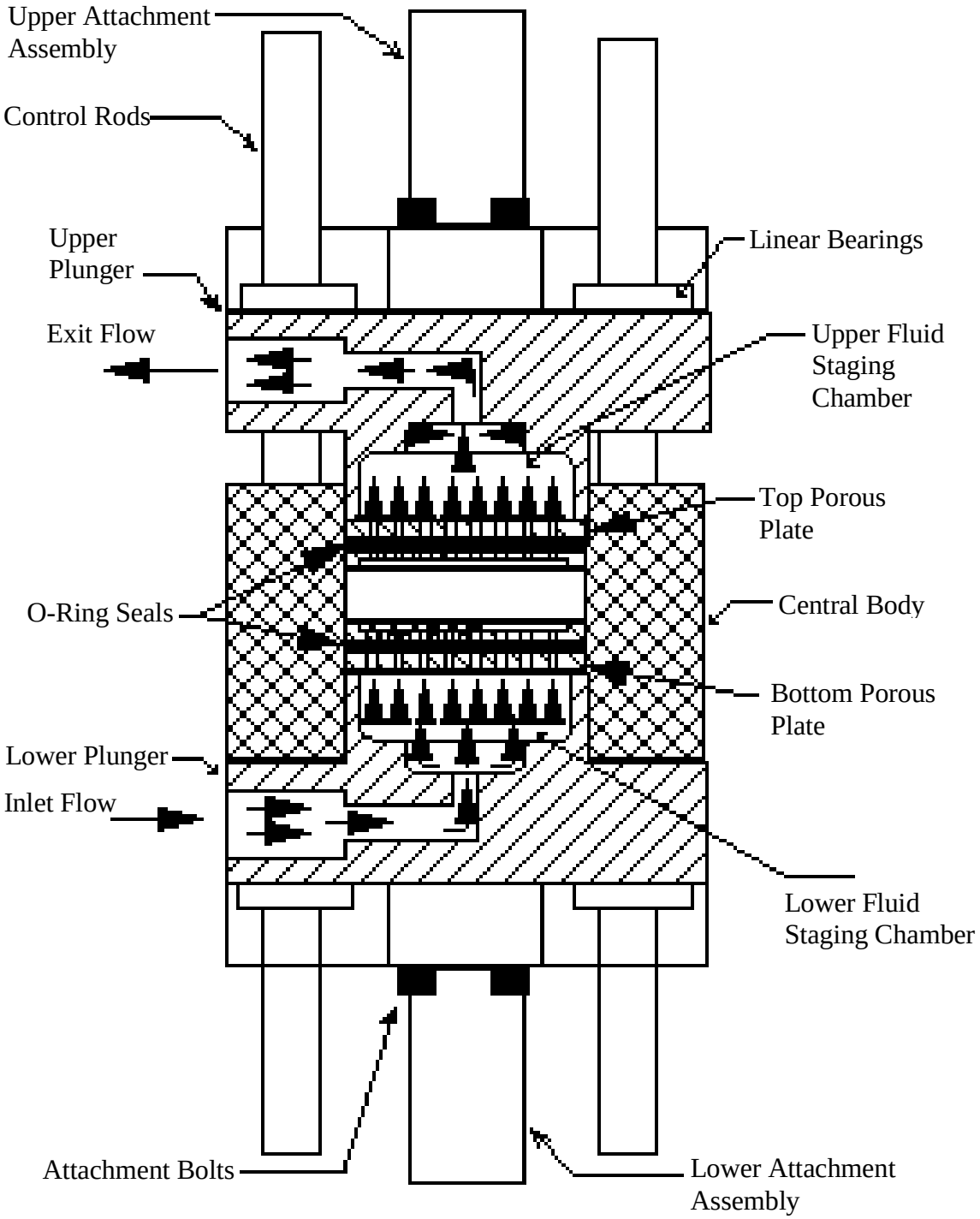

Figure 5.1: Schematic of the 5.08 cm x 5.08 cm through the thickness permeability fixture [35].

where W_T is the total weight of the ten plies and A is the cross-sectional area (5.08 cm x 5.08 cm). Tables 5.1 and 5.2 contain the areal weights for the samples used in the compaction and permeability testing.

Table 5.1 - Areal weights for 10 plies of Amoco EWC-600X 8HS used in the compaction testing.

Amoco's EWC-600X 8HS	Areal weight (ξ) (g/m^2)
sample 1 (11.50g)	4456.29
sample 2 (11.69g)	4528.57
sample 3 (11.64g)	4510.59

Table 5.2 - Areal weights for 10 plies of Amoco EWC-600X 8HS used in the permeability testing.

Amoco's EWC-600X 8HS	Areal weight (ξ) (g/m^2)
sample 1 (11.62g)	4502.41
sample 2 (11.55g)	4475.83
sample 3 (11.68g)	4525.27

5.2.3.COMPACTION TESTING

The bottom of the test fixture was placed on a cleaned, smooth steel plate which had been bolted to the test frame. The sample was placed in the test cavity carefully, ensuring that each ply was lying flat. The top of the fixture was lowered into position. The cross-head of the Instron was lowered until it touched the steel ball atop the fixture. Perfect alignment is necessary between the load frame and the top of the fixture to ensure a true point load and evenly applied pressure.

Since the top piece of the fixture was not attached to the Instron load frame, its weight must be accounted for. The weight of the upper piece was added to the applied

compaction load from the test machine to give the total applied compaction load. The applied compaction pressure, P_{comp}, was calculated using the following expression,

$$P_{comp} = \frac{F_{comp} + F_{top}}{A} \qquad (5.8)$$

where F_{comp} is the compaction force applied by the load frame, F_{top} is the force applied due to the weight of the top piece of the fixture, and A is the cross sectional area of the test section.

The load cell on the Instron was connected to Labview, the data acquisition system. The load frame was turned on along with the SCXI board and the power supply. The equipment was calibrated and data acquisition began. The preform was compressed to a thickness pre-determined by desired fiber volume fraction. The initial thickness, t, in inches, was determined as follows

$$t = \frac{m}{\rho v_f A}\frac{100}{2.54} + 0.025 \qquad (5.9)$$

where m is the weight of the 10 plies, ρ is the density of the graphite fiber, v_f is the starting fiber volume fraction, and A is the area of the plies.

The fiber volume fraction was calculated with the following equation,

$$v_f = \frac{\xi}{\rho_f t} \qquad (5.10)$$

where ξ is the areal weight, ρ_f is the density of the fiber, and t is the current thickness of the 10 plies.

Compaction pressure, thickness, and load were recorded at each fiber volume fraction. This continued until a fiber volume fraction of about 56% was reached, at which point the test concluded. All three samples were tested in the exact same manner.

5.2.4. PERMEABILITY TESTING

The permeability test procedure was the same as the compaction test procedure, with the addition of a pump to control the flow of the corn oil through the cavity. A Parker Hannifin Corp. Zenith Pump, with a 50 cc/min capability, was used to pump the corn oil.

The corn oil had a viscosity of 0.054 Pa-s at 23°C. The viscosity of the oil was measured at different temperatures and the data fit the following equation [35],

$$\eta = (-2.0496\ (T) + 101.54) / 1000 \qquad (5.11)$$

where η is the viscosity in Pa-s and T is temperature in °C.

The pressure transducer at the inlet was calibrated prior to beginning any tests. The O-ring was lubricated with O-ring grease and placed around the top of the fixture to

prevent oil from leaking out of the cavity. At each fiber volume fraction the pump was run at three different flow rates. The resulting pressure differentials associated with each flow rate were measured. Through the use of Darcy's law, the flow rate was related to the pressure drop across the preform at each fiber volume fraction. By plotting flow rate versus pressure drop and determining the slope of a linear least squares fit to the data, the permeability for each volume fraction was determined by [33],

$$S = \frac{slope \cdot \mu}{A} \qquad (5.12)$$

where μ is the viscosity of the fluid and A is the flow area.

The permeability testing concluded around 56% fiber volume fraction. The test cavity was drained of oil and cleaned for the next sample. All three samples were tested in the same manner.

5.3. RESULTS

5.3.1. COMPACTION

The data from the three tests were compiled into one data set. Figure 5.2 shows fiber volume fraction as a function of applied compaction pressure. A power law regression model was used to establish a relationship between the fiber volume fraction and the applied compaction pressure. The equation of the curve fit had the form

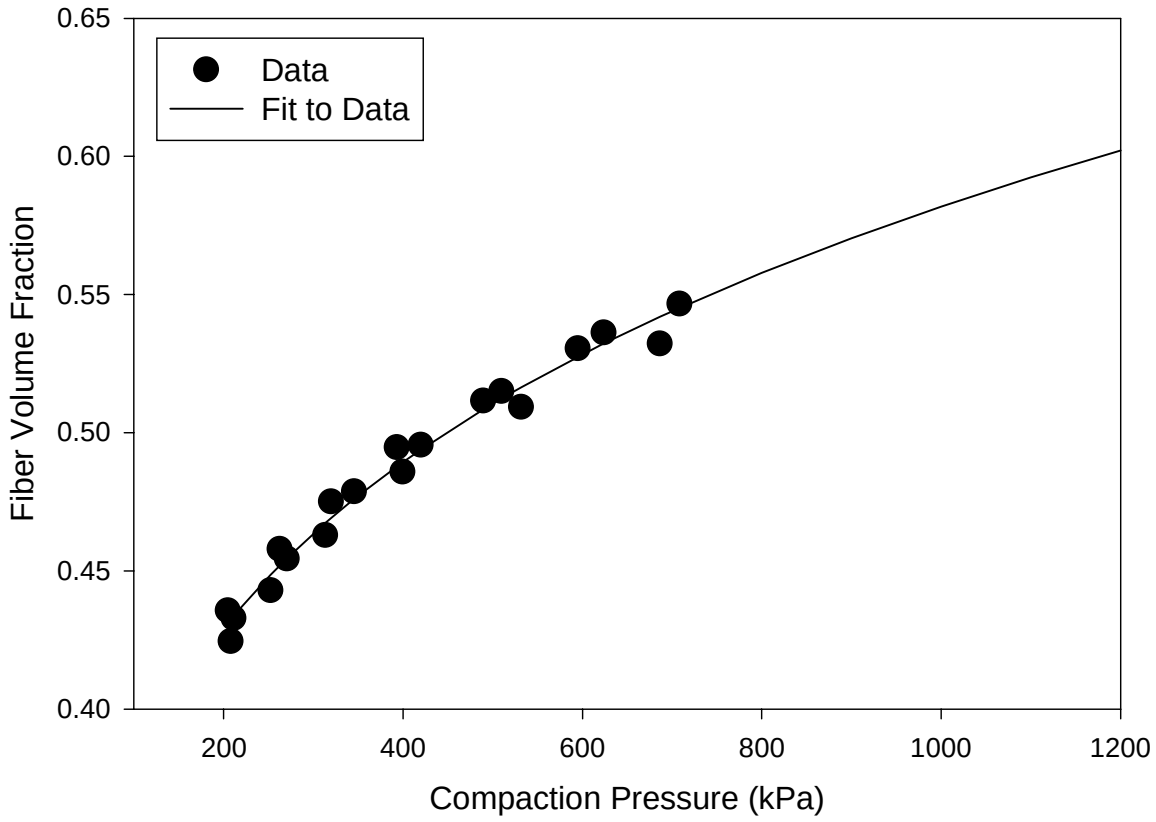

Figure 5.2: Fiber volume fraction as a function of applied compaction pressure for Amoco Thermalgraph™ EWC-600X 8HS graphite fabric.

$$\nu_f = a\ (\text{Compaction Pressure})^b \qquad (5.13)$$

where a and b are constants determined by the regression analysis. The experimental constants, a and b, for the Amoco EWC-600X 8HS are 0.1578 and 0.1889, respectively.

The curve shows an initial non-linear increase in fiber volume fraction as the load is applied**.** The waviness of the eight harness satin weave results in gaps between adjacent layers**.** As the compaction load is applied, these gaps are eliminated and the fibers are able to move and achieve an optimal state of compaction [33]. As the maximum preform deflection is reached, a significantly greater load is required to increase the fiber volume fraction. This is reflected by the linear relationship at higher loads.

The larger density of graphite fiber compared to carbon fiber led to significantly increased compaction pressures to reach the same fiber volume fraction. Even though the EWC-600X and the TTI IM7 [33] both have the same 8HS weave pattern, significant differences in compaction pressures were noted. The EWC-600X (ρ=2.18 g/cc) required approximately 1200 kPa to reach a fiber volume fraction of 0.6 where as the TTI IM7 (ρ=1.8 g/cc) only needed 100 kPa to reach the same fiber volume fraction.

5.3.2. THROUGH-THE-THICKNESS PERMEABILITY

Three 10 ply samples were tested to measure the through the thickness permeability of Amoco EWC-600X 8HS fabric. At each fiber volume fraction, three different flow rates were used. The equilibrium pressure difference, flow rate,

permeability, and mold height were recorded. Each test concluded at a fiber volume fraction of about 56%.

After all the tests were completed, the data were combined and permeability values were plotted as a function of fiber volume fraction. A power law regression model was used to fit a curve through the data. The power law fit had the form

$$S = c\,(v_f)^d \qquad (5.14)$$

where c and d were determined, by the curve fitting program, to be 3.38×10^{-16} and -8.40 respectively. Figure 5.3 shows the experimental data and curve fit for through the thickness permeability as a function of fiber volume fraction.

To ensure that Darcy's law applied in this case, pressure drop across the preform was plotted as a function of flow rate. Figure 5.4 shows that the pressure gradient increases linearly with flow rate. This validates the assumption that the fabric is a porous medium and that Darcy's law can be applied to this fabric [35].

Questions may arise on the validity of a steady state permeability test for the RFI process, because in the RFI process resin flow is into a dry preform not a previously saturated one. However, steady state permeability was assumed to be adequate on the basis of previous investigations [36] that showed there were negligible differences between steady state and advancing front permeabilities.

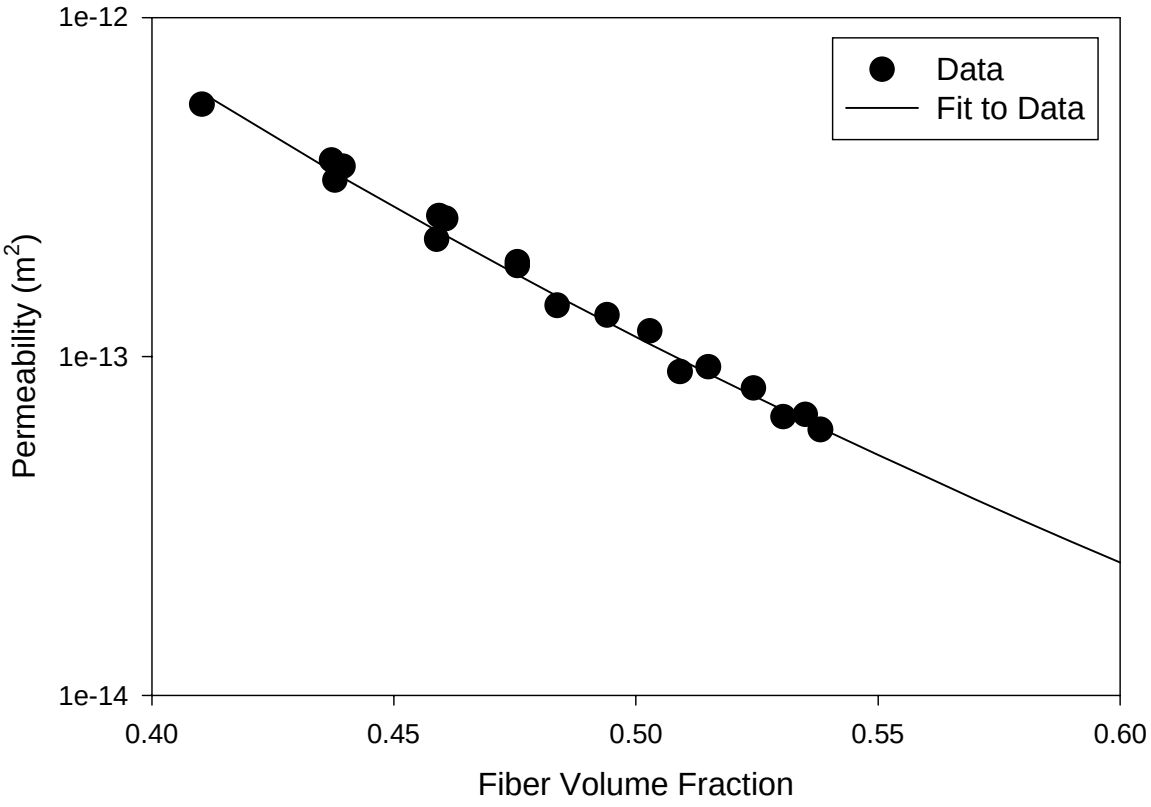

Figure 5.3: Permeability behavior for the EWC-600X 8HS graphite fabric in the through-the-thickness direction.

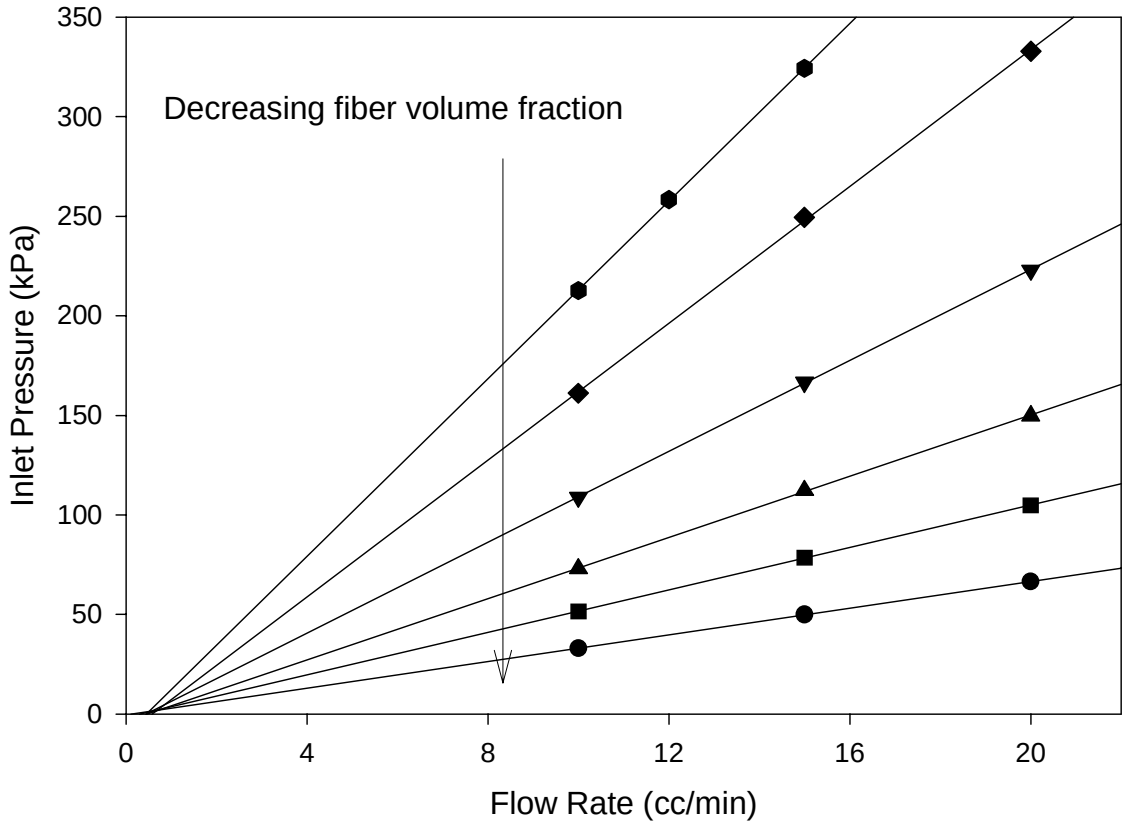

Figure 5.4: Inlet pressure as a function of flow rate for EWC-600X 8HS graphite fabric.

5.4. CONCLUSIONS

The relationship between compaction pressure and fiber volume fraction is very important in the RFI process since fiber volume fraction has a large influence on the mechanical properties of the composite part. By knowing this relationship, the preform can be compacted to the desired fiber volume fraction prior to resin injection. Since permeability characteristics of the fabric were determined as a function of fiber volume fraction, an understanding of the resin infiltration into a compacted preform can be achieved. Compaction and through the thickness permeability information are essential pieces of information in the RFI process.

CHAPTER 6: ONE-DIMENSIONAL FLOW SIMULATION

6.0 ONE DIMENSIONAL FLOW SIMULATION

A one dimensional flow model was developed to simulate the resin infiltration during the resin film infusion process. The resin film infusion process is a variation of the resin transfer molding process in which a hot-melt thermoset resin infiltrates a fabric preform. The RFI technique can be performed in a hot press, a vacuum oven, or an autoclave. Both flat plate and complex shape textile preforms have been succcessfully fabricated by the resin film infusion process.

A schematic illustration of the resin film infusion tooling of a flat panel is shown in Figure 6.1.

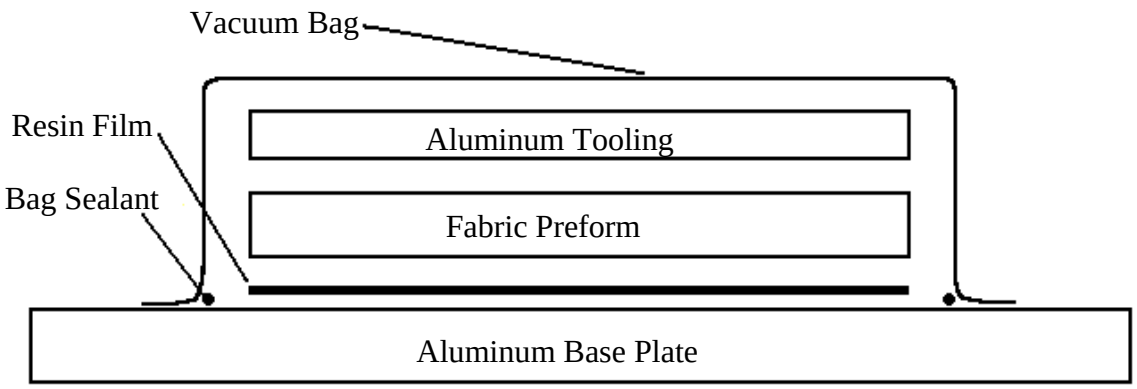

Figure 6.1: Exploded view of the Resin Film Infusion Setup.

A degassed hot-melt thermoset resin film is placed on the surface of the base plate. The thickness of the resin film depends on the mass of the resin required to completely infiltrate and wet-out the preform. The dry preform is placed on top of the resin film and the aluminum tooling is put in place. A vacuum bag is placed over the

tool and the entire assembly is put into an autoclave for infiltration and cure. A full vacuum is applied at the beginning of the cure and is maintained for the duration of the process, ensuring that all entrapped air is removed from the preform. Elevated pressure is applied to the assembly and held constant throughout the entire process. The pressure compacts the fabric preform to the specified fiber volume fraction and forces the resin into the preform. The tool assembly is heated according to a prescribed temperature cycle which decreases the resin viscosity, allowing for infusion and fiber wet-out, and cure of the resin saturated preform [6].

The flow is essentially one-dimensional since the resin film is placed beneath the preform and the flow is up through the layers of the fabric. Minimal in-plane flow takes place in a preform of simple geometry. The one-dimensional flow model takes into account the cure kinetics and viscosity models of the resin and the permeability and compaction characteristics of the fabric. Variables such as flow front, resin infiltration time, and time for the resin to fully cure are calculated by the model.

6.1. LITERATURE REVIEW

Assuming that the fibrous preform can be modeled as a porous medium, resin flow through a porous medium can be described by Darcy's Law. The one-dimensional, differential form of Darcy's Law can be written as

$$\frac{Q}{A} = \frac{-S_z}{\mu}\frac{dP}{dz} \qquad (6.1)$$

where Q is the volumetric flow rate, A is the cross-sectional area normal to the flow, S_z is the permeability in the z-direction, μ is the viscosity of the resin, and dP/dz is the pressure gradient across the thickness of the preform. The autoclave pressure is fixed during the RFI process, therefore the preform thickness and permeability should remain constant. The relationship between the superficial velocity and the interstitial velocity can be written as follows

$$\frac{Q}{A} = q_z = v_z \frac{A_{flow}}{A_{total}} = v_z \phi = \frac{dz}{dt}\phi \qquad (6.2)$$

where q_z is the superficial velocity, v_z is the interstitial velocity, ϕ is the porosity of the preform, and A_{flow} is the flow area. Substituting Equation (6.2) into Equation (6.1) and rewriting the pressure gradient as -ΔP/z yields the governing differential equation for one-dimensional, constant pressure resin infiltration.

$$\frac{dz}{dt}\phi = \frac{S_z}{\mu}\frac{\Delta P}{z} \qquad (6.3)$$

Integrating Equation (6.3), for the constant pressure injection case, while assuming permeability remains unchanged, yields the flow front position, z, as a function of time, t,

$$z^2 = \left(\frac{2S_z(P_i - P_o)}{\mu\phi} \right) t \qquad (6.4)$$

where P_i and P_o are the inlet and outlet pressures. The mold filling time, t_f, can be determined by rearranging Equation (6.4) as follows

$$t_f = \frac{z_f^2 \mu\phi}{2S_z(P_i - P_0)} \qquad (6.5)$$

Once infiltration is complete, the temperature of the mold assembly is raised to the final cure temperature and held at temperature until the resin achieves the specified cure state. The cure time for a specified cure temperature can be determined from the cure kinetics model of the resin system used.

In the present case, the model was used to conduct one-dimensional through-the-thickness flow simulations. Two cyanate ester resins and two eight harness satin fabrics were investigated. The resins were simulated to flow through 16 plies of fabric (approximately 6 mm thick). The simulation was used to determine flow front as a function of time as well as resin infiltration and cure times.

6.2. SIMULATION PROCEDURE

The one dimensional flow simulation written by Caba [37] was modified to fit the requirements of the cyanate ester resin systems. Two versions of the program were set up to accommodate the two different resins. The cure kinetics models and viscosity models of each resin were incorporated into the programs. The permeability and compaction data for the Amoco Thermalgraph™ EWC-600X 8HS and TTI IM7/8HS [33] fabrics were input into the programs. Table 6.1 summarizes the one dimensional flow simulations that were run.

Table 6.1: Summary of the four different one-dimensional flow simulations.

Simulation	Resin	Fabric
Run #1	954-3	EWC-600X 8HS
Run #2	954-2a	EWC-600X 8HS
Run #3	954-3	TTI IM7/8HS
Run #4	954-2a	TTI IM7/8HS

Table 6.2 summarizes the recommended autoclave temperature cycle used in the one-dimensional flow simulations.

Table 6.2: Manufacturer's recommended cure cycle used in the one-dimensional flow simulations [10].

Cure Cycle Step	Initial Temperature (°C)	Temperature Ramp (°C/min)	Duration (min)
First Ramp	20	+3	52.3
First Hold	177	0	120
Second Ramp	177	+3	14.3
Second Hold	220	0	60

The autoclave pressure used during the infiltration and cure is essential in compacting the preform to the desired fiber volume fraction. A fiber volume fraction of

0.6 was selected for the simulations and compaction pressures were calculated using Equation (5.13). Compaction pressures were calculated to be 1200 kPa for the EWC-600X 8HS and 100 kPa for the TTI IM7/8HS [33]. Selecting the fiber volume fraction in conjunction with Equation (5.10) also enabled the determination of the thickness of the compacted preform. Table 6.3 summarizes the compaction pressures and preform thicknesses used in the simulations.

Table 6.3: Summary of the compaction pressures and preform thicknesses used in the one-dimensional flow simulations.

Fabric	Pressure (kPa)	Preform Thickness (mm)
EWC-600X 8HS	1200	5.5
TTI IM7/8HS	100	6.2

Upon completion of the preliminary calculations, the simulations were run.

6.3. RESULTS

In each of the four simulations, the resins completely infiltrated the preforms. The fill times were significantly shorter for the 954-3 resin compared to the 954-2a due to its very low viscosity. Figures 6.2 - 6.9 contain plots of various parameters versus time for the different simulations.

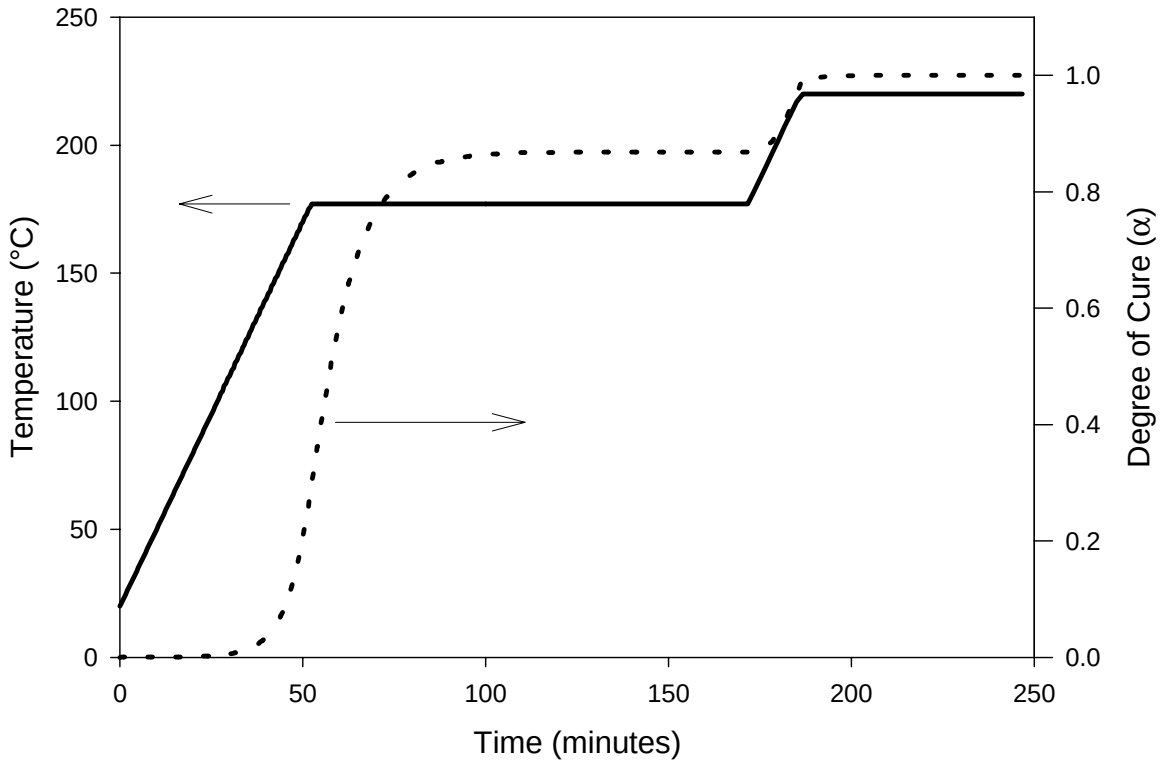

Figure 6.2: Temperature and degree of cure as a function of time for the 954-3 cyanate ester resin flowing through the EWC-600X 8HS graphite fabric.

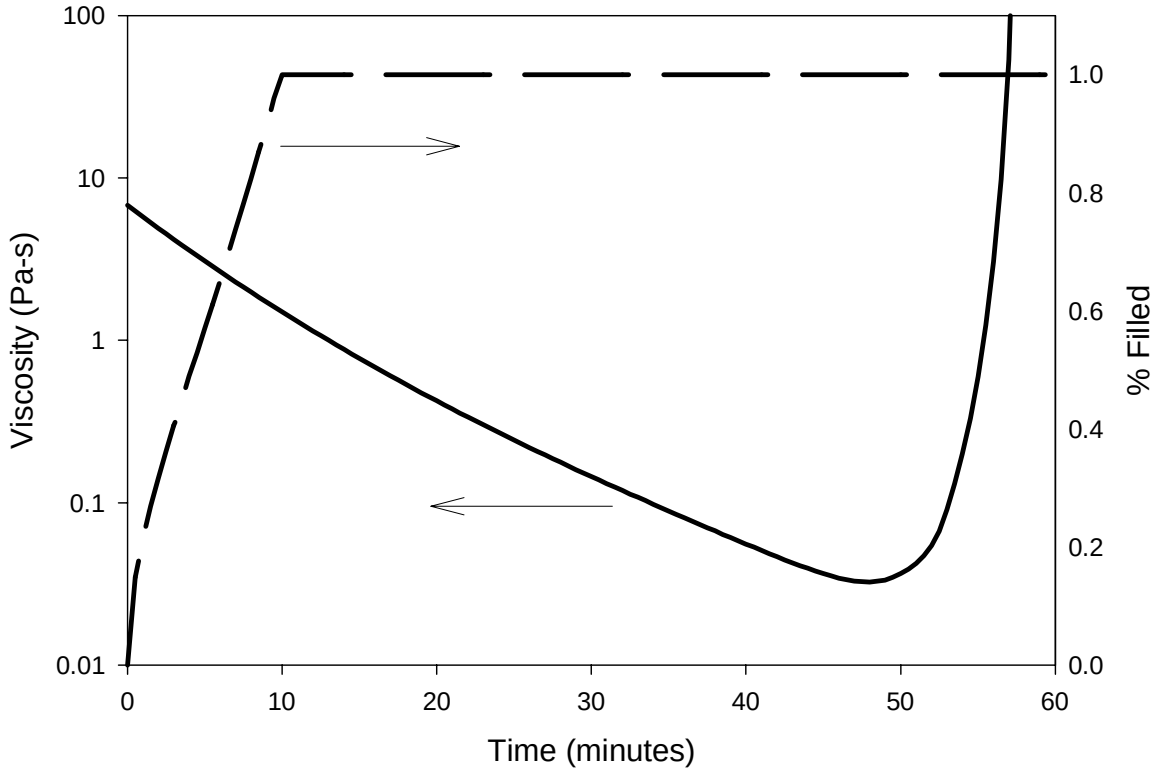

Figure 6.3: Viscosity and resin infiltration as a function of time for the 954-3 cyanate ester resin flowing through the EWC-600X 8HS graphite fabric.

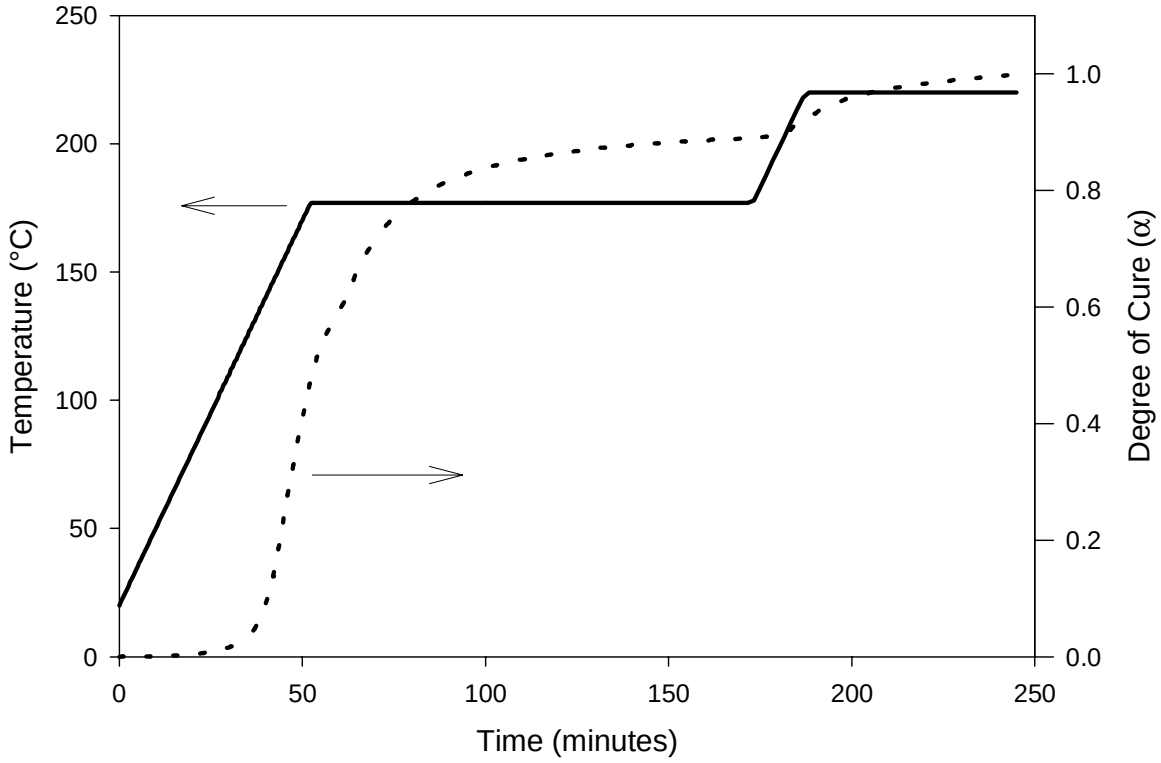

Figure 6.4: Temperature and degree of cure as a function of time for the 954-2a cyanate ester resin flowing through the EWC-600X 8HS graphite fabric.

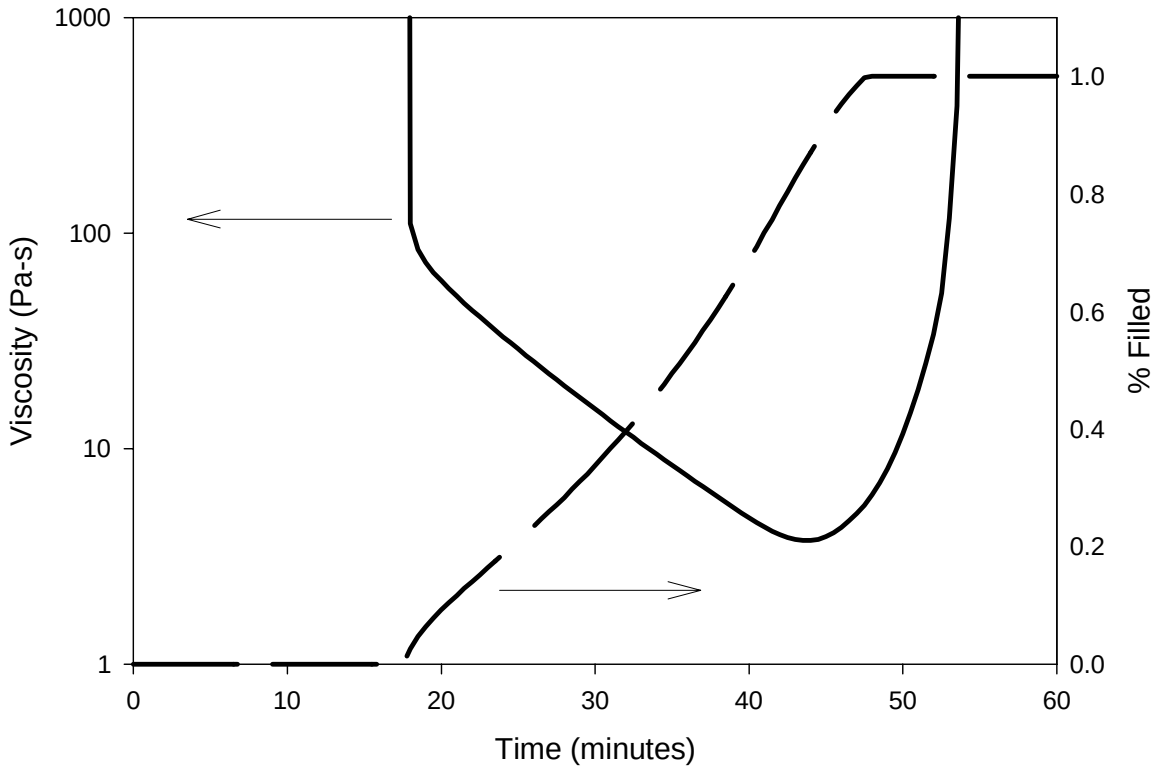

Figure 6.5: Viscosity and resin infiltration as a function of time for the 954-2a cyanate ester resin flowing through the EWC-600X 8HS graphite fabric.

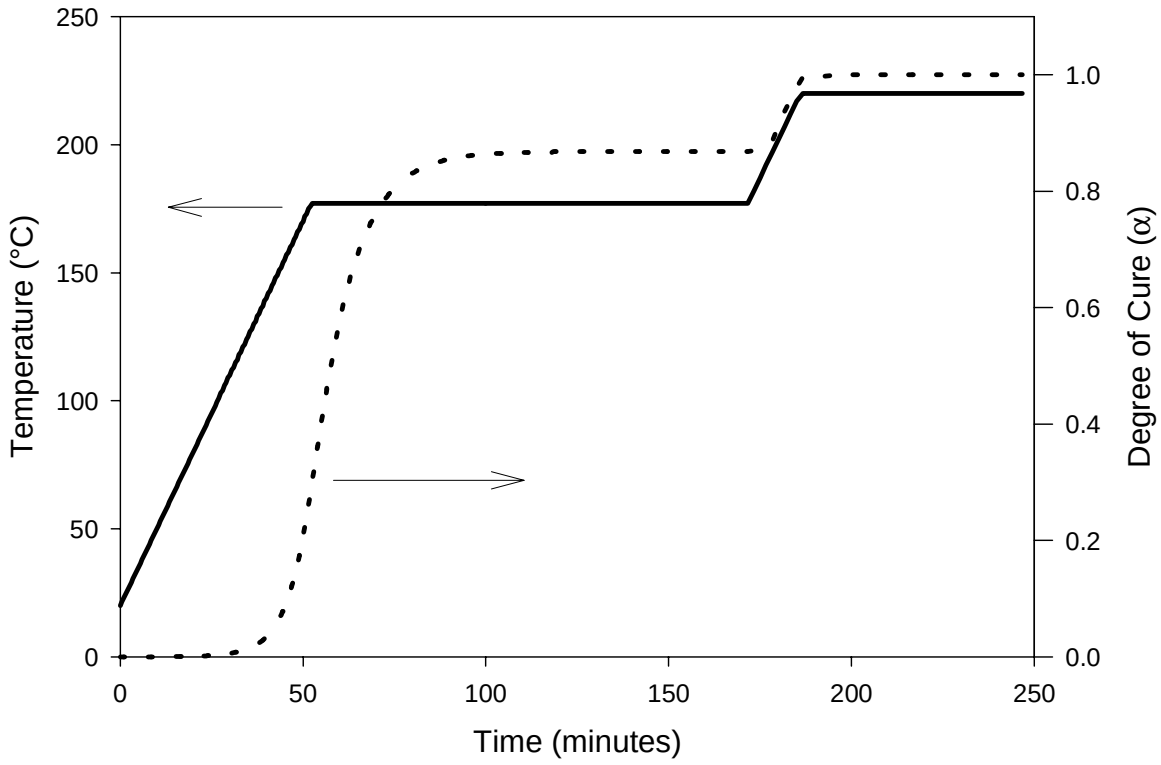

Figure 6.6: Temperature and degree of cure as a function of time for the 954-3 cyanate ester resin flowing through the TTI IM7/ 8HS carbon fabric.

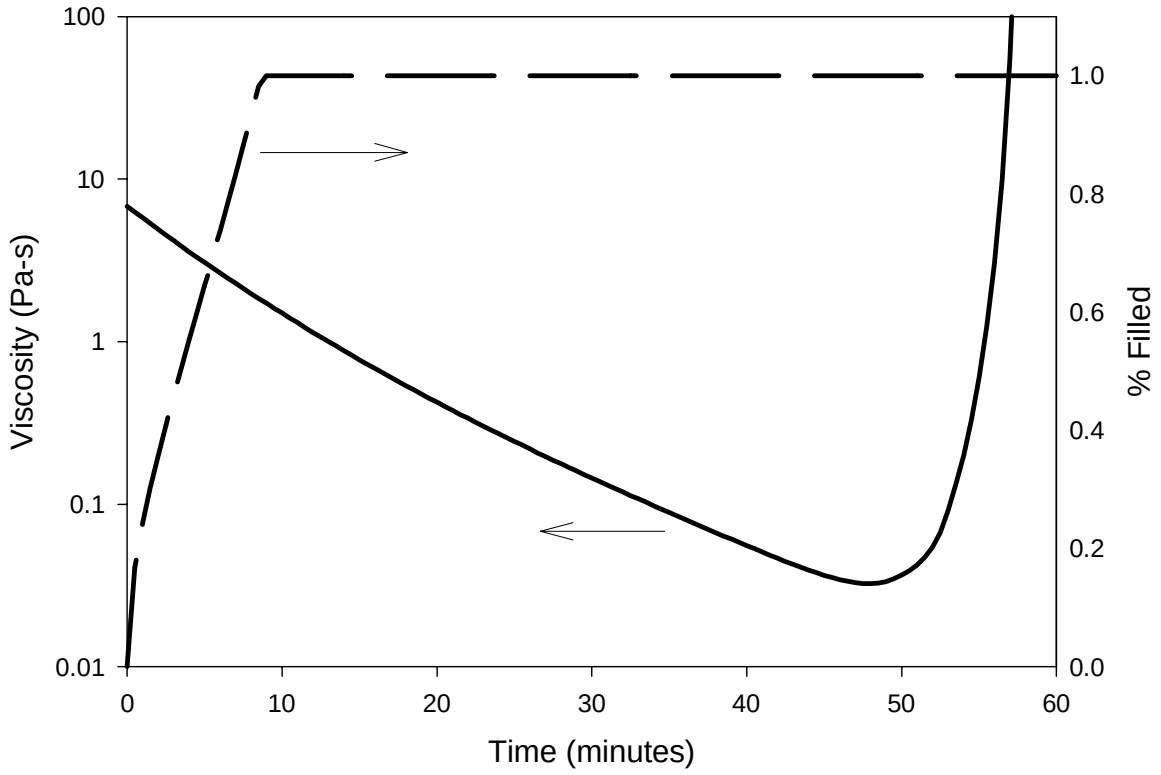

Figure 6.7: Viscosity and resin infiltration as a function of time for the 954-3 cyanate ester resin flowing through the TTI IM7/ 8HS carbon fabric.

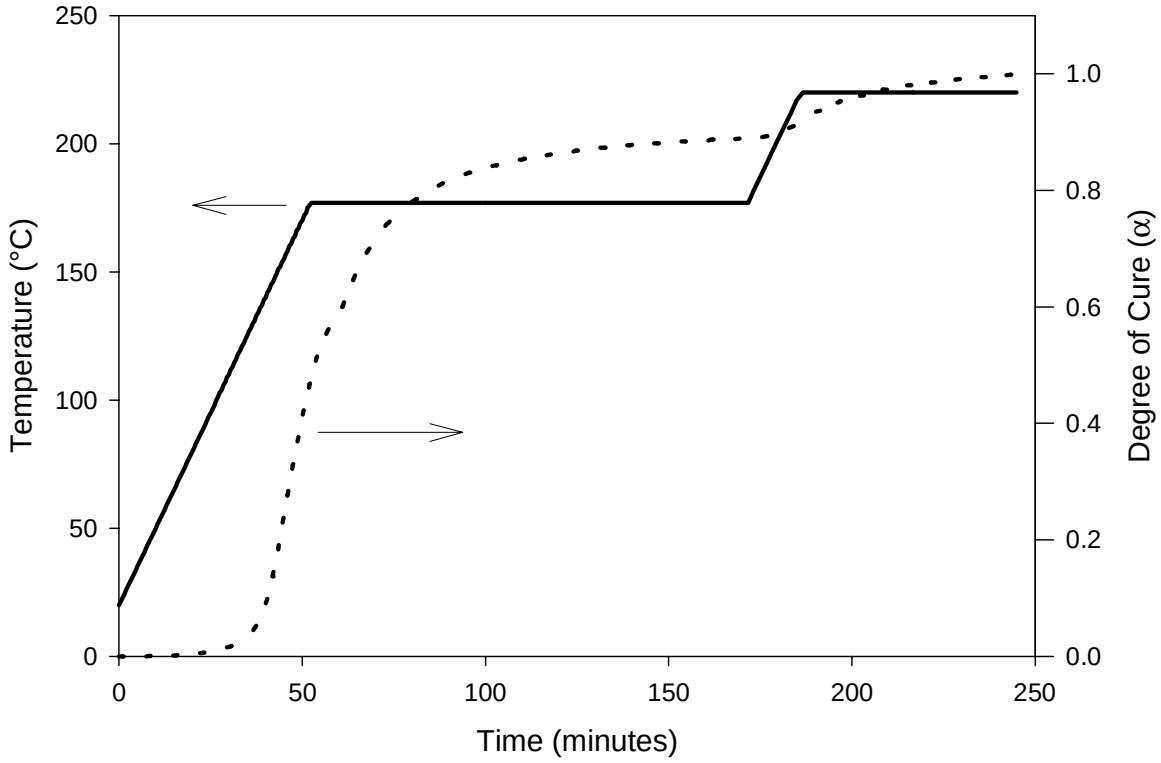

Figure 6.8: Temperature and degree of cure as a function of time for the 954-2a cyanate ester resin flowing through the TTI IM7/ 8HS carbon fabric.

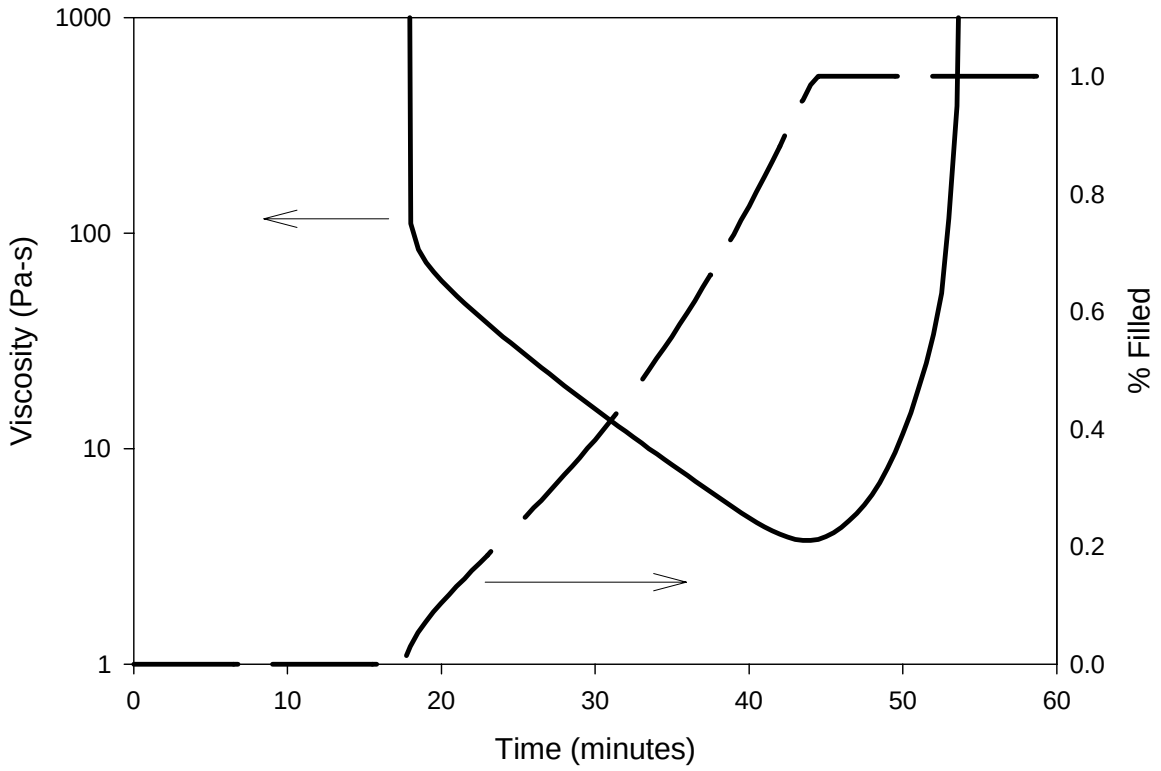

Figure 6.9: Viscosity and resin infiltration as a function of time for the 954-2a cyanate ester resin flowing through the TTI IM7/ 8HS carbon fabric.

6.4. CONCLUSIONS

The resin completely infiltrated the preform in all four flow simulations. Although the compaction pressure required to reach a fiber volume fraction of 0.6 was significantly higher for the EWC-600X 8HS, the resin infiltration times were almost identical to those of the TTI IM7/8HS. This is attributed to identical weave patterns, similar areal weights (4500 g/m^2 vs. 4190 g/m^2) , similar permeabilities, and similar thicknesses (5.5 mm vs. 6.2 mm). The 954-3 cyanate ester resin filled both fabrics in approximately 10 minutes, whereas the 954-2a toughened cyanate ester resin took approximately 45 minutes. The difference in times is due to the very low minimum viscosities experienced by the 954-3 resin. The one-dimensional flow simulations proved to be an informative tool when dealing with the resin film infusion process.

CHAPTER 7: CONCLUSIONS AND FUTURE WORK

7.0 CONCLUSIONS AND FUTURE WORK

7.1. CONCLUSIONS

The focus of this research was to characterize two cyanate ester resin systems and a new 8 harness satin graphite fabric weave, and to simulate the flow of the resins through the fabric. Cure kinetics and viscosity models were proposed for the resins. Permeability and compaction characteristics of the graphite fabric were also measured. The flow model took into account the resin and fabric characteristics and calculated parameters such as flow front position and infiltration time. A better understanding of the flow of a resin through the thickness of a preform was gained by running the one-dimensional flow simulations.

7.1.1. CURE-KINETICS

The four parameter / two part cure kinetics model developed by Castro and Macosko was used to characterize the 954-3 and 954-2a cyanate ester resin systems. Isothermal DSC along with residual dynamic scans were completed to determine the kinetics parameters. It was shown that, for a reasonable range of temperatures, the model fit the experimental data well for both resin systems. An accurate cure kinetics model is an essential parameter in a one-dimensional flow simulation.

7.1.2. VISCOSITY

An empirical viscosity model was fit to isothermal viscosity data of both cyanate ester resin systems. The initial viscosity and the degree of cure at gel were determined to be linear functions of temperature for both resins. The model parameters A and B were also determined to be linear functions of temperature. It was shown that the models fit the data over the entire range of temperatures.

7.1.3. COMPACTION AND PERMEABILITY

Amoco's EWC-600X 8HS fabric was characterized to determine the compaction and through-the-thickness permeability. Compaction tests showed a non-linear increase in fiber volume fraction at low compaction pressures followed by a linear increase at higher compaction pressures. The data were fit with a power law model and relatively high pressures (750 kPa) were required to reach a fiber volume fraction of 55%. Through the thickness permeability tests were performed on the fabric as well. Permeabilities ranged from $8x10^{-14}$ m^2 to $8x10^{-13}$ m^2 over a fiber volume fraction range of 42 to 55%, respectively. The data were fit with a power law model similar to that of the compaction data. A plot of flow rate versus compaction pressure was produced to ensure that the one-dimensional form of Darcy's law applied.

7.1.4. 1-D FLOW

Since the flow of the resin in the resin film infusion process is primarily through the thickness of the fabric, a one-dimensional flow and cure simulation was run. This simulation determined flow front position as a function of time as well as resin infiltration time and time required for the resin to fully cure. The previously determined cure-kinetics models and viscosity models as well as the permeability and compaction information of the fabrics were incorporated into the programs. Part thickness and an autoclave temperature pressure cycle were also input into the program. The simulation resulted in much shorter infiltration times for the 954-3 resin as opposed to the toughened 954-2a resin.

7.2. FUTURE WORK

7.2.1. FUTURE COMPACTION TESTING

Compaction testing of the EWC-600X 8HS graphite fabric should be continued on the 5.08 cm x 5.08 cm fixture up to fiber volume fractions of about 65%. A series of wet compaction tests should also be run to determine if a saturated preform affects the applied compaction pressure.

7.2.2. FUTURE PERMEABILITY CHARACTERIZATION

More permeability work should be performed on the EWC-600X 8HS fabric. In-plane permeability tests should be run in both the warp and fill directions. Advancing front permeability should also be measured considering the flow of the resin in the RFI process is into a dry preform not a previously saturated one.

7.2.3. MODEL VERIFICATION

The one dimensional flow model should be verified with experimental data. A composite panel should be fabricated using each of the four proposed combinations of resin and fabric. Pressure transducers should be used to monitor flow front and resin infiltration time, and results compared to model predictions.REFERENCES

References

1. Almen, G. R., P. D. Mackenzie, V. Malhotra, and R. K. Maskell. "Fiberite 954: cyanate ester systems." SPIE - Design of Optical Instruments, Vol. 1690, 1992, 288-294.

2. Almen, G. R., P. D. Mackenzie, V. Malhotra, and R. K. Maskell. "954: A Family of Toughened Cyanate Ester Resins." 23rd International SAMPE Technical Conference, October 21-24, 1991, 947-958.

3. Almen, G., P. Mackenzie, V. Malhotra, and R. Maskell. "Toughened Cyanates for Aerospace Applications." 35th International SAMPE Symposium, April 2-5, 1990, 408-413.

4. Yu-Hon-Wen and Young-Wen-Bin. "Optimal design of process parameters for resin transfer molding." Journal-of-Composite-Materials, Vol. 31, No. 11, 1997, 1113-1140.

5. Loos, A. C., J. D. MacRae. "Resin Film Infusion Process Simulation of Complex Wing Structures." Fifth NASA/DoD Advanced Composites Technology Conference, May 1995, 773-786.

6. Rohwer, K., B. Grossheim, and R. Burgess. "Stitched/Resin Film Infusion Manufacturing Technology Development for Transport Aircraft Composite Wing Structures." Sixth NASA/DoD Advanced Composites Technology Conference, June 1996, 167-189.

7. Loos, A. C. and J. D. MacRae. "A Process Simulation Model for the Manufacture of a Blade-Stiffened Panel by the Resin Film Infusion Process." Composites Science and Technology, Vol. 56, 1996, 273-289.

8. Shimp, D. A., and J. E. Wentworth. "Cyanate Ester-Cured Epoxy Resin Structural Composites." 37th International SAMPE Symposium, March 9-12, 1992, 293-305.

9. Osei-Owusu, A., G. C. Martin and J. T. Gotro. "Analysis of the Curing Behavior of Cyanate Ester Resin Systems." Polymer Engineering and Science, Vol. 31, No. 22, November 1991, 1604.

10. Almen, G., P. Mackenzie, V. Malhotra, and R. Maskell. "Cyanate / Thermoplastic Alloys." 21st International SAMPE Technical Conference, September 25-28, 1989, 304-314.

11. ICI Fiberite. Fiberite Data Sheets, November 1995, 1-12.

12. NASA Technical Paper, No. 2950, Nov. 1989, 1-27.

13. Amoco Performance Products, Inc. Product Information, Thornel, Thermalgraph™ Fabric EWC-600X, August 1995, 1-2.

14. Vali, P. S. The DuPont DSC 910 Operations Manual, Version 1.01, May 1989, 10-11.

15. Zukas, Walter X. and James T. Varnum. "Cure Studies of a Cyanate Ester Resin and Prepreg." Society of Plastics Engineers, 53rd Technical Conference, May 7-11, Vol. 41, 1995, 2761-2765.

16. Chen, Y. T. and C. W. Macosko. "Chemorheology of Polycyanate for Resin Transfer Molding." 24th International SAMPE Technical Conference, October 20-22, 1992, T630.

17. Deng, Y. and G. C. Martin. "Diffusion and Diffusion-Controlled Kinetics during Epoxy-Amine Cure." Macromolecules, Vol. 27, 1994, 5147-5153.

18. Deng, Y. and G. C. Martin. "Curing Characteristics of a Zinc-Catalyzed Cyanate Ester Resin System." ANTEC '94: Plastics: Gateway to the Future, Vol. 40, 1994, 1664-1666.

19. Jandel Corporation. Transforms and Nonlinear Regressions, User's Manual, Version 3.0, October 1995, 7.1-7.6.

20. Castro, J. M. and C. W. Macosko. "Studies of Mold Filling and Curing in the Reaction Injection Molding Process." AIChE Journal, Vol. 28, No. 2, March 1982, 250-253.

21. Brookfield Engineering Laboratories, Inc. Brookfield Viscometers / Rheometers, 1995, 16-19.

22. Batch, G. L. and S. Cumiskey. "Multilayer Compaction and Flow in Composites Processing." Proceedings of the 45th Annual Conference, February 12-15, 1990, Composites Institute, The Society of the Plastics Industry, Inc. (1990) Session 9A.

23. Darcy, H. Les Fontaines Publiques de la Villa de Dijon. Dalmount, 1856.

24. Gauvin, R. and M. Chibani. "Analysis of Composites Molding with Woven and Non Woven Reinforcements." Proceedings of the 45th Annual Conference, February 12-15, 1990, Composites Institute, The Society of the Plastics Industry, Inc. (1990) Session 9F.

25. Molnar, J. A., L. Trevino, and L. J. Lee. "Mold Filling in SRIM and RTM: Controlling a Critical Process Parameter," Modern Plastics, September 1989, 120-126.

26. Fracchia, C. A., J. Castro, and C. L. Tucker III. "A Finite Element/Control Volume Simulation of Resin Transfer Mold Filling." Proceedings of the American Society for Composites, Fourth Technical Conference, October 1989, 157-166.

27. Gebart, B. R., "Permeability of Unidirectional Reinforcements for RTM." Journal of Composite Materials, Vol. 26, No. 8, 1992, 1100-1133.

28. Galli, E. "Resin Transfer Molding: A Cost Effective Alternative." Plastic Design Forum, March/April 1982, 47-56.

29. Kim. Y. T., S. P. McCarthy, J. P. Fanucci, S. C. Nolet, and C. Koppernaes. "Resin Flow Through Fiber Reinforcements During Composite Processing," in L. D. Michelove et al. (eds.), 22nd International SAMPE Technical Conference, SAMPE, Covina, Ca., 1990, 709-723.

30. Skartsis, L., J. L. Kardos, and B. Khomami. "Resin Flow Through Fiber Beds During Composite Manufacturing Processes. Part I: Review of Newtonian Flow Through Fiber Beds." Polymer Engineering and Science, Vol. 26, No. 20, November 1986, 1434-1441.

31. Gutowski, T. G., Z. Cai, S. Bauer, D. Boucher, J. Kingery, and S. Wineman. "Consolidation Experiments for Laminate Composites." Journal of Composite Materials, Vol. 21, July 1987, 650-669.

32. Gutowski, T. G., T. Morigaki, and Z. Cai. "The Consolidation of Laminate Composites." Journal of Composite Materials, Vol. 21, February 1987, 172-188.

33. Hammond, V. H. "Verification of a Two-Dimensional Infiltration Model for the Resin Transfer Molding Process." Master's Thesis, Virginia Polytechnic Institute and State University, 1993.

34. Wiedeman, M. H. "An Infiltration/Cure Model for Manufacture of Fabric Composites by the Resin Infusion Process." Master's Thesis, Virginia Polytechnic Institute and State University, 1992.

35. Verghese, K. E. "Effects of Fiber Architecture and Through-the-Thickness Stitching on Permeability and Compaction of Textile Preforms." Master's Thesis, Virginia Polytechnic Institute and State University, 1996.

36. Hammond, V. H. and A. C. Loos. "The Effects of Fluid Type and Viscosity on the Steady-State and Advancing Front Permeability Behavior of Textile Preforms." Journal of Reinforced Plastics and Composites, Vol. 16, No. 1, 1997, 50-72.

37. Personal contact with A. Caba.

Vita

Paul Joseph Myslinski

Paul Joseph Myslinski was born on June 3, 1974 in Toms River, New Jersey. The son of Joe and Phyllis, Paul spent all of his life living near the beach in New Jersey. Paul also has two wonderful and supportive brothers, Brian and Lucas. Paul graduated from Toms River High School East in June of 1992, and enrolled at Virginia Tech in August of the same year. While an undergraduate, Paul was a member of SAMPE for two years, and spent a summer in Chicago working for Illinois Tool Works Research and Development. He graduated from Virginia Tech in May of 1996 with a B.S. in Materials Science and Engineering.

Paul entered graduate school in the fall of 1996. He enrolled in the Department of Materials Science and Engineering, to study composites manufacturing. He worked hard and completed his masters degree in December of 1997.